The Dissertation Committee for Arash Motamed Certifies that this is the approved version of the following dissertation:

Constitutive Modeling of Viscoelastic Behavior of Bituminous Materials

Committee:

Amit Bhasin, Supervisor

Kenneth M. Liechti

Jorge A. Prozzi

C. Michael Walton

John L. Tassoulas

Constitutive Modeling of Viscoelastic Behavior of Bituminous Materials

by

Arash Motamed, B.S.; M.S.; M.S.

Dissertation

Presented to the Faculty of the Graduate School of

The University of Texas at Austin

in Partial Fulfillment

of the Requirements

for the Degree of

Doctor of Philosophy

The University of Texas at Austin

December 2012

Dedication

This dissertation is dedicated to my family and teachers.

Acknowledgements

I deeply thank Professor Amit Bhasin, my Ph.D. supervisor, who has always been a great guide and support for me. I also would like thank Professor Kenneth M. Liechti, who co-supervised this research and broadened my vision towards the Mechanics of Materials. Furthermore, I appreciate the constructive feedbacks from the committee members: Professor Jorge A. Prozzi, Professor C. Michael Walton, and Professor John L. Tassoulas. Finally, I would like to acknowledge the Federal Highway Administration FHWA and Asphalt Research Consortium for supporting this study.

Constitutive Modeling of Viscoelastic Behavior of Bituminous Materials

Arash Motamed, Ph.D.

The University of Texas at Austin, 2012

Supervisor: Amit Bhasin

Asphalt mixtures are complex composites that comprise aggregate, asphalt binder, and air. Several research studies have shown that the mechanical behavior of the asphalt mixture is strongly influenced by the matrix, i.e. the asphalt binder. Therefore, accurate constitutive models for the asphalt binders are critical to ensure accurate performance predictions at a material and structural level. However, researchers who use computational methods to model the micromechanics of asphalt mixtures typically assume that (i) asphalt binders behave linearly in shear, and (ii) either bulk modulus or Poisson's ratio of asphalt binders is not time dependent. This research develops an approach to measure and model the shear and bulk behavior of asphalt binders at intermediate temperatures. First, this research presents the findings from a systematic investigation into the nature of the linear and nonlinear response of asphalt binders subjected to shear using a Dynamic Shear Rheometer (DSR). The DSR test results showed that under certain conditions a compressive normal force was generated in an axially constrained specimen subjected to cyclic torque histories. This normal force could not be solely attributed to the Poynting effect and was also related to the tendency of the asphalt binder to dilate when subjected to shear loads. The generated normal force changed the state of stress and interacted with the shear behavior of asphalt binder. This effect was considered to be an "interaction nonlinearity" or "three dimensional effect". A constitutive model was identified to accommodate this effect. The model was successfully validated for several different loading histories. Finally, this study investigated the time-dependence of the bulk modulus of asphalt binders. To this end, poker-chip geometries with high aspect ratios

were used. The boundary value problem for the poker-chip geometry under step displacement loading was solved to determine the bulk modulus and Poisson's ratio of asphalt binders as a function of time. The findings from this research not only improve the understanding of asphaltic materials behavior, but also provide tools required to accurately predict pavement performance.

Table of Contents

List of Tables

List of Figures

Chapter 1: Introduction

Computational methods are being increasingly used to model the mechanical response of asphalt composites based on the properties of their constituent materials (mineral aggregate, asphalt binder, and air). These methods are also used in a micromechanics framework to characterize damage evolution in the composites. Computational methods not only save time and resources in evaluating the performance of different asphalt mixtures, but they also allow industry to innovate and develop newer technologies to design more efficient highway structures and materials. However, the success of computational methods is contingent upon the accuracy of the constitutive relationships that are used to describe the constituent materials behavior.

The mechanical properties of the asphalt binder or mastic, the matrix in the asphalt mixture composite, are time and temperature dependent and have a lower stiffness compared to the inclusions (aggregate particles). Several research studies have demonstrated that the properties of the asphalt binder significantly influence the overall mechanical response of the asphalt mixture composite (*Di Benedetto et al., 2004; Delgadillo, 2008*). Therefore, accurate constitutive relationships for the asphalt binder are crucial to ensure accurate predictions of the mixture behavior. However, a review of the literature indicates that computational methods to model the micromechanics of asphalt mixtures typically employ two assumptions pertaining to the asphalt matrix: (i) it is linearly viscoelastic in shear, and (ii) either the bulk modulus or Poisson's ratio is time independent.

Computational methods to model the micromechanics of asphalt mixtures typically utilize a linearly viscoelastic (LVE) model to characterize the matrix (e.g., *You and Dai, 2007*). To obtain the linearly viscoelastic properties, a dynamic shear rheometer (DSR) (*Anderson et al., 1994*) is typically used and test data are fitted to a linearly viscoelastic constitutive model such as power law or Prony series. However, several

research studies demonstrated that asphalt binders exhibit a nonlinear stress-strain relationship, except under very low stresses and strains (*Anderson et al., 1994; Bahia et al., 2001; Airey et al., 2004; Kim and Little, 2004; Delgadillo, 2008*).

Airey et al. (*2004*) investigated the rheological behavior of bituminous paving materials to determine the LVE region within which the stress-strain relationship is independent of the magnitude of stress or strain. They demonstrated that for mixtures, the LVE limit for strain was on the order of 0.01% while this limit for asphalt binder was at least 100 times greater (1% strain). This raises a very pertinent question as to whether the asphalt binder experiences stresses that exceed its LVE limit in mixtures subjected to typical service loads.

Several studies have tried to examine the range of stresses experienced by the asphalt binder within the asphalt mixture composite using finite element analysis (*Kose, 2001; Lakes et al., 2002*). Kose (*2001*) illustrated that on an average the local strain in the binder was about 8 to 510 times more than the far field strain in the mixture. Other studies corroborated these findings (*Masad et al., 2001; Drakos et al., 2001*). These studies concluded that asphalt binder experiences a range of local stresses within the mixture that is typically one to two orders of magnitude higher than the far field strain, and there is no unique level of strain that can be regarded as representative of what binders experience in a typical mixture. It can be synthesized from these studies that the asphalt binder will have a nonlinearly viscoelastic response when used in a mixture subjected to typical service loads. Therefore, developing a constitutive model that accurately describes the behavior of the binder at high level of stress and strain is required to accurately predict mixture performance. Consequently, it is important to investigate the nature of nonlinearly viscoelastic response of the asphalt binder as well as to develop and use appropriate constitutive relationships in micromechanical formulations. This research investigates the sources of nonlinear response in asphalt binders subjected to shear, and also introduces a thermodynamic-based constitutive equation to model these nonlinearities.

With regards to the Poisson's ratio and bulk modulus, different assumptions are typically employed regarding the time-dependent behavior of the bulk modulus of asphaltic materials during computational modeling. For example it can be assumed that the material is elastic in dilatation [e.g., in the work of You et al. (*2007*)]. This assumption implies that the Poisson's ratio changes with time while the bulk modulus in constant. An alternative to this assumption is that the bulk modulus and shear modulus have similar time dependency [e.g., in the works of Kim and Lutif (*2008*), and Karki (*2010*)]. This assumption, which is known as synchronous shear and bulk moduli, implies that the Poisson's ratio does not change with time. Finally, some studies have also assumed the asphalt binder to be incompressible (*Read and Whiteoak, 2003; Al-Khateeb et al., 2006; Delgadillo, 2008*; *Johnson, 2010; Luo and Lytton, 2011*). This implies that the bulk modulus is infinite and the Poisson ratio is 0.5. Investigating the validity of these assumptions is also important to ensure the accuracy of computational models at the material and mixture length scale. Although many researchers have measured the bulk modulus of asphalt mixtures (*Lee, 1976; Stroup-Gardiner et al., 1997; Read, 2000; Long, 2001; Maher and Bennert, 2008; Kim et al., 2010*), there have only been few studies (*Kim, 2009; Di Benedetto et al., 2007*) intended to measure the bulk modulus of asphalt binders at intermediate temperatures. Since these approaches, were either not successful or hard to implement, this study further investigates the time-dependence of the bulk modulus of asphalt binders.

In summary, this research investigates the sources of nonlinear response in asphalt binders subjected to shear (Chapter 2) and introduces a thermodynamic-based constitutive equation to model these nonlinearities (Chapter 3). This study also further investigates the viscoelastic behavior of asphaltic materials by measuring the time-dependence of the bulk modulus of asphalt binders (Chapter 4).

Chapter 2: Interaction Nonlinearity in Asphalt Binders[1]

2.1. OVERVIEW

Asphalt mixtures are complex composites that comprise aggregate, asphalt binder, and air. Several research studies have shown that the mechanical behavior of the asphalt mixture is strongly influenced by the matrix, i.e. the asphalt binder. Characterization and a thorough understanding of the binder behavior is the first and crucial step towards developing an accurate constitutive model for the composite. Accurate constitutive models for the constituent materials are critical to ensure accurate performance predictions at a material and structural level using micromechanics. This chapter presents the findings from a systematic investigation into the nature of the linear and nonlinear response of asphalt binders subjected to different types of loading using the Dynamic Shear Rheometer (DSR). Laboratory test data show that a compressive normal force is generated in an axially constrained specimen subjected to torsional shear. This research investigates the source of this normal force and demonstrates that the asphalt binder can dilate when subjected to shear loads. This chapter also presents the findings from a study conducted to investigate the source of nonlinearity in the asphalt binder. Test results demonstrate that the application of cyclic shear loads results in the development of a normal force and a concomitant reduction in the dynamic shear modulus. This form of nonlinear response is referred to as an "interaction nonlinearity". A combination of experimental and analytical tools is used to demonstrate and verify the presence of this interaction nonlinearity in asphalt binders. The findings from this study highlight the

1- A significant portion of this chapter has been published in the Journal of Mechanics of Time Dependent Materials; Motamed, A., Bhasin, A., Liechti, K.M.: Interaction nonlinearity in asphalt binders. *J. Mech. Time-Depend. Mater.* 16(2), 145-167 (2012*a*)

importance of modeling the mechanical behavior of asphalt binders based on the overall stress state of the material.

2.2. INTRODUCTION AND MOTIVATION

Asphalt mixtures are composite that comprise mineral aggregate, asphalt binder, and air. Computational methods are frequently used to model the mechanical response of an asphalt composite based on the properties of its constituent materials. These methods are also used in a micromechanics framework to characterize damage evolution in the composite (*Lakes et al., 2002*).

The accuracy of computational methods is contingent upon the accuracy of two important inputs: the internal structure or geometry of the composite and the constitutive relationship for the materials in the composite. The mechanical properties of the asphalt binder, the matrix in an asphalt mixture composite, are time and temperature dependent and have a lower stiffness compared to the inclusions (aggregate particles). The properties of the asphalt binder govern the overall mechanical response of the asphalt mixture composite (*Di Benedetto et at., 2004; Delgadillo, 2008*). Therefore, an accurate constitutive relationship for the asphalt binder is crucial to ensure accurate predictions of the mixture behavior.

Computational methods to model the micromechanics of asphalt mixtures typically utilize a linearly viscoelastic (LVE) model to characterize the matrix (*You and Dai, 2007*). To obtain the linearly viscoelastic properties, a dynamic shear rheometer (DSR) (*Anderson et al., 1994*) is typically used and test data are fitted to linearly viscoelastic constitutive models such as the Christensen–Anderson–Marasteanu (CAM) model (*Marasteanu and Anderson, 1999*), Burger's four-element model, power law, or Prony series. However, several research studies indicate that asphalt binders exhibit a nonlinear stress-strain relationship, except under very low stresses and strains (*Anderson et al., 1994; Bahia et al., 2001; Airey et al., 2004; Kim and Little, 2004; Delgadillo, 2008*).

Airey et al. (*2004*) investigated the rheological behavior of bituminous paving materials to determine the LVE region within which the stress-strain relationship is

independent of the magnitude of stress or strain. They demonstrated that for mixtures, the LVE limit for strain applied to the mixture was on the order of 0.01% while this limit for asphalt binder was at least 100 times greater (1% strain). This raises a very pertinent question as to whether the asphalt binder experiences stresses that exceed its LVE limit in mixtures subjected to typical service loads.

Several studies have tried to examine the range of stresses experienced by the asphalt binder within an asphalt mixture using finite element analysis with images of asphalt mixture specimens (*Kose, 2001; Lakes et al., 2002*). Kose (*2001*) illustrated that on average the local strain in the binder was about 8 to 510 times more than the far field strain in the mixture. Other studies corroborated these findings (*Masad et al., 2001; Drakos et al., 2001*). These studies concluded that asphalt binder experiences a range of local stresses within the mixture that is typically one to two orders of magnitude higher than the far field strain, and there is no unique level of strain that can be regarded as representative of what binders experience in a typical mixture. Therefore, developing a constitutive model that accurately describes the behavior of the binder at high level of stress and strain is required to accurately predict mixture performance. It can be synthesized from these studies that the asphalt binder will have a nonlinearly viscoelastic response when used in a mixture subjected to typical service loads. Consequently, it is important to investigate the nature of nonlinearly viscoelastic response of the asphalt binder as well as to identify and use appropriate constitutive relationships in micromechanical formulations.

This chapter investigates the nature of nonlinearly response of asphalt binders. The following two sections present a brief review of the different sources of nonlinearity as well as a brief review of the models commonly used to describe the nonlinearly viscoelastic response of asphalt and other materials. Subsequently, this chapter presents the findings from a study conducted to investigate the nature of nonlinearly viscoelastic response in asphalt binders.

2.3. BACKGROUND ON SOURCES OF NONLINEAR RESPONSE

Nonlinearity in stress-strain relationships can be due to different mechanisms. In general, four different sources of stress-strain nonlinearity are recognized in the literature: material nonlinearity, geometrical nonlinearity, interaction nonlinearity, and intermodal nonlinearity.

2.3.1. Material Nonlinearity

Material nonlinearity is due to an inherent dependence of the stress-strain relationship on the magnitude of stress or strain. Material nonlinearity can be observed even at low strain levels (*Findley, 1976; Lakes, 2009*). There are several models available to describe this type of nonlinear response. Among these, the nonlinear power law and Schapery's nonlinear constitutive model (*Schapery, 1969*) have been used to some extent in the asphalt pavement industry to describe the intrinsic nonlinear response of asphaltic materials. Schapery (*1969*) used the thermodynamic principles of an irreversible process and experimental observations to describe the material's nonlinearly viscoelastic behavior in terms of its linearly viscoelastic properties and appropriate stress and time scaling functions. Schapery's model for uniaxial loading at constant temperature is

$$\varepsilon(t) = g_0 J_0 \sigma(t) + g_1 \int_0^t J[\psi(t) - \psi(\tau)] \frac{d(g_2\, \sigma(\tau))}{d\tau} d\tau, \tag{2.1}$$

where

$$\psi(t) = \int_0^t \frac{d\xi}{a_\sigma[\sigma(\xi)]} \ , \ \psi(\tau) = \int_0^\tau \frac{d\xi}{a_\sigma[\sigma(\xi)]} \ ,$$

and t is the time of interest; τ and ξ are the integration variables; $\sigma(t)$ is the applied stress at time t; g_0, g_1, and g_2 are material properties that are a function of stress; $\psi(t)$ and $\psi(\tau)$ are reduced time variables; $a_\sigma[\sigma(\xi)]$ is a shift factor that scales (modulates) the time and is a function of stress; J_0 is the time independent compliance, J is the linearly viscoelastic compliance (creep compliance). The creep compliance indirectly depends on

stress through the reduced time variables. This model incorporates five functions (g_0, g_1, g_2, $a_\sigma[\sigma(\xi)]$, J) and a constant (J_0) and can be used to describe different types of nonlinearities (*Findley, 1976; Lakes, 2009*). By setting $g_0 = g_1 = g_2 = a_\sigma[\sigma(\xi)] = 1$, the model reduces to the Boltzmann linear superposition integral.

The multiple integrals method is another approach to model the nonlinear response of viscoelastic materials and other nonlinear systems. Although the implementation of multiple integrals is difficult (*Findley, 1976*), it provides insight into some sources of nonlinear response, including cross interactions in multistep loading. This will be further discussed in section 2.6.3.

2.3.2. Geometric Nonlinearity

Geometric nonlinearity is related to large deformations and violations of simple mathematical approximations in the kinematic equations and the assumptions of infinitesimal deformation theory. In this case, consideration of the finite deformation/strain theory is necessary (*Biot, 1965; Fung, 1965; Shuku, 2009*). Infinitesimal deformation theory assumes that a body does not deform excessively under loading and therefore the deformation obtained using this theory would be geometrically linear. At low stress and strain levels, there is no coupling between shear and normal stresses. For small strains in homogeneous isotropic materials (*Gould, 1983; Sadd, 2009*)

$$\varepsilon_{ij} = \frac{1}{E}[(1+\nu)\,\sigma_{ij} - \nu\,\delta_{ij}\,\sigma_{kk}], \tag{2.2}$$

where ε_{ij} is the strain component, σ_{ij} is the stress component, E is the modulus of elasticity, ν is the Poisson's ratio, and δ_{ij} is the Kronecker delta. For example, consider a cylindrical tube specimen subjected to torsion shear. For small deformations it is expected that only shear strains will result in the specimen and the normal strain would be zero. However, at large deformations, the linear relation between deformation and strain does not hold any more and other higher terms are required (*Biot, 1965; Fung,*

1965; Sadd, 2009). In addition, large deformations and changes in geometry under torsion will result in the elongation of a circular specimen in the axial direction or the generation of an axial force if axial deformation is constrained. This is referred to as the Poynting effect in solids (*Poynting, 1909*). The normal force in a cylindrical tube with constrained ends subjected to torsion is (*Freudenthal and Ronay, 1966*)

$$N = -\frac{1}{4} G \pi \psi^2 (a^4 - b^4), \tag{2.3}$$

and the axial strain in the same geometry when the ends are allowed to move is (*Freudenthal and Ronay 1966*)

$$\varepsilon \approx \frac{1}{4} \frac{G}{E} \psi^2 (a^2 + b^2) = \frac{1}{12} \gamma (1 + \frac{b^2}{a^2}), \tag{2.4}$$

where N is the normal force, G is the shear modulus, E is the elastic modulus, ψ is the uniform angle of twist, a is the outer radius, and b is the inner radius.

2.3.3. Interaction Nonlinearity

In this type of nonlinearity, the material response changes depending on the state of stress within the material; i.e., the stress-strain response for a given mode of load such as shear varies due to the presence of other load components such as normal force. In other words, interaction nonlinearity is a way to incorporate the three dimensional effects. This phenomenon has been recognized in polymeric materials. For example, Lu and Knauss (*1999*) investigated interaction nonlinearity in Polymethyl Methacrylate (PMMA). They demonstrated that the shear compliance of PMMA depends on the state of stress. Figure 2.1 shows the influence of interaction nonlinearity for a neat polymer tested in simple torsion (shear), torsion with axial tension, and torsion with axial compression. As can be seen, the shear compliance in the presence of axial tension or compression is different from the shear compliance in the absence of these stresses, even though the applied shear stress was the same in all three cases. Lu and Knauss attributed

this interaction nonlinearity to the change in free volume in the polymer. Similar effects were noted by Popelar and Liechti (*1997; 2003*) for epoxy and urethane adhesives. The effect of shear was implemented in a modified free volume theory which has since been applied to epoxies that are used for bonding composite reinforcements to existing civil structures (*Park and Liechti, 2003; Park et al., 2004; Park et al., 2006*). Hygrothermal effects were incorporated into the theory in a natural and consistent manner.

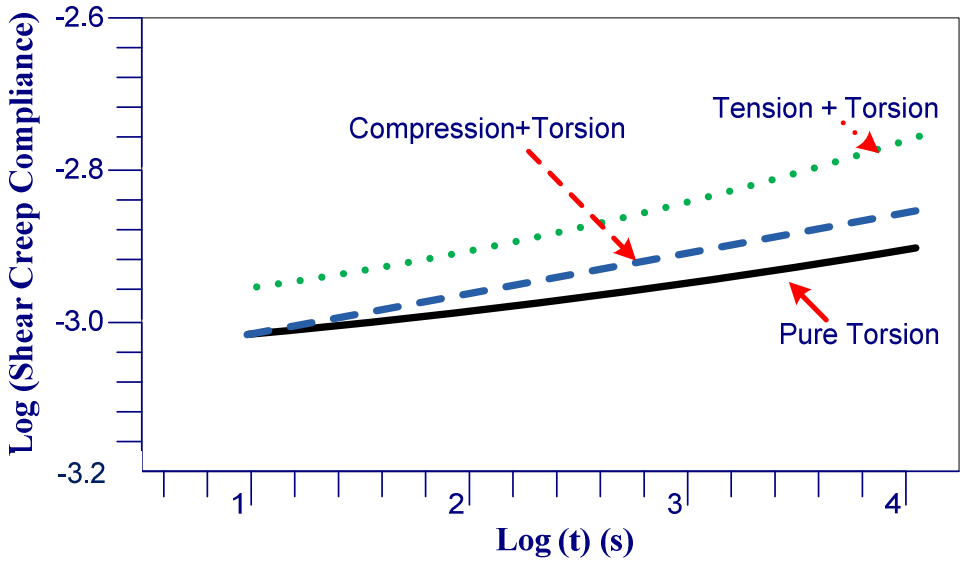

Figure 2.1: Shear creep compliance curves for pure torsion and torsion with superimposed tension or compression for PMMA. Change in creep compliance with multiaxial load illustrates interaction nonlinearity, Adapted form Lu and Knauss (*1999*).

2.3.4. Intermodal Nonlinearity

Intermodal nonlinearity is observed when there is more than one type of deformation mechanism acting simultaneously (*Brinson, 2008*). One example is the yielding and buckling in columns. This type of nonlinearity is unlikely to occur in asphalt binders or mixture.

While previous studies (*Airey et al., 2004; Delgadillo, 2008; Masad et al., 2008*) have used the DSR to demonstrate the nonlinearly viscoelastic response of asphalt binders, very little work has been done to fully explain the mechanisms that result in this response. Knowledge of these mechanisms is the first crucial step required to develop an accurate constitutive relationship for asphalt binders. In summary, there are several mechanisms that result in nonlinear stress-strain response of material. The following section presents the approach and findings from a systematic investigation into the sources of nonlinear response observed during the laboratory testing of asphalt binders.

2.4. PRELIMINARY INVESTIGATION

2.4.1. Materials and Test Method

Two modified binders were selected with different performance grades following the Superpave© specification: PG 82-22 and PG 76-22. The reason for selecting modified binders for this study was that the nonlinearity was more pronounced in modified binders. A DSR (Model TA AR2000Ex) was used to measure the mechanical response of the asphalt binders when subjected to different loading conditions. Two different test temperatures were used to investigate the influence of temperature on the nonlinear response of asphalt binders: 28^oC and 40^oC. These temperatures were well above the glass transition temperature, T_g, of asphalt binders; which range from -30^oC to -5^oC. The device is capable of measuring the axial force in the presence of an axial deformation constraint so that any geometrical nonlinearity could be addressed quantitatively. For the initial stage of this investigation, the effect of aging was not incorporated and all tests were conducted on un-aged binders.

2.4.2. Test Geometry

The selection of an appropriate test geometry for use with the DSR is critical to the investigation of the nonlinear response. There are two different geometric configurations that are typically used to test asphalt binders with a DSR at intermediate to high temperatures. The first and most common is the solid cylindrical specimen between two parallel plates with the top plate being subjected to torsion and the bottom plate being fixed. In this case, the shear strain rate $\dot{\gamma}$ at any point is

$$\dot{\gamma} = \frac{r \,.\, \Omega}{h}, \tag{2.5}$$

where r is the radial distance from the axis of rotation, h is the height of the specimen, and Ω is angular speed of the top plate. Since $\dot{\gamma}$ depends on the distance from the axis of rotation, the material will be subjected to different strain rates and stress levels at different radial positions within the specimen. As a result, in the case of a material that exhibits a nonlinear response, the measured response with the parallel plate geometry is an average of the non-uniform response across the cross section of the specimen unless a thin walled tube is used. In addition, the use of parallel plate has other disadvantages such as instability when the specimen is subjected to repeated creep and recovery at intermediate to high temperatures (*Motamed and Bahia, 2011*). Therefore, it is recommended that the parallel plate geometry not be used to determine the true material properties (*Carreau et al., 1997; Motamed and Bahia, 2011*).

The second configuration, although not as commonly used for asphalt binders, is the cone and plate geometry. The difference between the cone and plate geometry and the parallel plate geometry is that the former has a conical shaped top plate. This geometry ensures that the shear strain rate is approximately uniform throughout the specimen (*Carreau et al., 1997*):

$$\dot{\gamma} = \dot{\gamma}_{\theta\phi} = \frac{\sin\theta}{r}\left[\frac{\partial}{\partial\theta}\left(\frac{V_\phi}{\sin\theta}\right)\right] \approx -\frac{\Omega}{\theta_0}, \tag{2.6}$$

where θ_0 is the angle of the cone plate, r is the radial location of a point, θ is the angle in the vertical plane and ϕ is the angle in the horizontal plane following the spherical coordinate system (Figure 2.2). Since the cones that are used in DSR measurements are such that $\theta > 84^{\circ}$, $sin\ \theta$ is approximately equal to unity and the shear rate can be regarded as constant throughout the cross-section. Therefore, this geometry, which is more suitable for accurate measurement of material properties, was selected to characterize the behavior of the asphalt binders in this study. The parallel plate geometry was also subsequently used for limited verification of some of the findings. The diameters of both the cone and parallel plates were 25 mm. Two different cone plate angles were used in this study; one had a cone angle of 5° (5:45:03) and truncation gap of 146 μm, and the second one had a cone angle of 2° (2:17:42) and a truncation gap of 56 μm. A gap size of 1 mm was selected for testing with the parallel plate in accordance with the Strategic Highway Research Program (*SHRP*) specifications.

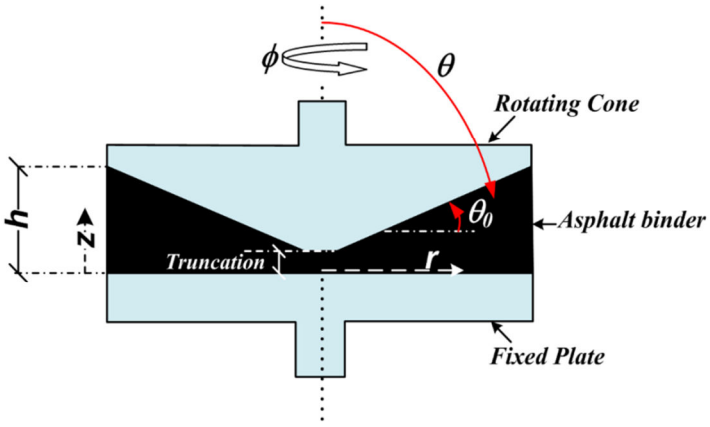

Figure 2.2: Cone and plate geometry.

2.4.3. Test Procedure and Data Collection

A stress sweep was conducted to determine the linearly viscoelastic limit of the asphalt binder. The frequency of oscillation was 0.1 Hz and 10 cycles were applied at each shear stress level. Our analytical simulation of oscillatory test showed that the transient effect will only last for almost 5 cycles. This was also verified by measuring the

material response in the laboratory. Therefore, applying 10 cycles of the oscillatory load is enough to overcome the initial transient effect. The rationale for selecting this low frequency was to enhance the time dependent response of the material. The stress amplitude was varied from 100 Pa to 48.1 kPa in eight equal steps. The minimum stress amplitude of 100 Pa was selected to ensure that the lowest stress was well within the linearly viscoelastic limit of the binder. Several researchers (*Delgadillo, 2008; Huang, 2008*) have reported that asphalt binders behave linearly at this stress level. The maximum stress amplitude was selected based on the maximum torque capacity of instrument. This stress amplitude was still below the maximum local stress experienced by the matrix part of asphalt mixture under typical traffic load levels (*Huang, 2004*).

An important consideration while running the stress sweep test was to record the normal force experienced by the plates. Figure 2.3 shows the results from the stress sweep test for the PG 82-22 at 40°C. Figure 2.3*a* illustrates both the applied shear stress as well as the average normal stress generated during the test. Figures 2.3*b* and 2.3*c* illustrate the reduction in dynamic shear modulus G^* with an increase in the stress amplitude indicating the onset of nonlinear response. This nonlinear response can be observed even at stress amplitudes that are as low as *7* kPa. G^*, which is the ratio of stress amplitude to strain amplitude under sinusoidal oscillatory loading, can be decomposed into its components, G' (storage modulus) and G'' (loss modulus) (*Brinson, 2008; Lakes, 2009*):

$$G' = G^*.\cos(\delta), \tag{2.7}$$

and

$$G'' = G^*.\sin(\delta), \tag{2.8}$$

where δ is the phase angle which is a measure of delay in response. In order to better represent this nonlinearity, G' and G'' are also shown in Figures 2.3*b* and 2.3*c*. Each test was done with three replicates with consistent results. Other binder-temperature combinations showed similar results.

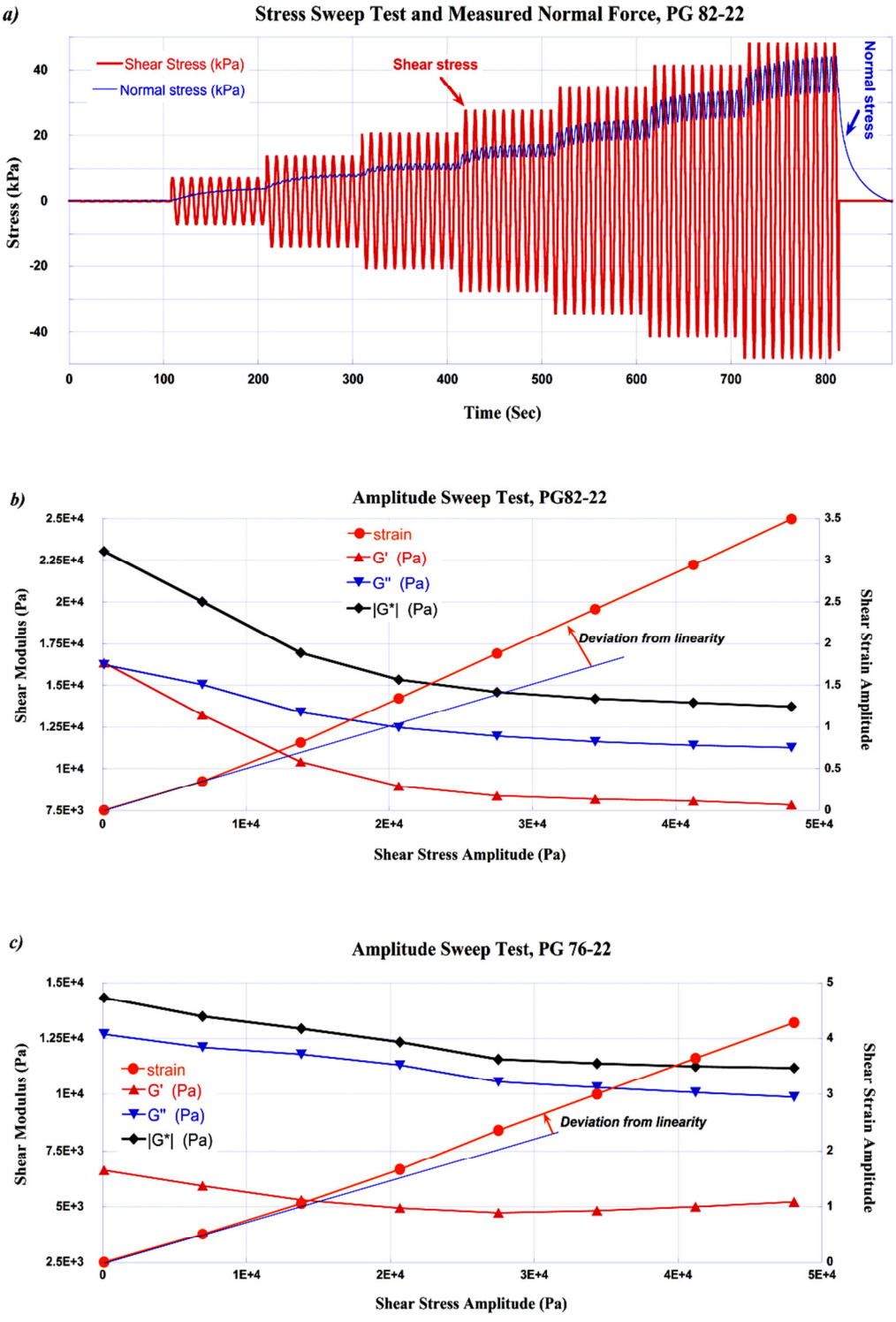

Figure 2.3: Stress amplitude sweep test using cone and plate geometry at 40°C.

The following observations can be made from these results. First, the results clearly show that torsion results in the generation of a normal force when the specimen is confined axially and the gap is not allowed to change. Second, the asphalt binder behaves nonlinearly, i.e., the complex modulus depends on the stress level.

In order to verify the tendency of the asphalt binder to deform axially, a shear stress sweep was conducted on the same material by allowing it to deform axially. The parallel plate geometry was required to conduct this test as it allows the adjustment of the gap size during the test in such a way that the net normal force is maintained at zero. A shear stress sweep was run on the same materials and the change in gap size was measured during the test. Figure 2.4 shows the change in shear complex modulus and specimen's height with shear stress level. As can be seen, having no axial constraint allows the specimen to expand or deform axially.

Similar to the case with constrained gap using cone and plate (Figure 2.3), the shear complex modulus decreased with increasing stress even in the absence of the normal force. This can easily be explained by considering the associated increase in free volume, which will cause the material to become softer and consequently result in a reduction of G^*.

The following two hypotheses are proposed based on the aforementioned observations:

(i) The normal force under constant gap develops either due to the Poynting effect or an increase in the free volume of the asphalt binder.

(ii) The asphalt binder exhibits an interaction nonlinearity, i.e., the complex stress state (normal stresses combined with the applied shear stress) is responsible for the deviation from the linearly viscoelastic response of the material.

The following two sections provide further analyses in support of these hypotheses.

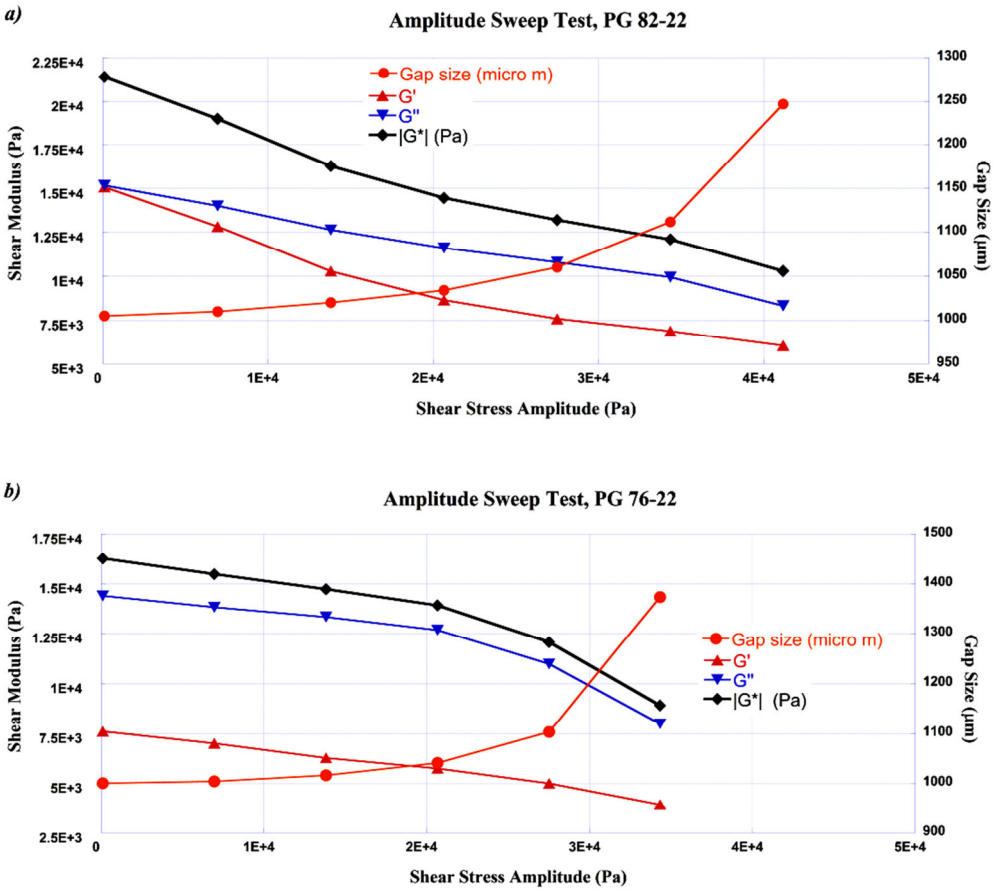

Figure 2.4: Stress sweep test using parallel plates geometry, no confinement, at 40°C.

2.5. Sources of Normal Force in a Specimen Subjected to Torsion

This section investigates the source of the normal force under simple torsion. The emergence of the normal force under simple shear can be due to the Poynting effect (geometric nonlinearity) or dilatation of asphalt binder (increase in free volume). To examine the contribution of large deformations or geometric nonlinearity, the test specimen was modeled (Figure 2.5) using commercially available finite element software, ABAQUS.

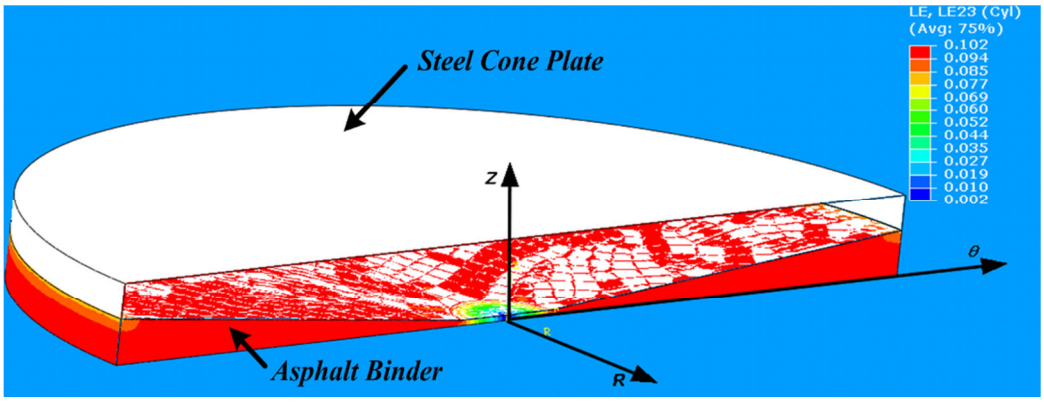

Figure 2.5: The cross section of cone and plate FE model, in cylindrical coordinate.

A creep test was conducted at a shear stress level of 100 Pa at 40°C, using the DSR to obtain the linearly viscoelastic properties of each asphalt binder. The measured creep compliance followed a power law very closely. Accordingly, the following power-law based interrelationship was used to obtain the shear relaxation modulus from the measured creep compliance (*Leaderman, 1958*):

$$G(t)\ J(t) = \frac{\sin(n\pi)}{n\pi}, \tag{2.9}$$

where *J(t)* is the shear creep compliance, *G(t)* is the shear relaxation modulus, and *n* is the exponent in the power law. Finally, the shear relaxation modulus from Equation 2.9 was fitted to obtain the Prony series constants that were used to describe the material response in the ABAQUS software (*ABAQUS Manual, 2007*):

$$\frac{G(t)}{G_0} = 1 - \sum_{i=1}^{N} \bar{g}_i^P (1 - e^{-\frac{t}{\tau_i}}), \tag{2.10}$$

where *G(t)* is the shear relaxation modulus, G_0 is the instantaneous modulus, and $\bar{g}_i^P$ - and τ_i - are the relative moduli and time constants, respectively. Figure 2.6 displays the measured data and all these fits to it and the derived shear modulus for the asphalt binder with performance grade PG of 82-22.

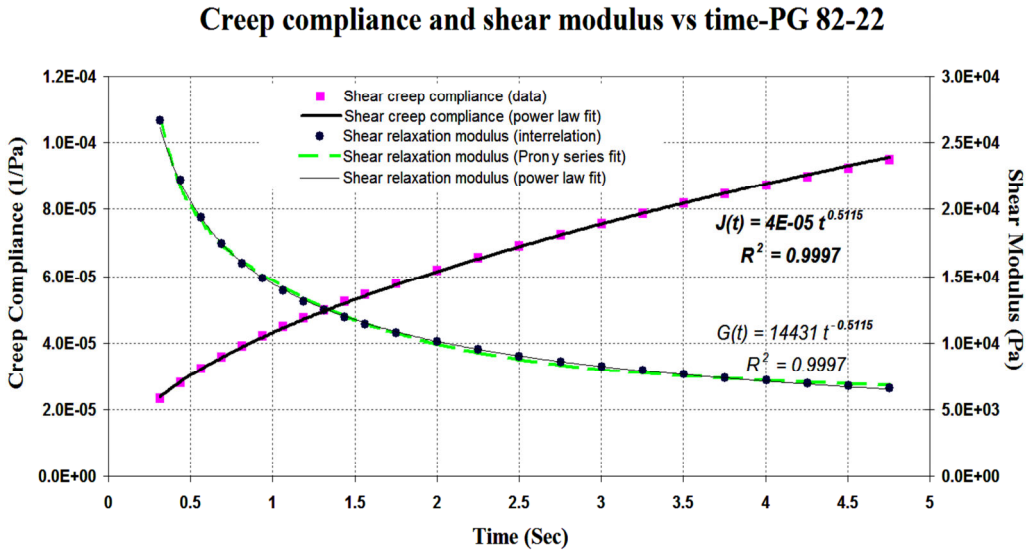

Figure 2.6: Creep test result and demonstration of power-law based interrelation.

After modeling the geometry in ABAQUS and assigning the material properties given above, the FE model was verified by simulating a few creep tests at stress levels other than the one that was used to obtain the model constants. Figure 2.7 illustrates that the FE simulation results are in good agreement with laboratory test data obtained at 1 kPa and 40°C. The amount of normal force developed during the creep was negligible and therefore no interaction nonlinearity was observed.

Finally, to examine the potential contribution of the Poynting effect to the normal force measured during the stress sweep test (Figure 2.3*a*), the test was computationally simulated at different stress amplitudes. At a very low stress amplitude of 0.1 kPa, the strain amplitude and G^* from the FE simulation matched the measured data very well. By increasing the stress amplitude the material response from the simulation remains linear because of the assumption of linearly viscoelasticity in the simulation (G^* is constant at all stress amplitudes) whereas the G^* measured in the laboratory reduced with an increase in the stress amplitude. Consequently, at higher stress amplitudes the shear strain measured in the lab was greater than the shear strain predicted from the FE simulation. For example, at a stress amplitude of 6.9 kPa, the measured G^* was reduced by almost 13 percent (Figure 2.3*b*). In order to compare the measured normal force to the predicted normal force from the FE simulation (which is derived from Poynting effect), the shear

stress in the simulation was adjusted such that the resulting shear strain amplitude matched the measured shear strain amplitude. In other words, the normal force due to the Poynting effect from the simulation was compared to the measured normal force at the same strain amplitude. Figure 2.8 illustrates this comparison at a strain amplitude of 34 percent for PG 82-22 at 40°C.

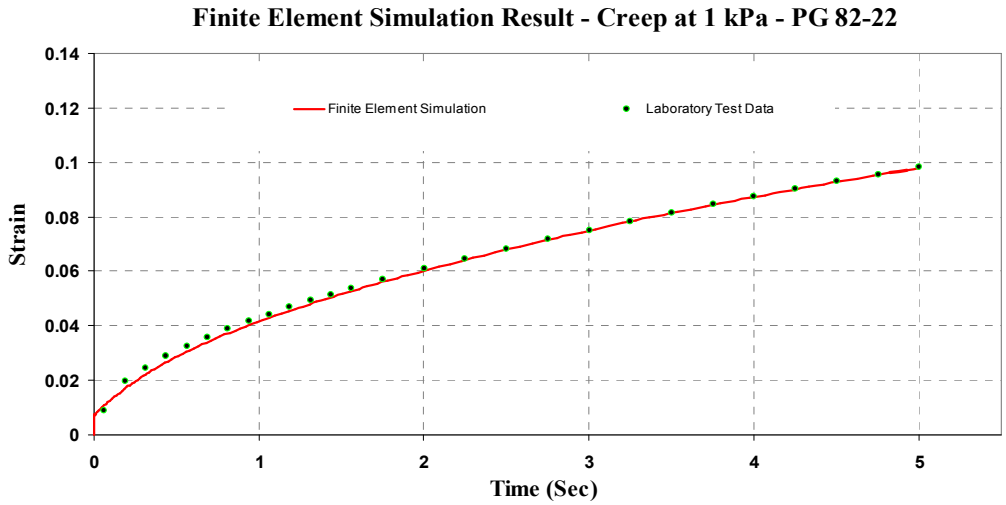

Figure 2.7: Verification of FE model using creep laboratory test data at 1kPa and 40°C.

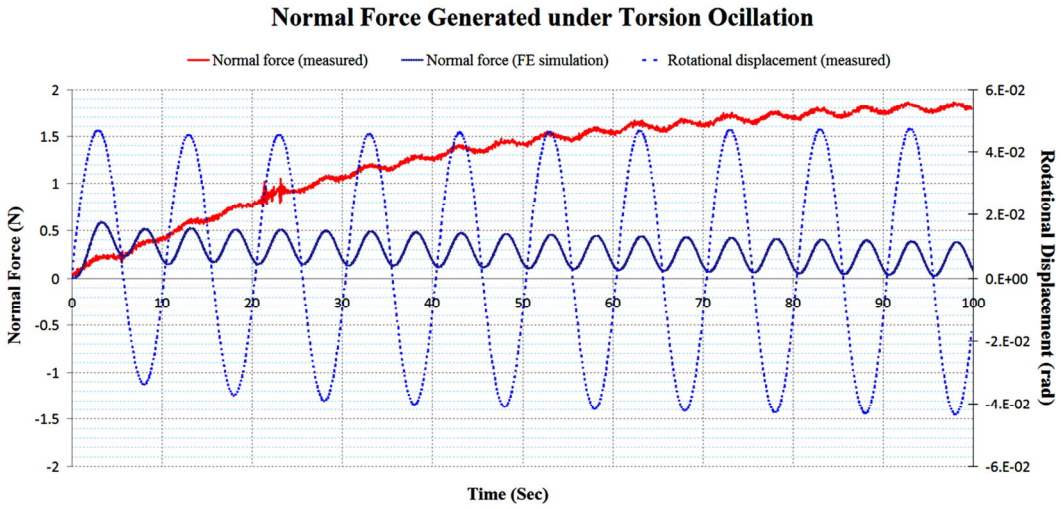

Figure 2.8: Normal force measured and calculated using simulation, at strain amplitude of 34 percent.

As can be seen, once the applied strain reached steady state (due to some start-up transient effects in the viscoelastic material and instrument), only a fraction of the total generated normal force can be explained by the Poynting effect or geometric nonlinearity of the specimen under torsional loading. Therefore, it is speculated that the residual normal force is due to dilatation and change in free volume of the asphalt binder. In the field of polymers, the concept of free volume and dilatation due to the application of axial forces was investigated by Knauss and Emri (*1981*). Popelar and Liechti (*2003*) extended this concept by including the dilatation and change in free volume of polymers subjected to shear forces. In the field of asphalt, the concept of free volume has been used to explain phenomena such as the deformation of pure binder at temperatures above glassy transition (*Cheung and Cebon, 1997*).

The contribution of the Poynting effect or geometric distortion nonlinearity to the generation of normal force increases at higher strain amplitudes. It is also noteworthy that laboratory data show that the normal force increases in the first few cycles and reaches an asymptotic value while in simulation the normal force relaxes very slowly as the numbers of cycle progress. The reduction in the simulated normal force may be due to the assumption of a time independent or constant Poisson's ratio; therefore, the change in bulk modulus occurs at the same rate as shear modulus, which may not be realistic. This assumption will be further investigated in Chapter 4.

2.6. SOURCE OF NONLINEARITY

This section investigates the nature of nonlinearly viscoelastic response of the asphalt binder. First, laboratory tests were conducted to validate the hypothesis of an interaction nonlinearity in asphalt binders. Subsequently, a systematic investigation was carried out to eliminate other potential sources of nonlinear response and further verify the hypothesis of interaction nonlinearity.

2.6.1. Interaction Nonlinearity

The following tests were conducted using the cone and plate geometry to verify the hypothesis that the interaction of normal and shear stresses was the source of the nonlinear response. A series of time sweep tests at different stress amplitudes with rest periods in between were conducted. The time sweeps were conducted at five different stress amplitudes on the same specimen, using cone and plate geometry. The shear stress amplitudes were 0.1 kPa, 5 kPa, 10 kPa, 20 kPa, and 40 kPa. The test frequency was kept the same as before; 0.1 Hz. The time sweep at each stress amplitude consisted of 10 cycles and the shear complex modulus was measured at the end of each cycle. A two-minute rest period was introduced between each time sweep to allow the normal force developed in the previous time sweep to relax (although in retrospect it was discovered that complete relaxation was not achieved during the two-minute rest period following the application of high stress amplitudes). Time sweeps at each stress amplitude were repeated twice before proceeding to the next stress level. Results from the second repeat were compared to the first repeat to detect any permanent change or damage to the material during the loading period.

Figure 2.9 shows the test results for the above test procedure including the change in normal force as the cycles progress, at 40°C. The ten sets of data correspond to the time sweep at the five stress amplitudes repeated twice with each time sweep separated by two minutes of rest period. The data indicate that at low stress levels the normal force is negligible and the complex modulus remains constant. At higher stress levels, in the first few cycles where there is only a small amount of normal force, the complex modulus is the same as the complex modulus at low stress levels. However, after a few cycles as the normal force increases the complex shear modulus decreases. Furthermore, at each stress level the results from the two repeats are identical indicating very little or no permanent change or damage to the material. A comparison of the evolution of normal stress and decrease in G^* from Figure 2.9 clearly illustrates the strong correlation and interaction between the normal force and complex shear modulus.

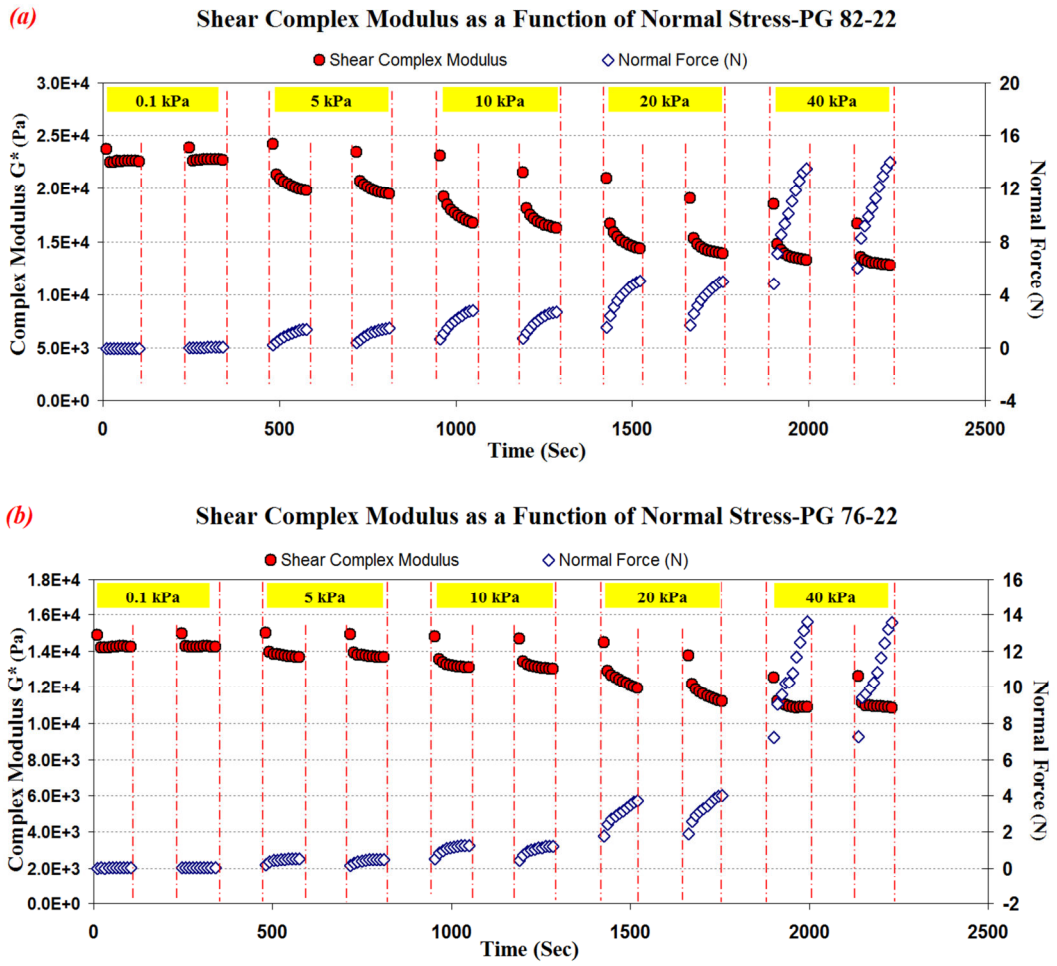

Figure 2.9: Time sweep tests at different stress levels and 40°C; with two repeat at each stress level to detect any damage, with two minutes rest period between each time sweep.

Similar phenomena were also observed at the lower temperature of 28°C. By decreasing the temperature, the time required for normal force to relax increases. Consequently, a residual normal force was observed even after the two-minute relaxation period.

In the following subsections, other sources that can possibly result in the nonlinear response of asphalt binders are investigated. More specifically, (*i*) the possibility of damage and intrinsic material nonlinearity was investigated by conducting

creep and recovery at different stress levels, (*ii*) the effect of loading history on nonlinear response was examined using the concept of multiple integrals, and finally (*iii*) the possibility of self-heating in asphalt binder and material softening was investigated experimentally.

2.6.2. Intrinsic Nonlinearity and Damage

Creep and recovery tests at different stress levels were conducted to determine the nature of nonlinear response of the asphalt binder. The creep part of the test was five seconds long. This loading time was long enough to collect the time dependent response of material for the time window of interest. The selected loading time was much greater than the rise time of the instrument, which is on the order of 10^{-4} second. This ensured the accuracy of the measured data. On the other hand, the loading time was not too long to risk damage to the material and cause tertiary flow. In this context, tertiary flow refers to the accelerated unstable creep that is preceded by steady-state creep, due to the change in material or creation of microcracks and cavities (*Lakes, 2009*). Research performed by Delgadillo (*2008*) showed that tertiary flow mainly happens after almost 10 seconds at high stress levels (such as 30 kPa) and temperatures (such as 46°C), Figure 2.10.

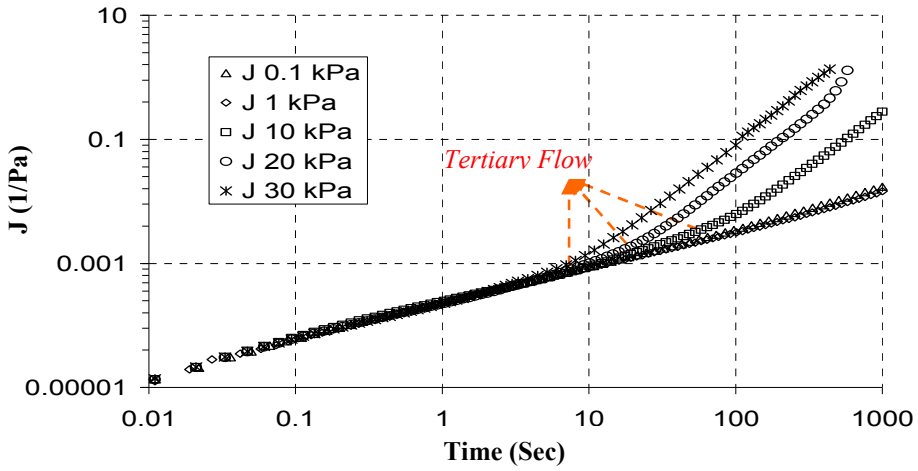

Figure 2.10: Tertiary flow in asphalt binder with PG 64-34 at 46°C and high stress levels. Creep compliance changes after 10 seconds of creep (*Delgadillo, 2008*).

The recovery time was considered long enough to achieve significant recovery; 1000 seconds. The stress level ranged from a low stress of 0.1 kPa to a high stress of 40 kPa (close the highest possible stress that instrument could apply). Six different stress levels were selected to obtain the material response: 0.1kPa, 1kPa, 5kPa, 10kPa, 20kPa, and 40kPa. As was the case of time sweeps in section 2.6.1, creep and recovery at each stress level were repeated twice before proceeding to the next stress. Results from the second repeat were compared to the first repeat in order to detect any permanent change or damage to the material during the loading period (Figure 2.11).

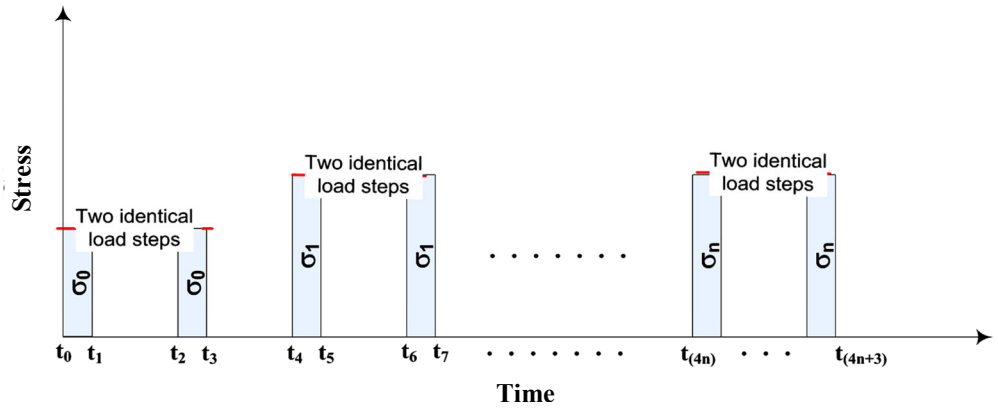

Figure 2.11: Schematic of creep and recovery test protocol.

An identical response under same loading condition would be an indication that no damage or permanent change in the material has occurred. Figure 2.12 shows the creep and recovery result for asphalt binder PG 82-22 at 40°C and different stress levels.

Creep and recovery test results show that asphalt binders behave as a linearly viscoelastic material and no damage occurs at stress levels below 40 kPa. Also, the normal force generated during these tests was minimal. Similar results obtained for asphalt binder PG 76-22, which are not presented for brevity reasons. This is in agreement with Delgadillo's experiment (in Figure 2.10, creep compliances measured at different stress levels are the same before occurrence of tertiary flow). These results

demonstrate that intrinsic material nonlinearity and damage are not contributing to the decrease in dynamic modulus observed during cyclic loading. Consequently, this analysis further corroborates the hypothesized interaction nonlinearity.

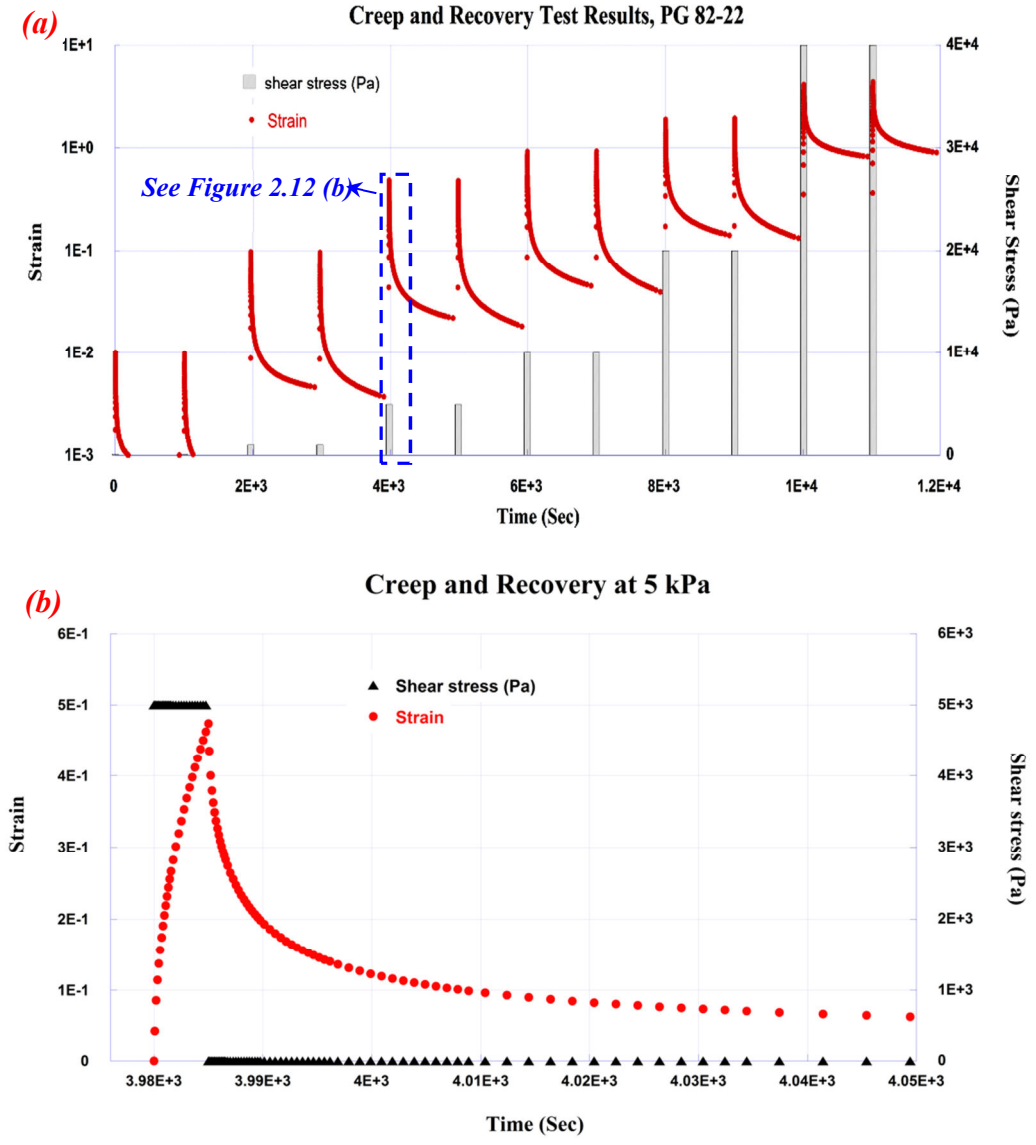

Figure 2.12: Creep and recovery test results at 40°C and different stress levels, PG 82-22.

2.6.3. Nonlinearity due to Loading History

Another potential source of nonlinear response is the influence of loading history. The linear response of a material from independent creep tests at different stress levels is a required but not sufficient condition for the material to be intrinsically linear. In other words, a material subjected to a series of creep (or dynamic) loads at low stress levels could still exhibit a nonlinear response due to the stress history. Further details on this type of nonlinear response can be found in Findley et al. (*1976*).

The effect of loading history on asphalt binder behavior was examined using the multiple integrals method. The multiple integrals method was first developed by Volterra and Frechet and later on, Rivlin and Green generalized it to three dimensions (*Findley, 1976*). They derived the multiple integrals equation using the principles of continuum mechanics. Findley (*1976*) used another approach that extends the linear superposition to the nonlinear range and considers interactions between loading steps to arrive at an identical model (shown here using three terms):

$$\begin{aligned}\varepsilon(t) = &\int_0^t \varphi_1(t-\tau_1)\frac{\partial\sigma(\tau_1)}{\partial\tau_1}d\tau_1 \\ &+\int_0^t\int_0^t \varphi_2(t-\tau_1,t-\tau_2)\frac{\partial\sigma(\tau_1)}{\partial\tau_1}\frac{\partial\sigma(\tau_2)}{\partial\tau_2}d\tau_1\,d\tau_2 \\ &+\int_0^t\int_0^t\int_0^t \varphi_3(t-\tau_1,t-\tau_2,t-\tau_3)\frac{\partial\sigma(\tau_1)}{\partial\tau_1}\frac{\partial\sigma(\tau_2)}{\partial\tau_2}\frac{\partial\sigma(\tau_3)}{\partial\tau_3}d\tau_1\,d\tau_2\,d\tau_3\,,\end{aligned} \tag{2.11}$$

where t is the time of interest, the τ_i are the time variables of integration, and φ_i are the time-dependent material functions. Multiple integrals can be considered as an extension of linear superposition that includes the interaction terms to account for the nonlinear response. Multistep creep and recovery tests are typically used to determine the time dependent kernels for a material. These tests should include different stress levels as well as different loading time intervals. The tediousness of procedure demands some type of simplifications to make the model practical (*Findley, 1976*). However an advantage of the

model is that it is comprehensive and flexible so that it can be applied to a broad range of nonlinear systems besides nonlinearly viscoelastic systems (*Schetzen, 1980*).

To examine the effect of loading history, a multistep loading was considered for which the Equation 2.11 can be rewritten as (for N load steps)

$$\begin{aligned}\varepsilon(t) &= \sum_{i=0}^{N}(\Delta\sigma_i)\varphi_1(t-t_i) \\ &+ \sum_{i=0}^{N}\sum_{j=0}^{N}(\Delta\sigma_i)(\Delta\sigma_j)\varphi_2(t-t_i,t-t_j) \\ &+ \sum_{i=0}^{N}\sum_{j=0}^{N}\sum_{k=0}^{N}(\Delta\sigma_i)(\Delta\sigma_j)(\Delta\sigma_k)\varphi_3(t-t_i,t-t_j,t-t_k).\end{aligned} \tag{2.12}$$

In the case of two-step loading ($\Delta\sigma_0$ at t_0 and $\Delta\sigma_1$ at t_1) the response (strain) for the time after t_1 will not only include the summation of the two responses from each step but also all possible cross products to account for nonlinearity. The higher order material functions, φ_2 and φ_3 , have two and three time dependent parameters, respectively, to accommodate the second and third order interactions between stress increments. For two-step loading, Equation 2.12 reduces to the following form:

$$\begin{aligned}\varepsilon(t) &= \left[(\Delta\sigma_0)\,\phi_1(t)+(\Delta\sigma_0)^2\phi_2(t,t)+(\Delta\sigma_0)^3\phi_3(t,t,t)\right] \\ &+ \left[(\Delta\sigma_1)\,\phi_1(t-t_1)+(\Delta\sigma_0)^2\phi_2(t-t_1,t-t_1)+(\Delta\sigma_0)^3\phi_3(t-t_1,t-t_1,t-t_1)\right] \\ &+ \left[2(\Delta\sigma_0)(\Delta\sigma_1)\phi_2(t,t-t_1)+3(\Delta\sigma_0)^2(\Delta\sigma_1)\phi_3(t,t,t-t_1)\right. \\ &+ \left.3(\Delta\sigma_0)(\Delta\sigma_1)^2\phi_3(t,t-t_1,t-t_1)\right].\end{aligned} \tag{2.13}$$

For an intrinsically linear material, the functions φ_2 and φ_3 reduce to zero for all time arguments, thus reducing Equations 2.11 and 2.12 to the familiar form of the Boltzmann superposition principle. Intrinsic nonlinearity of the material is accommodated by time functions with similar time arguments, e.g., $\varphi_2(t, t)$. Nonlinearity due to stress history is accommodated by time functions with dissimilar time arguments, e.g., $\varphi_2(t, t-t_1)$. The nonlinearity due to stress history reflects the influence of residual strain or stored energy on material behavior. Special cases arise when time functions with similar time

arguments (such as $\varphi_2(t, t)$ and $\varphi_3(t-t_1, t-t_1, t-t_1)$) are zero but non-zero for dissimilar time arguments (such as $\varphi_2(t, t-t_1)$). In these cases, the material does not exhibit intrinsic nonlinearity but exhibits history dependent nonlinearity. In other words, one can expect a linear response when comparing strains from independent creep tests with stresses $\Delta\sigma_0$ and $\Delta\sigma_0+\Delta\sigma_1$ and a nonlinear response when the two-step loading (or any arbitrary stress history) is applied. This is further illustrated in Figure 2.13; the residual strain at the end of step one directly affects the response in the second and third step. This is what is referred to as second order interactions for dissimilar time arguments and shown by solid arrows. This residual strain which directly affect the response in the second and third steps, will also affect the third step indirectly through its effect on the second step. In other word, the first step affect the second step and the response of the second step which is already affected by first step will affect the third step. This is what is referred to as third order interaction and shown by dashed arrows. Further details on this type of nonlinearity can be found in Findley (*1976*).

For a material that exhibits history dependent nonlinearity, the recovery part of a creep-recovery test cannot be predicted using the Boltzmann superposition principle with the creep data. Similarly, the creep response from a multi-step test cannot be predicted using the Boltzmann superposition principle with the creep data from the first step. These two approaches were used to investigate whether asphalt binders exhibit history dependent nonlinearity. First, a power law equation was fitted to the creep data, then the recovery response was predicted using Boltzmann superposition and compared with the measured recovery (Figure 2.14). As can be observed, the prediction is in good accord with the experiment showing the absence of cross interaction or history dependence for this material.

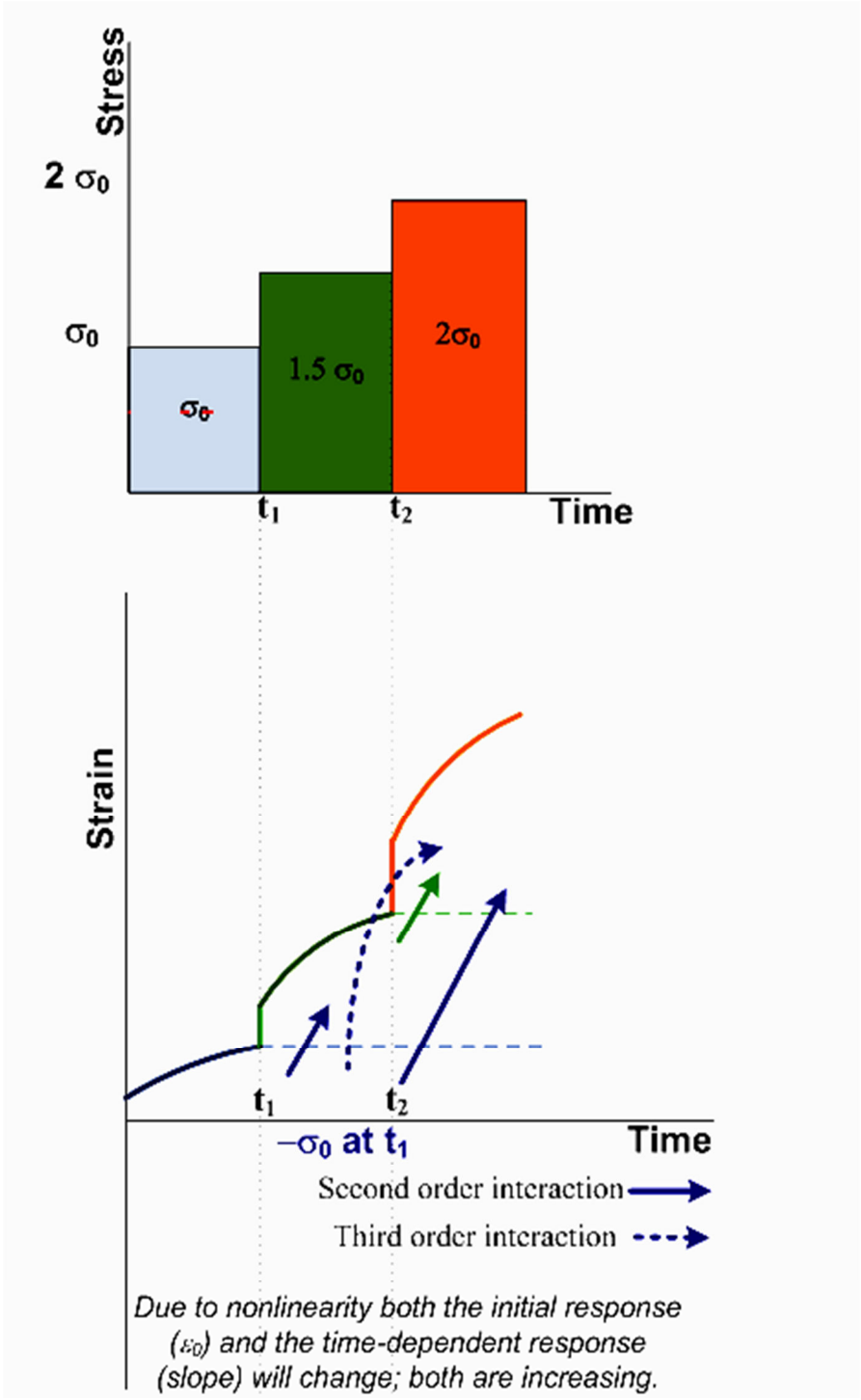

Figure 2.13: Three step loading. Demonstration of cross interaction of loading steps in multiple integrals method.

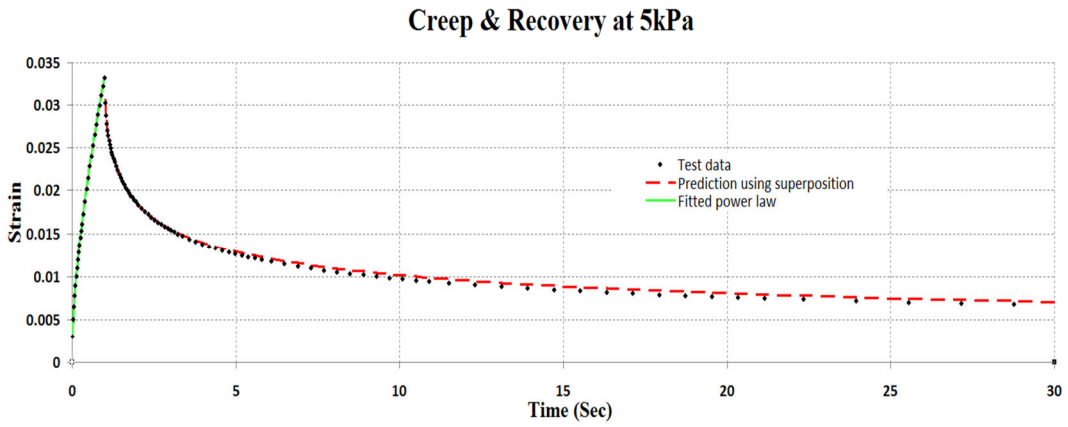

Figure 2.14: Creep and recovery test result on PG76-22 at 5kPa stress level and 28°C, 1 second creep and 300 seconds recovery.

To further investigate the existence (or absence) of cross interaction between load steps in loading history, a two-step creep loading with different load increments was applied. The magnitude of normal force and therefore the interaction nonlinearity during the two-step creep was not significant. First a power law equation was fitted to the first step of creep data, then the Boltzmann superposition was used to predict the material response under two step creep, Figure 2.15.

Figure 2.15: Two step creep loading on PG 82-22 at 40°C.

As can be seen, the prediction is in good agreement with the experimental data. This further corroborates the lack of cross interaction or history dependence between loading steps. Consequently, it was concluded that the loading history did not contribute to the nonlinearity or reduction in G^* observed during the amplitude sweep tests.

2.6.4. Self / Hysteretic Heating

The dissipation of energy and liberation of heat is one of most important issues in cyclic loading. This phenomenon is known as self / hysteretic heating. The reason for this heat generation is the viscous nature of the material (*Riddell et al., 1966*). A phase difference between the stress and strain creates the hysteresis loop over any complete cycle. Part of this energy will cause changes in the material and the rest will be released as heat (*Haward, 1994*). Dissipative heating can cause changes in temperature. In some materials, this change in temperature can lead to softening or an overall change in mechanical behavior. Hysteretic heating has been well studied for metals (*Taylor and Quinney, 1934*) and solid polymers (*Tormey and Britton, 1963; Schapery, 1965; Molinari and Germain, 1996; Rittel, 2000; Dinzart et al., 2008*).

Considering the fact that the stiffness of asphalt binders is sensitive to changes in temperature, it was speculated that the observed decrease in G^* during cyclic loading might be partially due to self-heating and the softening associated with the increase in temperature.

To consider this possibility, a thermocouple was placed inside the asphalt binder specimen to monitor the specimen temperature during the test (Figure 2.16). It was observed that the temperature remains almost constant (within +/-0.1°C, the precision level of thermocouple) in the bulk of specimen during the cyclic test. Thus it was concluded that self-heating did not contribute to the observed reduction of G^* during amplitude sweep test.

The small ratio of specimen volume to its surface boundaries can explain why the temperature was observed to be constant during the test. Having a large boundary

maintained at a constant temperature allowed efficient transmission of heat from within the specimen to the surface and did not allow the bulk of specimen temperature to increase. Therefore, despite the generation of hysteretic heat, the specimen temperature remained unchanged.

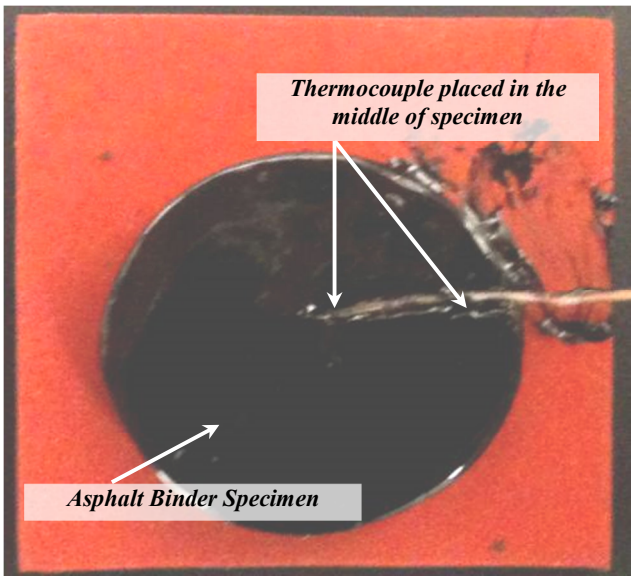

Figure 2.16: Placing thermocouple inside the DSR specimen to record the change in temperature during the test.

2.7. DISCUSSION AND CONCLUSION

The literature shows that localized stress concentrations in an asphalt mixture can result in very high and complex stress/strain states in asphalt binder. Therefore it is important to develop a comprehensive constitutive model for asphalt binder that is capable of reflecting the true response of the material under these stress states.

This study evaluated the response of two asphalt binders subjected to a range of cyclic stress levels using a Dynamic Shear Rheometer (DSR). The results demonstrate that asphalt binder specimens subjected to cyclic shear loads with stress amplitudes of 5 kPa and above, while axially constrained, experience the generation of a compressive

axial force that changes the state of stress within specimen. The contribution of excessive geometric distortion to the generation of normal force was examined using finite element simulation. FE simulation revealed that the normal force generated under pure torsion can only be partially attributed to geometric distortion or the Poynting effect. The change in free volume and tendency of the specimen to axially dilate must be considered to fully explain the normal force that was observed in the laboratory tests.

It was also observed that asphalt binder subjected to cyclic loads over a range of stress amplitudes exhibits nonlinear behavior even at stress amplitudes as low as 5 kPa. This observation was consistent with the findings from other research studies. However, the decrease in dynamic modulus observed during a stress sweep test is commonly attributed to intrinsic nonlinearity of the material or damage. A systematic study was conducted to investigate the nature of nonlinear response in asphalt binders. The results from this study demonstrate that the nonlinear response of asphalt binders observed using measurements with the DSR can be explained by considering the interaction between normal stresses and applied shear stresses, referred to here as an interaction nonlinearity or three dimensional effects. Softening due to hysteretic heating or stress history dependence did not contribute significantly to the observed nonlinear response.

In summary, asphalt binders experience a change in free volume or dilatation when subjected to shear stresses, which in turn leads to an interaction nonlinearity. In other words, the response of the asphalt binder to shear stresses also depends on the magnitude of axial stress. Given the fact that asphalt binders are used as the matrix in asphalt mixture composites that experience a variety of stress states due to traffic loads, an appropriate constitutive model for asphalt binders must be capable of accommodating interaction nonlinearity. One such model is the Schapery's nonlinearly viscoelastic model that is calibrated against the octahedral shear stresses to account for the stress state within the material. The detailed development, calibration, and validation of this model is presented in the following chapter.

Chapter 3: Constitutive Modeling of the Nonlinearly Viscoelastic Response of Asphalt Binders in Shear[1]

3.1. OVERVIEW

A Dynamic Shear Rheometer (DSR) is again used to characterize the nonlinearly viscoelastic properties of asphalt binders in shear at intermediate or high temperatures. In Chapter 2, the DSR test results showed that under certain conditions a compressive normal force was generated in an axially constrained specimen subjected to cyclic torque histories. This normal force could not be solely attributed to the Poynting effect and was also related to the tendency of the asphalt binder to dilate when subjected to shear loads. The generated normal force changed the state of stress and interacted with the shear behavior of asphalt binder. This effect was considered to be an "interaction nonlinearity" or "three dimensional effect". This concept is explored further in this chapter by developing a fundamental approach to modeling the observed behavior. In this approach, the octahedral shear stress is used to represent the three dimensional stress state in Schapery's model of nonlinearly viscoelastic behavior. The model was successfully validated for several different loading histories. These results highlight the importance of modeling the mechanical behavior of asphalt binders based on the three dimensional stress state of the material.

1- A significant portion of this chapter has been published in the Journal of Mechanics of Time Dependent Materials; Motamed, A., Bhasin, A., Liechti, K.M.: Constitutive modeling of the nonlinear viscoelastic response in asphalt binders; incorporating three dimensional effects. *J. Mech. Time-Depend. Mater.,* (2012*b*) DOI: 10.1007/s11043-012-9178-9

3.2. INTRODUCTION AND MOTIVATION

Hot Mix Asphalt (HMA) is a composite that comprises mineral aggregate, asphalt binder, and air. Computational methods are frequently used to model the mechanical response of an asphalt composite based on the properties of its constituent materials. These methods are also used in a micromechanics framework to characterize damage evolution in the composite. The accuracy of such results is contingent upon the accuracy of the constitutive relationship used to describe the materials behavior in the composite. The mechanical properties of the asphalt binder (the matrix or continuous phase) are time and temperature dependent. Asphalt binder also has a significantly lower stiffness compared to the aggregate particles (inclusions). The properties of the asphalt binder have a significant influence on the overall mechanical response of the asphalt mixture composite (*Di Benedetto et al., 2004, Delgadillo, 2008*). Therefore, an accurate constitutive relationship for the asphalt binder is crucial to ensure accurate predictions of the mixture behavior.

Computational methods to model the micromechanics of asphalt mixtures typically use linear viscoelasticity to characterize the asphalt binder or the continuous phase (*You and Dai, 2007*). Furthermore, dynamic shear rheometers (DSR) are typically used to measure the viscoelastic properties of the asphalt binder. Test data from the DSR are typically fitted to linearly viscoelastic constitutive models such as the Christensen–Anderson–Marasteanu (CAM) model (*Marasteanu and Anderson, 1999*), Burger's four-element model, power law, or Prony series. However, several research studies indicated that asphalt binders behave in a nonlinear manner, except under very small stresses and strains (*Anderson et al., 1994; Bahia et al., 2001; Airey et al., 2004; Kim and Little, 2004; Delgadillo, 2008*).

Airey et al. (*2004*) investigated the rheological behavior of bituminous paving materials to determine the linearly viscoelastic region within which the stress-strain relationship is independent of the magnitude of stress or strain. They demonstrated that for mixtures, the linear viscoelastic limit for strain applied to the mixture was on the order of 0.01% while this limit for asphalt binder was at least 100 times greater (1%

strain). This raises a very pertinent question as to whether the asphalt binder experiences stresses that exceed its linear viscoelastic limit, in mixtures subjected to typical service loads.

Several studies have examined the range of stresses experienced by the asphalt binder within an asphalt mixture using finite element analysis (*Kose, 2001; Lakes et al., 2002*). Kose (*2001*) demonstrated that the local strain in binder was 8 to 510 times higher than the far field strain applied to the mixture. Other studies corroborated these findings (*Masad et al., 2001; Drakos et al., 2001*). It can be deduced from these studies that asphalt binders will experience a nonlinearly viscoelastic behavior when used in mixtures and subjected to typical service loads. Therefore, developing a constitutive model that accurately describes the behavior of the binder at high levels of stress and strain is necessary to accurately predict mixture performance.

To this end, this research investigated the nature of nonlinear behavior of asphalt binders under torsion (Chapter 2). Test results demonstrated that, under certain test conditions, the application of cyclic shear loads resulted in the development of normal forces with a concomitant reduction in the dynamic shear modulus. This observation was confirmed in subsequent finite element analyses of the test and was referred to as an "interaction nonlinearity" or three dimensional effect. This chapter extends the study of interaction nonlinearity by modeling this phenomenon. In this approach the octahedral shear stress is used to represent the three dimensional stress state in material. Schapery's nonlinearly viscoelastic constitutive equation (*1969*) was then adopted and its parameters were obtained as a function of the octahedral shear stress. The model was validated by comparing the solutions from modeling with the results from tests under several different loading histories.

Section 3.3 of this chapter presents a brief review of models that are currently used to describe the nonlinear behavior of asphaltic materials. This is followed in Section 3.4 by a review of other nonlinear models for viscoelastic materials in general and the justification for the most appropriate model for asphalt binders. Section 3.5 presents details regarding the experimental procedures. Finally, a methodology is presented in

Sections 3.6 for obtaining the model parameters along with a validation of the proposed model. The model predictions were in good agreement with the measured laboratory test data. The findings from this study highlight the importance of modeling the mechanical behavior of asphalt binders based on the overall stress state of the material.

3.3. BACKGROUND

3.3.1. Current Models of the Nonlinearly Viscoelastic Response of Asphaltic Materials

Most of the literature on modeling the nonlinear behavior of asphaltic materials is limited to modeling the nonlinear behavior due to plastic flow and damage. Lai and Anderson (*1973*) developed a model in which the hot mix asphalt deformation was separated into two parts, nonlinear viscous (irrecoverable) strain ε^V and nonlinear viscoelastic (recoverable) strain ε^{VE}:

$$\varepsilon(t) = \varepsilon^V + \varepsilon^{VE} = \int_0^t \dot{\varepsilon}^V(\xi)\, d\xi + \int_0^t (t-\xi)^n \left[C_1 + C_2\, \sigma(\xi)\right] \dot{\sigma}(\xi)\, d\xi, \tag{3.1}$$

where t is the time of interest; $\varepsilon(t)$ is the total strain as a function of time; $\sigma(\xi)$ is the stress history; and C_1, C_2, and n are material constants. In this model, a strain hardening principle was used to describe the rate of viscous strain and a modified superposition principle was applied to describe the nonlinearly viscoelastic response. Lai and Anderson (*1973*) used this model to represent the behavior of hot mix asphalt under compressive stress and obtained the materials constants by performing multiple creep and recovery tests on hot mix asphalt specimens. Although the model had a mechanical basis and showed promising results, the objective of the study was not to make a connection between hot mix asphalt performance and its constituent properties. In other words, Lai and Anderson's macro-scale model could only predict the response for tested mixtures and was not suitable for implementation in micromechanics models.

In an attempt to correlate asphalt binder properties and hot mix asphalt performance, Reinke et al. (*2006*) investigated the effect of stress level on the behavior of

asphalt binders and performance of asphalt mixtures. They introduced the concept of stress viscosity factor S_V:

$$S_V = \eta^* \times \tau_{0.7\eta^*}, \tag{3.2}$$

where η^* is the complex viscosity of the binder in the linearly viscoelastic region, and $\tau_{0.7\eta^*}$ is the stress level at which η^* decreases to 70 percent of its initial value. They used an empirical approach and found a good correlation between the stress viscosity factor of binders and permanent deformation in mixtures. This was an improvement in the characterization of asphalt binders. However, since this approach is mostly empirical, it is limited in its ability to be implemented in micromechanics computational models.

To overcome this limitation, Delgadillo (*2008*) resorted to a mechanics-based approach to model the nonlinear response and tertiary flow in asphalt binders. In this context, tertiary flow refers to the accelerated unstable creep that is preceded by steady-state creep, due to the change in material or creation of microcracks and cavities (*Ferry, 1980; Lakes, 2009*). Delgadillo (*2008*) decomposed the total response (strain) into permanent and recoverable strain to propose a constitutive equation to predict the total strain for any arbitrary stress history *(Delgadillo, 2008)*:

$$\gamma(t) = \int_0^t \dot{\gamma}_p(\xi) d\xi + \int_0^t J_r(t-\xi) \frac{d\tau(\xi)}{d\xi} d\xi, \tag{3.3}$$

where ξ is the time integration variable, $\tau(\xi)$ is the stress history, J_r is the recoverable creep compliance, and $\dot{\gamma}_p(\xi)$ is the permanent strain rate. Delgadillo conducted a series of creep and recovery tests for different combinations of stress level and loading duration, and measured the total and permanent strain for any of these combinations. The data for both total and permanent strain were fitted to a power law equation with two arguments *(Delgadillo, 2008)*:

$$\begin{aligned} \gamma\ (t,\tau) &= k_1\, t^{m1}\ \tau^{p1} + k_2\, t^{m2}\ \tau^{p2}, \\ \gamma_p(t,\tau) &= k_1\, t^{m3}\ \tau^{p1} + k_2\, t^{m4}\ \tau^{p4}, \end{aligned} \tag{3.4}$$

where γ and γ_p are the total and permanent shear strain, respectively; t is the time in seconds; τ is the shear stress in kPa; and k_i, m_i, and p_i are the material constants. Finally, the recoverable strain was found by subtracting the functional form of the permanent strain from the functional form of total strain. Finding the γ_p and J_r equations, the total response of asphalt binder under any loading history can be predicted using Equation 3.3. Delgadillo and Bahia (*2010*) demonstrated the relationship between the nonlinearity of asphalt binders and asphalt mixture permanent deformation.

Masad et al. (*2008*) took a different approach to model the nonlinearly viscoelastic response of asphalt binders. They used a nonlinearly viscoelastic model, proposed by Schapery (*1969*), to predict the response of asphalt binders. Details of this model are presented in Section 3.4.5. To characterize the asphalt binders, they used a DSR and conducted a series of stress amplitude sweep tests (shear stress applied with varying amplitudes following a sinusoidal form) at different temperatures. They considered the stress amplitude at each cycle to be the representative stress at that cycle. They then used this to estimate the parameters for the nonlinearly viscoelastic model. To validate the model, they simulated the test using a finite element program and compared it to the measured results. In a similar work, Huang (*2008*) separated the viscoelastic (recoverable) and viscoplastic (irrecoverable) responses in the Multiple Stress Creep and Recovery (MSCR) test conducted on asphalt binders. By using a nonlinear model instead of the Boltzmann linear superposition integral, he reduced the amount of error in estimating the irrecoverable strain.

Lately, there has been considerable progress in characterizing and modeling the nonlinear response of asphalt binders. However, these constitutive models consider material intrinsic nonlinearity or damage and plasticity to be the sources of nonlinear response. This study (Chapter 2) demonstrated that, under certain conditions, the material response is significantly affected by the three-dimensional state of stress and the associated interaction nonlinearity. Therefore, it is imperative that the constitutive models for asphalt binders and mixtures account for this form of nonlinearity in addition to the

intrinsic material nonlinearity. The next section presents a brief discussion on the sources of nonlinearly viscoelastic response in an undamaged asphalt binder.

3.3.2. Sources of Nonlinear Response in Asphalt Binders

Nonlinearity in the stress-strain relationship in asphalt binders can be due to several different mechanisms. In general, five potential sources of stress-strain nonlinearity can be considered for an undamaged asphalt binder: intrinsic material nonlinearity, geometric nonlinearity, interaction nonlinearity, softening due to self-heating, and history dependent nonlinearity. In Chapter 2, these different potential sources of nonlinearity were investigated using results from a DSR. The following is a brief summary of the findings from this study:

First, axially constrained asphalt binder specimens subjected to sinusoidal cyclic loads with stress amplitudes of 5 kPa and above, at an intermediate temperature, resulted in the generation of a compressive axial force. Based on finite element simulations, the generated normal stress was partially attributed to the tendency of the specimen to deform axially when subjected to torsion and partially to the change in free volume and tendency of asphalt binder to dilate. The tendency of the specimen to deform axially when subjected to torsion is referred to as geometric nonlinearity or Poynting effect in solids (*Poynting, 1909*). The normal force in a cylindrical specimen with constrained ends subjected to torsion is (*Freudenthal and Ronay, 1966*)

$$N = -\frac{1}{4} G \pi \psi^2 a^4 , \tag{3.5}$$

where N is the normal force, G is the shear modulus, ψ is the uniform angle of twist, a is the cylinder radius.

Second, asphalt binder subjected to a stress sweep test exhibits nonlinear behavior (reduction in complex modulus with increase in stress amplitudes) even at stress

amplitudes as low as 5 kPa. This observation was consistent with the findings from other research studies (*Airey et al., 2004; Delgadillo, 2008; Masad et al., 2008*). However, the decrease in complex modulus observed during a stress sweep test is commonly attributed to intrinsic nonlinearity of the material or damage. It was demonstrated that the observed nonlinear response under the test conditions could be explained by considering the interaction between normal stresses and applied shear stresses, referred to here as interaction nonlinearity or three-dimensional effects. This interaction nonlinearity can exist in addition to intrinsic material nonlinearity.

Interaction nonlinearity has been recognized in polymeric materials. For example, Lu and Knauss (*1999*) investigated interaction nonlinearity in polymethyl methacrylate (PMMA). They demonstrated that the shear compliance of PMMA depends on the state of stress; the shear compliance in the presence of axial tension or compression is different from the shear compliance in the absence of these stresses, even though the applied shear stress was the same in all three cases. Lu and Knauss attributed this interaction nonlinearity to the change in free volume in the polymer. Similar effects were noted by Popelar and Liechti (*1997, 2003*) for epoxy and urethane adhesives. The effect of shear was implemented in a modified free volume theory, which has since been applied to epoxies used as structural adhesives *(Park and Liechti, 2003; Park et al., 2004; Park et al., 2006*). Park and Liechti incorporated hygrothermal effects into the theory in a natural and consistent manner. In summary, interaction nonlinearity or three-dimensional effects must be considered in developing a robust constitutive model for asphalt binder. The following section reviews common nonlinearly viscoelastic models and their ability to incorporate interaction nonlinearity.

3.4. ADOPTING A NONLINEARLY VISCOELASTIC CONSTITUTIVE EQUATION

Material nonlinearity is due to the inherent dependence of the stress-strain relationship on the magnitude of load. Material nonlinearity can be observed even at low strain levels (*Findley, 1976; Lakes, 2009*). A literature review reveals that more than ten different constitutive equations have been developed in the last four decades to model the nonlinearly viscoelastic response of materials. This section briefly reviews the relevant models with the intention of identifying the most appropriate approach to modeling intrinsic and interaction nonlinearity in asphalt binders. The models are grouped based on their generic approach.

3.4.1. Phenomenological Constitutive Equations

This category of models includes, but is not limited to, *Bailey-Norton's Nonlinear Creep Power Law* and *Findley's Nonlinear Creep Power Law*. The power law behavior of materials under creep has been reported by many researchers. *Bailey-Norton's Nonlinear Creep Power Law* (*Bailey, 1935; Norton, 1929*) is one of the earliest equations developed to model nonlinear creep response:

$$\varepsilon(t,\sigma) = A\sigma^m t^n, \tag{3.6}$$

where σ is the stress level, t is time, $\varepsilon(t,\sigma)$ is the strain as a function of stress and time, and m and n are material constants. This model is intended to predict the initial and steady state creep response of materials. Because the slope of strain response in steady state of creep is constant, the material constant n is typically considered to be one. This implies that the strain rate (slope) during steady state creep is only a function of stress level:

$$\frac{d\varepsilon}{dt} = A\sigma^m. \tag{3.7}$$

Findley (*1976*) introduced another form of *Nonlinear Power Law*, in which the linear power law equation was modified by using a normalized function of stress:

$$\varepsilon(t) = \varepsilon_0 \sinh\left(\frac{\sigma}{\sigma_0}\right) + m\, t^n \sinh\left(\frac{\sigma}{\sigma_n}\right), \tag{3.8}$$

where σ is the stress level; and ε_0, σ_0, σ_n , m, and n are material constants. The motivation for using the power law equation is to have a simple model with a few material constants and obtain a reasonable approximation. In other words, the power law sacrifices accuracy for the sake of simplicity. However, since these models do not accommodate the history (no integral), they can only be used for step loading (creep) and do not account for recovery. The second limitation of the power law equation is the continuous increase of strain with time, regardless of material behavior. In other words, the power law equation cannot model the long time rubbery plateau behavior of thermo-set materials. This is typically resolved by using a Prony series (a series of power law terms) with a sufficient number of terms. The third limitation is the sensitivity of n to experimental errors and noise in data; in order to calculate n accurately, the creep test should be of sufficiently long duration. Hiel and coworkers (*1984*) demonstrated that the use of the recovery portion of a creep-recovery test can decrease the time required to determine n by a factor of ten. These issues restrict the application of *power law* models.

3.4.2. Extensions of Linear Superposition

The second group of model is based on the extensions of linear superposition. For instance, *Nonlinear Superposition* is a modified form of the Boltzmann integral that accommodates the loading history (the integral). The only difference between *Nonlinear Superposition* and Boltzmann integral is that the creep compliance is not only a function of time but also a function of stress level:

$$\varepsilon(t) = \int_0^t J(t-\tau, \sigma(\tau)) \frac{d\sigma(\tau)}{d\tau} d\tau. \tag{3.9}$$

The creep compliance can be found by running several creep tests at different stress levels. The functional form of the compliance curve depends on the stress level. Although this approach does not account for the cross interactions from multiple load steps, it can describe some specific types of nonlinear behavior. For example, *Quasi-linear Viscoelasticity (QLV)* is a specific case of *Nonlinear Superposition*. The *QLV* equation was originally introduced by Schapery (*1962*), and later was used by Fung (*1972*) to model the behavior of soft tissues. This model considers creep compliance as a product of two separable kernels (time-dependent and stress-dependent kernels):

$$J(t-\tau,\sigma(\tau)) = J(t)\,.\,f(\sigma). \tag{3.10}$$

In this model the shape of the creep compliance curve is independent of stress level. This is because the stress kernel contributes only a scalar multiplier to the kernel of time. This means that the creep compliance curves at different stress levels will be parallel to each other on a log-scale plot. Darvish and Crandall (*2001*) successfully used this model to describe the nonlinear behavior of brain tissue. This model is adequate to describe the mechanical response of soft tissues and is used by researchers in biomechanics and medical engineering. However, only a few other materials show such a simple behavior (*Lakes, 2009*). Our preliminary analysis showed that this approach is not suitable to model the nonlinear behavior of asphalt binders.

Modified Superposition is another approach that not only includes the stress sensitivity of response under a step load, but also accounts for the most recent load history. Unlike regular superposition, *Modified Superposition* removes all previous loading history (until the last step) and adds the current load step (Figure 3.1). For instance, the material response under two-step loading (σ_0 applied at t_0 and the load level changes to σ_1 at t_1) is

$$\varepsilon(t) = f(\tau_0, t-t_0) - f(\tau_0, t-t_1) + f(\tau_1, t-t_1), \quad for\, t > t_1 \tag{3.11}$$

where $f(\tau_0,t)$ is the material response (strain) under constant load of τ_0 at time zero. This function can be a nonlinear function of stress. The material response can be generalized for N step loading as

$$\varepsilon(t) = \sum_{i=0}^{N} f(\tau_i, t-t_i) - f(\tau_{i-1}, t-t_i) \; . \tag{3.12}$$

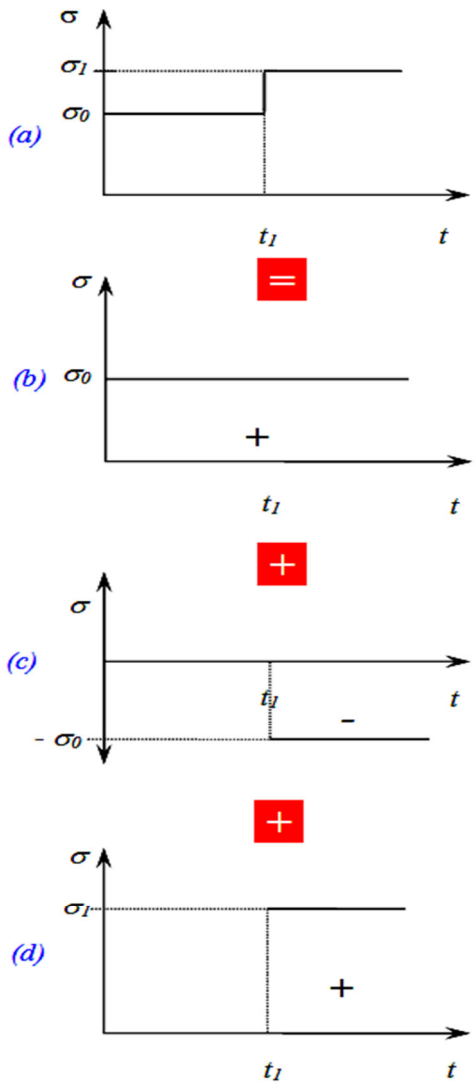

Figure 3.1: Modified Superposition.

For infinitesimal load steps, when N approaches infinity

$$\begin{aligned}
\varepsilon(t) &= \lim_{N\to\infty}\sum_{i=0}^{N}\lim_{\Delta\tau_i\to 0} f(\tau_i, t-t_i) - f(\tau_i-\Delta\tau_i, t-t_i) \\
&= \lim_{N\to\infty}\sum_{i=0}^{N}\lim_{\Delta\tau_i\to 0} f(\tau_i, t-t_i) - f(\tau_i-\Delta\tau_i, t-t_i)\ \frac{\Delta\tau_i}{\Delta\tau_i} \\
&= \lim_{N\to\infty}\sum_{i=0}^{N}\lim_{\Delta\tau\to 0} \frac{f(\tau_i+\Delta\tau_i, t-t_i) - f(\tau_i, t-t_i)}{\Delta\tau_i}\Delta\tau_i \\
&= \int_0^t \frac{f(\partial\tau(\zeta), t-\zeta)}{\partial\tau(\zeta)}\, d\tau(\zeta) \\
&= \int_0^t \frac{f(\partial\tau(\zeta), t-\zeta)}{\partial\tau(\zeta)}\,\frac{d\tau(\zeta)}{d\zeta} d\zeta.
\end{aligned} \tag{3.13}$$

This final integral form was introduced by Turner (*1966*). Although this approach is appropriate for many materials, it does not consider all cross interactions as the *Multiple Integral* method does (*Findley, 1976*).

3.4.3. Displacement Based Equations

This group of models was developed to predict relaxation stress under displacement loading. *Finite Linear Viscoelasticity* theory was originally introduced by Coleman and Noll (*1961*). Lianis (*1963*) used an approximate form of this theory and described the stress relaxation in terms of three material constants and four relaxation functions. McGuirt and Lianis (*1969*) used the approximate approach to describe the stress relaxation in incompressible isotropic materials under unconfined uniaxial relaxation tests. They determined three relaxation functions by conducting three relaxation tests at different extension levels, as a function of a fourth unknown relaxation function. The material constants were determined by allowing these tests to reach equilibrium. A two-step relaxation test was then conducted to determine the fourth relaxation function independent of the others. This method was applied by several researchers to model the relaxation stress in polymers and the results were satisfactory

(*Findley, 1976*). However, this method was introduced only for relaxation tests and no equivalent creep formulation has been reported (*Findley, 1976*). *Elastic Fluid Theory* is another well-known displacement-based model. This model (also known as the *BKZ* model) was first developed by Bernstein, Kearsley, and Zapas (*1963*) to capture the nonlinear behavior of elastic fluids. Bernstein et al. (*1963*) used the Equation 3.14 to model the relaxation stress in elastomers:

$$\sigma(t) = \int_0^t A(t-\tau)\, f(\varepsilon_g(\tau))\, d\tau, \tag{3.14}$$

where *A(t)* is a function of time, ε_g is the generalized strain measure which is appropriate for large deformations:

$$\varepsilon_g = \frac{1}{2}(\lambda^2 - 1), \qquad \lambda = \frac{l}{l_0}, \tag{3.15}$$

where the λ is the extension ratio, l is the deformed length, and l_0 is the initial length. It is noteworthy that for the unconfined uniaxial step loading relaxation test on incompressible isotropic materials, both the *BKZ* and the *Finite Linear Viscoelasticity* approach reduce to the same expression. Even though the *BKZ* model worked well with elastomers, it was not so successful for moderate strain levels in other materials such as polypropylene and poly-vinyl-chloride (*Findley, 1976*). The second issue with this model is that no equivalent creep formulation has been developed.

3.4.4. Nonlinear Mechanical Analogue Models

Nonlinear Mechanical Analogue models are another important group that use the analogy between the material behavior and mechanical element combinations. One advantage of these models is that they provide a mechanical analogue of the mechanisms involved in material behavior. For instance, nonlinear viscoelasticity can be modeled by considering Burger or other mechanical models with nonlinear spring and dashpot elements:

$$E_i = E_i(\sigma), \quad \mu_i = \mu_i(\sigma), \quad \tau_i = \tau_i(\sigma), \tag{3.16}$$

where σ is stress level, E_i are the spring moduli, μ_i are dashpot viscosities, and τ_i are the relaxation times. In this case, all these material properties are functions of stress. To determine the constitutive equation we first need to determine the stress-dependent functions in Equation 3.16. Then, the stress-strain relationship is obtained by introducing these functions in the stress-strain differential equation and solving it. Another example is the generalized Kelvin model with nonlinear spring elements and linear dashpot elements, the constitutive equation for creep compliance would become (*Brinson and Brinson, 2008*)

$$J(t) = \sum_{i=1}^{n} \frac{f_i(\sigma)}{E_i}(1 - e^{\frac{-t}{\tau_i}}), \tag{3.17}$$

where J is the creep compliance, $f_i(\sigma)$ are functions of stress. As can be seen, there are three parameters in each Kelvin element arrangement that must be defined. By increasing the number of required elements (n), difficulties in determining model parameters from experimental data increase considerably. This makes the use of such models difficult in practice.

The methods that have been discussed thus far were mainly capable of modeling material nonlinear behavior under certain conditions. In the case of multiple loading steps or continuously varying loads, a more general and flexible model is required.

3.4.5. Thermodynamic-based Equation

Schapery (*1969*) proposed a constitutive model for nonlinear viscoelasticity which he verified using the thermodynamic principles of an irreversible process and experimental observations. Schapery's model for uniaxial loading at a constant temperature is

$$\varepsilon(t) = g_0 J_0 \sigma(t) + g_1 \int_0^t J[\psi(t) - \psi(\tau)] \frac{d(g_2\ \sigma(\tau))}{d\tau} d\tau, \tag{3.18}$$

where

$$\psi(t) = \int_0^t \frac{d\xi}{a_\sigma[\sigma(\xi)]};\ \psi(\tau) = \int_0^\tau \frac{d\xi}{a_\sigma[\sigma(\xi)]},$$

where t is the time of interest; τ and ξ are the integration variables; $\sigma(t)$ is the applied stress at time t; g_0, g_1, and g_2 are material properties that are a function of stress; $\psi(t)$ *and* $\psi(\tau)$ are reduced time variables; $a_\sigma[\sigma(\xi)]$ is a shift factor that scales (modulates) the time and is a function of stress; J_0 is the time independent compliance, J is the linear viscoelastic compliance (creep compliance). The creep compliance indirectly depends on stress through the reduced time variables. This model incorporates five functions (g_0, g_1, g_2, $a_\sigma[\sigma(\xi)], J$) and a constant (J_0) and can be used to describe different types of nonlinearities (*Findley, 1976; Lakes, 2009*). By setting $g_0 = g_1 = g_2 = a_\sigma[\sigma(\xi)] = 1$, the model reduces to the Boltzmann linear superposition integral. When all of these parameters other than $a_\sigma[\sigma(\xi)]$ are set to unity, the model reduces to Knauss's free volume model (*Knauss and Emri, 1981*). They studied the thermo-rheology of high polymers and associated the change in mechanical behavior of polymers to the change in free volume. Using this concept, they introduced a unifying parameter that explains the change in material behavior due to changes in temperature, water concentration, and also volume dilatation based on changes in free volume. The *Modified Superposition* is also a special form of *Schapery*'s model when g_1 and a_σ are set to unity. It should be noted that none of these parameters (g_0, g_1, g_2, and a_σ) are fundamental physical or thermodynamic constants and need to be determined through creep and recovery tests at different stress levels. As mentioned earlier, Huang (*2008*) used Schapery's nonlinear constitutive model to describe the intrinsic nonlinear response of asphaltic materials.

3.4.6. Multiple Integrals Method

The *Multiple Integrals* method is another powerful approach to modeling the nonlinear response of viscoelastic materials. The *Multiple Integrals* method was first developed by Volterra and Frechet. Green and Rivlin (*1957, 1960*) used the principles of continuum mechanics and generalized this model to three dimensions. Findley (*1976*) used another approach that extends the linear superposition for nonlinear viscoelasticity by considering the interactions between loading steps, and arrived at an identical formulation (shown here using three terms):

$$\begin{aligned}\varepsilon(t) = & \int_0^t \varphi_1(t-\tau_1)\frac{\partial\sigma(\tau_1)}{\partial\tau_1}d\tau_1 \\ & + \int_0^t\int_0^t \varphi_2(t-\tau_1, t-\tau_2)\frac{\partial\sigma(\tau_1)}{\partial\tau_1}\,\frac{\partial\sigma(\tau_2)}{\partial\tau_2}d\tau_1\,d\tau_2 \\ & + \int_0^t\int_0^t\int_0^t \varphi_3(t-\tau_1, t-\tau_2, t-\tau_3)\frac{\partial\sigma(\tau_1)}{\partial\tau_1}\,\frac{\partial\sigma(\tau_2)}{\partial\tau_2}\frac{\partial\sigma(\tau_3)}{\partial\tau_3}d\tau_1\,d\tau_2\,d\tau_3\end{aligned} \tag{3.19}$$

where t is the time of interest, the τ_i are the time variables of integration, and φ_i are the time-dependent material functions. *Multiple Integrals* can be considered as an extension of linear superposition that includes interaction terms to account for the nonlinear response. For an intrinsically linear material, the functions φ_2 and φ_3 reduce to zero for all time arguments reducing Equation 3.19 to the familiar form of the Boltzmann superposition principle. The intrinsic nonlinearity of the material is accommodated by time functions with similar time arguments, e.g., $\varphi_2(t, t)$. Nonlinearity due to stress history is accommodated by time functions with dissimilar time arguments, e.g., $\varphi_2(t, t\text{-}t_1)$. The nonlinearity due to stress history reflects the influence of residual strain or stored energy on material behavior. Special cases arise when time functions with similar time arguments (such as $\varphi_2(t, t)$ and $\varphi_3(t\text{-}t_1, t\text{-}t_1, t\text{-}t_1)$) are zero, and with dissimilar time arguments (such as $\varphi_2(t, t\text{-}t_1)$) are non-zero. In these cases, the material does not exhibit intrinsic nonlinearity but exhibits history dependent nonlinearity. In other words, one can expect a linear response when comparing strains from independent creep tests with

stresses $\Delta\sigma_0$ and $\Delta\sigma_0+\Delta\sigma_1$ and a nonlinear response when the two-step loading (or any arbitrary stress history) is applied. Therefore, the multiple integrals method provides insight into nonlinearity due to loading history (cross interactions).

Multistep creep and recovery tests are typically used to determine the time dependent kernels of a material. These tests include different stress levels as well as different loading time intervals. The tediousness of this procedure demands some simplifications to make the model practical (*Findley, 1976*). However, an advantage of the model is that it is comprehensive and flexible and thus can be applied to a broad range of nonlinear systems besides nonlinearly viscoelastic systems (*Schetzen, 1980*).

The *Multiple Integral* formulation has a very general form and many viscoelastic models can be derived as a special case of the *Multiple Integrals*. For example, when second and third order interactions are neglected, the model reduces to a linear Boltzmann integral. By restricting the kernels to be only the function of the smallest time argument (the most recent occurrence), the *Multiple Integral*s reduces to the *Modified Superposition*. *Multiple Integrals* can also be used to model the interaction nonlinearity in compressible materials. By making some simplifications, it is possible to incorporate the effect of axial load on the torsion shear strain:

$$\varepsilon_{12}(t) = \int_0^t G_1\,\dot{\tau}\,d\xi_1 \;+\int_0^t\int_0^t G_3\,\dot{\tau}\,\dot{\sigma}\;d\xi_1\,d\xi_2 + \int_0^t\int_0^t\int_0^t (G_2\,\dot{\tau}^3 + G_4\,\dot{\sigma}^2\,\dot{\tau}\,\varphi_3)\,d\xi_1\,d\xi_2\,d\xi_3\,, \tag{3.20}$$

where $\dot{\tau}$ and $\dot{\sigma}$ are the torsion and axial stress rate, respectively; G_1, G_2, G_3, and G_4 are four independent kernels. Note that all of these terms are functions of time ξ_i. The terms that include $\dot{\sigma}$ quantify the effect of axial stress on the torsion shear strain. This model has been used by many researchers to model the nonlinearly viscoelastic behavior of materials. For example, Erman and Onaran in 1974 used multiple integrals to model the time dependent behavior of nonlinear orthotropic materials such as wood and fiber composite plastic under combined stresses and step loading (*Findley et al., 1976*). The results were in good agreement with experimental data.

3.4.7. A Nonlinearly Viscoelastic Model for Asphalt

Among the models discussed earlier, *Multiple Integrals* and *Schapery*'s equation are the most promising methods to model the nonlinearly viscoelastic behavior of asphalt binders. For this study, *Schapery's* model was selected over *Multiple Integrals* because of its advantages for future implementation in numerical schemes (*Huang, 2008*). It should also be noted that obtaining the time kernels for *Multiple Integrals* model is more involved and requires more testing (discussed in Section 3.4.6).

To have a better understanding of Schapery's model, the application of this model is illustrated for creep and recovery tests on materials that follow power law behavior. Consider a viscoelastic response under a constant step load σ_0. For a given stress, the functions g_0, g_1, g_2, and a_σ, have a constant value and the material response is given as

$$\varepsilon(t) = g_{0,\sigma_0} J_0 \sigma_0 + g_{1,\sigma_0} g_{2,\sigma_0} \sigma_0 J(\frac{t}{a_{\sigma,\sigma_0}}). \tag{3.21}$$

For a material with a creep compliance that follows a power law,

$$\varepsilon(t) = g_{0,\sigma_0} J_0 \sigma_{0,\sigma_0} + g_{1,\sigma_0} g_{2,\sigma_0} \sigma_0 (\frac{t}{a_{\sigma,\sigma_0}})^n, \tag{3.22}$$

where t is time and n is the material constant. By decomposing the total strain into its elastic ε_E and viscoelastic ε_{VE} components we have

$$\begin{aligned} \varepsilon_E &= g_0 J_0 \sigma_0, \\ \varepsilon_{VE} &= g_1 g_2 \sigma_0 J(\frac{t}{a_\sigma}) = g_1 g_2 \sigma_0 (\frac{t}{a_\sigma})^n. \end{aligned} \tag{3.23}$$

Comparing the elastic response in *Schapery's* Equation 18 to that of a linear model, the former has an additional factor of g_0. Thus, g_0 is considered to be the correction factor for nonlinearity in the elastic response. This is similar to using a nonlinear spring in the elastic part of a mechanical analogue model. Considering the viscoelastic response in log-log scale,

$$Log[\varepsilon_{VE}] = Log[g_1 g_2 \sigma_0 (\frac{t}{a_\sigma})^n] = Log[g_1 g_2] + Log[\sigma_0 (\frac{t}{a_\sigma})^n], \tag{3.24}$$

it can be seen that $Log[g_1 g_2]$ shifts the creep compliance curve vertically and that the a_σ, which scales the time, shifts the graph horizontally. These shifts move the linearly time dependent part of the prediction model and match it with the measured material response. This procedure is very similar to making a master curve using the Time Temperature Superposition principle, and in the literature is called the Time Stress Superposition principle. Both of these principles are based on the assumption that the deformation mechanism at different temperatures and stress levels is the same, but at a different rate.

3.5. EXPERIMENTAL

This section describes the materials and experiments used in this research. This includes the details regarding the test procedures used to model and verify nonlinear viscoelasticity in asphalt binders.

3.5.1. Materials and Test Method

Two modified binders were selected with different performance grades following the Superpave© specification: PG 82-22 and PG 76-22. The reason for selecting modified binders for this study was that the nonlinearity is more pronounced in modified binders. A DSR (Model TA AR2000Ex) was used to measure the mechanical response of the asphalt binders when subjected to different loading conditions. Two different test temperatures were used to investigate the influence of temperature on the nonlinear response of asphalt binders: 28^oC and 40^oC. These temperatures were well above the glass transition temperature, T_g, of asphalt binders; which range from -30^oC to -5^oC. The device is capable of measuring the axial force in the presence of an axial deformation constraint so that any geometrical nonlinearity and asphalt binder dilatation could be addressed quantitatively. For this investigation, the effects of aging were not incorporated and all tests were conducted on un-aged binders.

3.5.2. Test Geometry

The selection of an appropriate test geometry for use with the DSR is critical to the investigation of the nonlinear response. There are two different geometric configurations that are typically used to test asphalt binders with a DSR at intermediate to high temperatures. The first and most common one is the parallel plates. Since in this geometry strain rate depends on the distance from the axis of rotation, the material will be subjected to different strain rates and stress levels at different radial positions within the specimen. As a result, in the case of a material that exhibits a nonlinear response, the measured response with the parallel plate geometry is an average of the non-uniform response across the cross section of the specimen unless a thin-walled tube is used. In addition, the use of parallel plate has other disadvantages as discussed in Section 2.4.2.

The second configuration, not commonly used for asphalt binders, is the cone and plate geometry. The difference between the cone and plate geometry and the parallel plate geometry is that the former has a conical shaped top plate. This geometry ensures that the shear strain rate is approximately uniform throughout the specimen as indicated in Section 2.4.2. Therefore, this geometry, which is more suitable for accurate measurement of material properties, was selected in this study to characterize the behavior of the asphalt binders. The diameter of the cone and plate was 25 mm. Two different cone plate angles were used; one had a cone angle of 5° (5:45:03) and a truncation gap of 146 μm, and the second had a cone angle of 2° (2:17:42) and a truncation gap of 56 μm.

3.5.3. Test Procedure and Data Collection

A stress sweep was conducted to determine the linear viscoelastic limit of the asphalt binder. The oscillation frequency was 0.1 Hz, and 10 cycles were applied at each shear stress level. Our analytical simulation of oscillatory tests showed that the transient effect only lasts for about 5 cycles. This was also verified by measuring the material response in the laboratory. Therefore, 10 cycles of the oscillatory load were considered to be adequate to overcome any initial transient effects. The rationale for selecting the low frequency of 0.1 Hz was to enhance the time dependent response of the material. The

stress amplitude was varied from 100 Pa to 48.1 kPa in eight equal steps. The minimum shear stress amplitude of 100 Pa was selected to ensure that the lowest stress was well within the linear viscoelastic limit of the binder. Previous researchers (*Delgadillo, 2008; Huang, 2008*) have reported that asphalt binders behave linearly at this stress level. The maximum shear stress amplitude of 48.1 kPa was selected based on the maximum torque capacity of instrument. This level was still below the maximum local stress experienced by the matrix part of asphalt mixture under typical traffic load levels (*Huang, 2004*).

An important consideration while running the stress sweep test was to record the normal force experienced by the plate. Figure 3.2 shows the results from the stress sweep test for the asphalt binders under study at $40^{\circ}C$. Figure 3.2*a* illustrates both the applied shear stress as well as the average normal stress generated during the test. Figures 3.2*b* and 3.2*c* illustrate the reduction in dynamic shear modulus G^* with an increase in the shear stress amplitude as well as the generated normal force indicating the onset of the nonlinear response. This nonlinear response can be observed even at stress amplitudes that are as low as 7 *kPa*. Each test was replicated three times with consistent results. Other binder-temperature combinations showed similar results.

The laboratory measurements clearly show that torsion results in the generation of a normal force when the specimen is confined axially and the gap is not allowed to change. Second, the asphalt binder behaves nonlinearly, i.e., the complex modulus depends on the stress level.

Chapter 2 demonstrated that the normal force develops in asphalt binder DSR specimens with a constant gap due to both the Poynting effect and an increase in the free volume of the asphalt binder. Furthermore, the generated normal force affects the shear behavior of asphalt binders and causes a change in shear modulus. This form of nonlinear response is referred to as an interaction nonlinearity. The results also showed that the generated normal force is more significant when the specimen geometry has a high aspect ratio and the applied shear stress is high. The next section presents the modeling of the interaction nonlinearity, followed by validations of the proposed model under different loading histories.

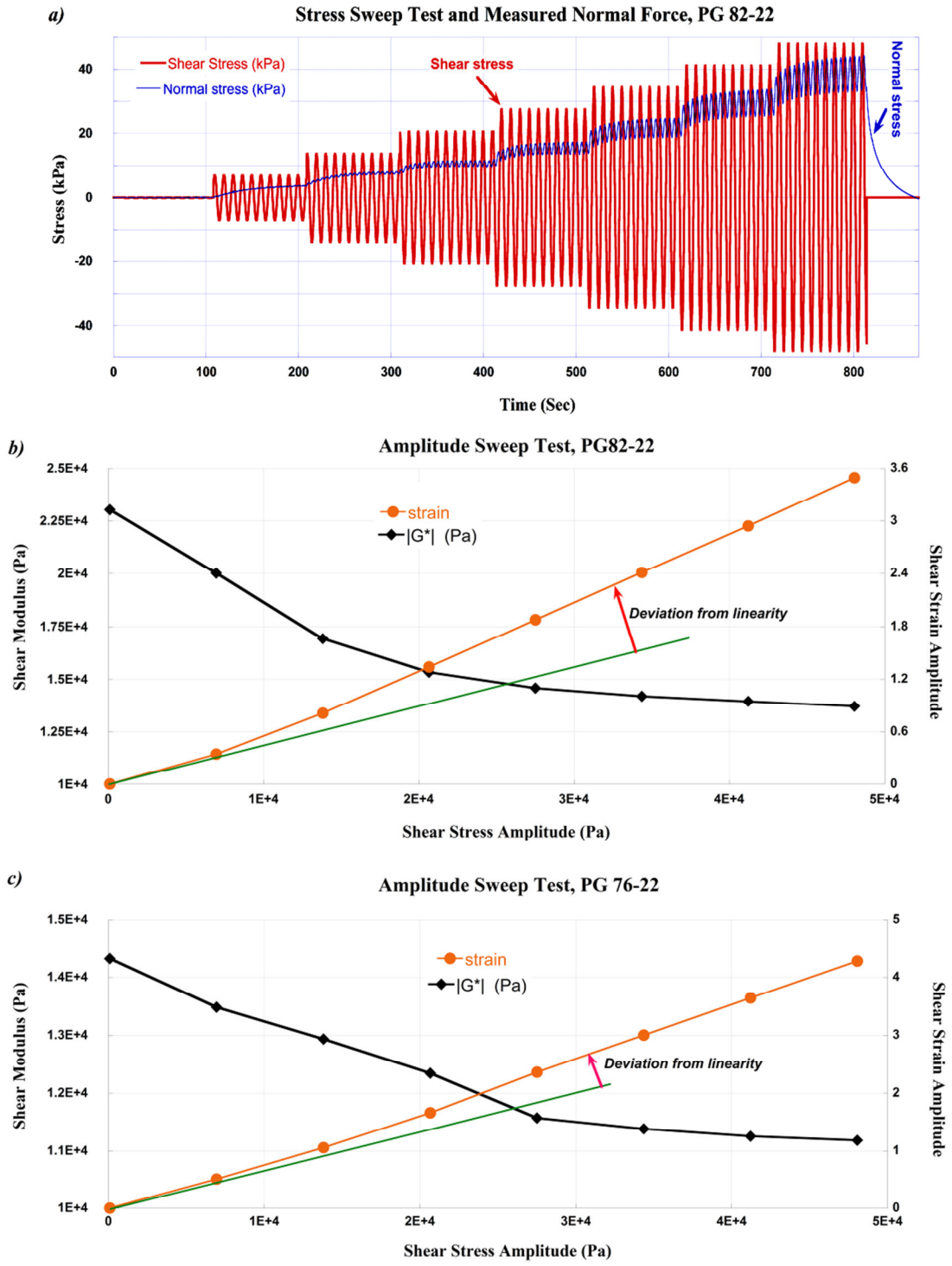

Figure 3.2: Stress amplitude sweep test at 40°C using cone and plate geometry.

3.6. MODELING

The nonlinear behavior of asphalt binders under stress sweep tests could be due to material intrinsic nonlinearity or the interaction of normal stresses with the shear behavior of asphalt binders. In this study, the octahedral shear stress, which includes the effects of any induced normal stresses, was used to represent the overall state of stress in the material. In order to model the nonlinear behavior of asphalt binder, Schapery's nonlinear viscoelastic equation was adopted such that the nonlinear material parameters were functions of the octahedral shear stress. Creep and recovery tests at different levels of octahedral shear stress are required to calibrate the model and obtain the nonlinear material parameters (g_0, g_1, g_2, and a_σ in Equation 3.18) as a function of octahedral shear stress. The normal force cannot be controlled (by changing the gap size) for cone and plate geometry, since the gap size is fixed. Thus, to measure the creep and recovery response of asphalt binders at different levels of octahedral shear stress, the author first conducted an amplitude sweep test to generate the normal force in the specimen. A few seconds after the amplitude sweep test, while the generated normal force was gradually relaxing, the author conducted a series of short duration creep and recovery tests (creep and recovery snapshots) at different magnitudes of normal force. The following subsections describe the procedure used to obtain material parameters in more detail.

3.6.1. Test Method

To obtain the linear creep compliance of the asphalt binder, creep and recovery tests were conducted at a low stress level of 0.1 kPa. The creep and recovery test consisted of 5 second creep and 500 second recovery. The selected loading time was much greater than the rise time of the instrument, which is on the order of 10^{-4} second. Figure 3.3 shows the test results for the first 100 seconds.

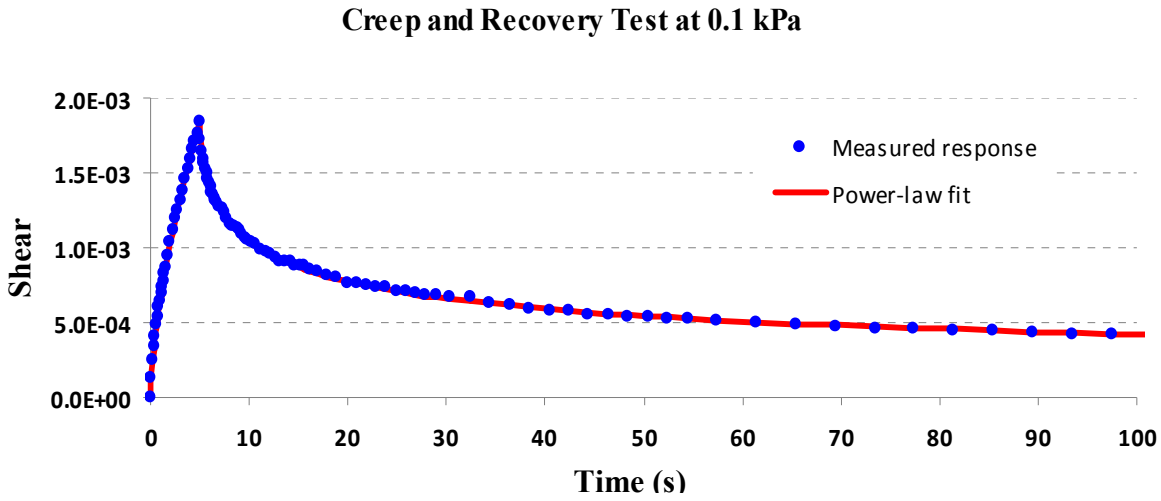

Figure 3.3: Shear creep and recovery test at stress level of 0.1 kPa and 28°C using cone and plate geometry.

As can be seen, power law model adequately represents the response of the material:

$$J(t) = J_0 + J\,t^n, \tag{3.25}$$

where J_0, J, and n are linear material constants. It should be noted that due to higher sensitivity of these constants to the test duration in creep, these material constants were obtained using only the recovery test data (*Hiel et al., 1984*). The linearity of the response was verified by conducting creep and recovery tests at the higher stress level of 5 kPa.

The next step was to obtain the nonlinear material parameters (g_0, g_1, g_2, and a_σ) as a function of octahedral shear stress. This requires conducting creep and recovery tests at different levels of octahedral shear stress. To generate the normal stress within the DSR specimen, a shear stress sweep test was conducted. The frequency of oscillation was 0.1 Hz and 10 cycles were applied at each shear stress level. The shear stress amplitude was varied from 100 Pa to 48.1 kPa in eight steps with equal increment. The test geometry was a cone and plate with a cone angle of 2° (2^o:17′:42″) and a truncation gap of 56 μm. The stress sweep test resulted in the generation of a significant normal stress due

to dilatation and Poynting effect, as discussed earlier. The test temperature was $28^{\circ}C$, so that the relaxation of the normal force could easily be observed. After completing a stress sweep test, a series of creep and recovery tests were conducted at 20 kPa as the normal stress was relaxing. The corresponding creep and recovery snapshots consisting of 1 second loading and 90 seconds recovery are shown in Figure 3.4. Each snapshot captures the material behavior at a specific level of interaction (between normal stress and shear properties). These creep recovery cycles produced an insignificant change in the normal force. Figure 3.5 is a close-up of the second snapshot in Figure 3.4 for the first 10 seconds. As can be seen, the normal force does not vary significantly during the first 10 seconds of creep and recovery and therefore can be considered to be constant. The next subsection presents the stress analysis for the cone and plate geometry that is required for calibrating the model.

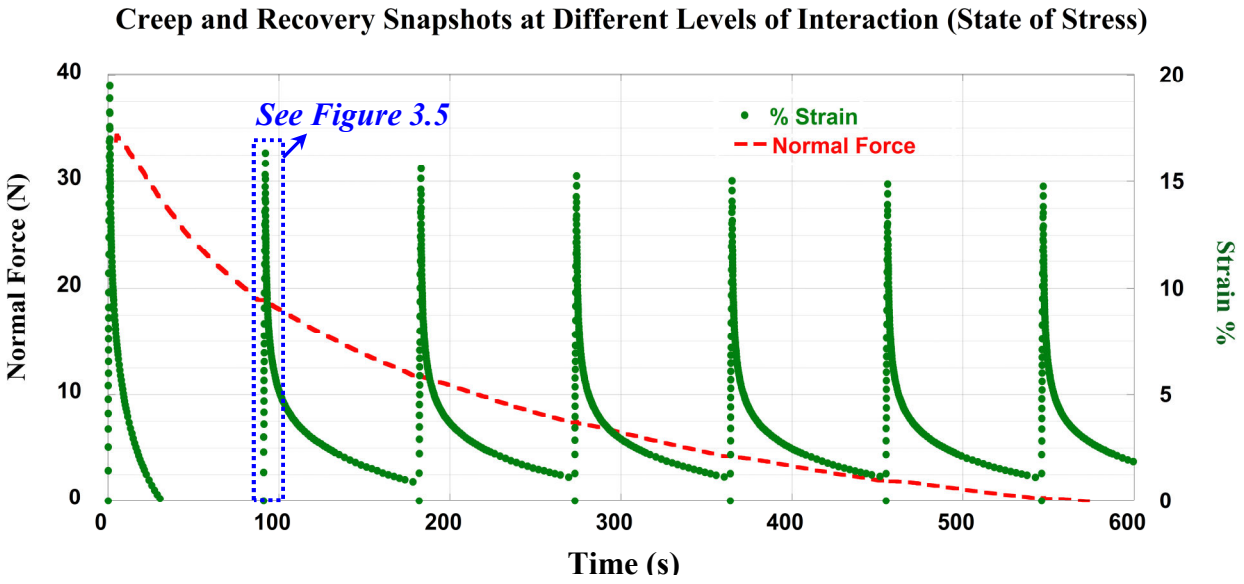

Figure 3.4: A series of creep and recovery tests conducted after the stress sweep test to obtain the nonlinear model parameters at different levels of octahedral shear stress, at 20 kPa shear stress level and at 28°C using cone and plate geometry.

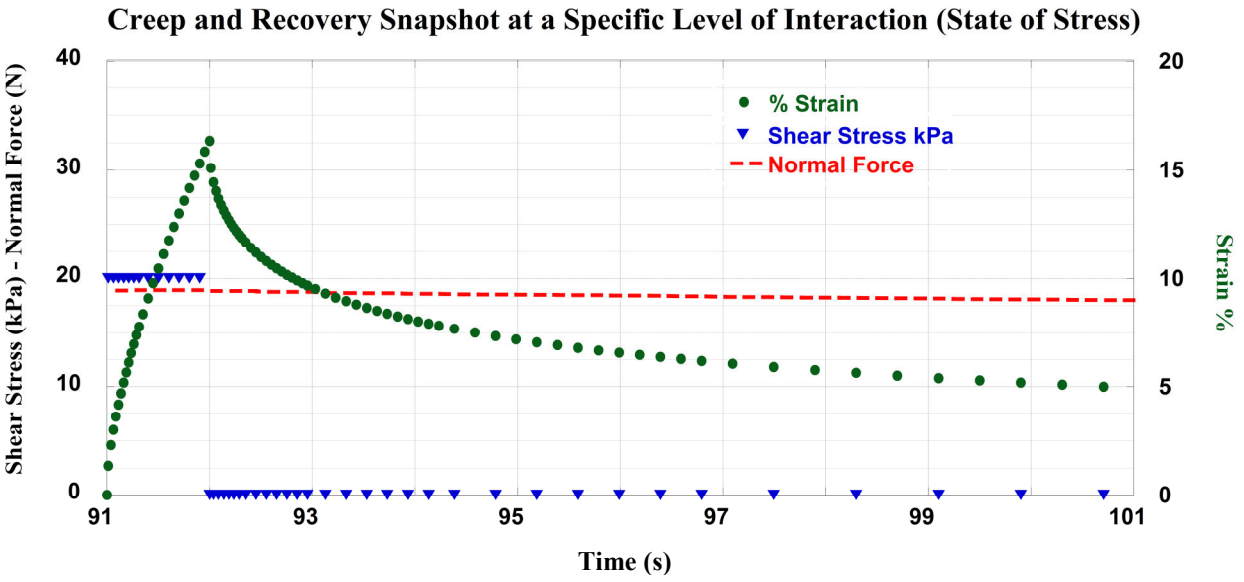

Figure 3.5: Close-up of Figure 3.4. Creep and recovery test at 20 kPa shear stress level and at 28°C following a shear stress sweep. The normal force does not vary significantly in the first few seconds of creep and recovery.

3.6.2. Stress Analysis and Model Calibration

The appearance of a normal force as a result of torsion indicated a coupling between applied shear stress $\tau_{\phi\theta}$ and normal stresses. It was assumed that there is no coupling between the applied shear $\tau_{\phi\theta}$ and other shear stress components ($\tau_{r\theta}$ and $\tau_{r\phi}$). Using three equilibrium equations in spherical coordinates (*Sadd, 2009*) as

$$\frac{\partial \sigma_r}{\partial r}+\frac{1}{r}\frac{\partial \tau_{r\theta}}{\partial \theta}+\frac{1}{r\,Sin(\theta)}\frac{\partial \tau_{r\phi}}{\partial \phi}+\frac{1}{r}[2\sigma_r-\sigma_\phi-\sigma_\theta+\tau_{r\theta}\,Cot(\theta)]+F_r=0, \tag{3.26a}$$

$$\frac{\partial \tau_{r\theta}}{\partial r}+\frac{1}{r}\frac{\partial \sigma_\theta}{\partial \theta}+\frac{1}{r\,Sin(\theta)}\frac{\partial \tau_{\phi\theta}}{\partial \phi}+\frac{1}{r}[(\sigma_\theta-\sigma_\phi)\,Cot(\theta)+3\tau_{r\theta}]+F_\theta=0, \tag{3.26b}$$

$$\frac{\partial \tau_{r\phi}}{\partial r}+\frac{1}{r}\frac{\partial \tau_{\phi\theta}}{\partial \theta}+\frac{1}{r\,Sin(\theta)}\frac{\partial \sigma_\phi}{\partial \phi}+\frac{1}{r}[2\tau_{\phi\theta}\,Cot(\theta)+3\tau_{r\phi}]+F_\phi=0, \tag{3.26c}$$

and equating $\tau_{r\theta}$, $\tau_{r\phi}$, and setting the body force vector $\underset{\sim}{F}$ to zero provides us with a

system of differential equations:

$$\frac{\partial \sigma_r}{\partial r} + \frac{1}{r}[2\sigma_r - \sigma_\phi - \sigma_\theta] = 0, \tag{3.27a}$$

$$\frac{1}{r}\frac{\partial \sigma_\theta}{\partial \theta} + \frac{1}{r\,Sin(\theta)}\frac{\partial \tau_{\phi\theta}}{\partial \phi} + \frac{1}{r}[(\sigma_\theta - \sigma_\phi)\ Cot(\theta)] = 0, \tag{3.27b}$$

$$\frac{1}{r}\frac{\partial \tau_{\phi\theta}}{\partial \theta} + \frac{1}{r\,Sin(\theta)}\frac{\partial \sigma_\phi}{\partial \phi} + \frac{1}{r}[2\tau_{\phi\theta}\ Cot(\theta)] = 0. \tag{3.27c}$$

Due to the rotational symmetry, we have

$$\frac{\partial \sigma_\phi}{\partial \phi} = \frac{\partial \tau_{\theta\phi}}{\partial \phi} = 0. \tag{3.28}$$

Therefore, Equation 3.27 reduces to

$$\frac{\partial \sigma_r}{\partial r} + \frac{1}{r}[2\sigma_r - \sigma_\phi - \sigma_\theta] = 0, \tag{3.29a}$$

$$\frac{\partial \sigma_\theta}{\partial \theta} + [(\sigma_\theta - \sigma_\phi)Cot(\theta)] = 0, \tag{3.29b}$$

$$\frac{\partial \tau_{\phi\theta}}{\partial \theta} + [2\tau_{\phi\theta}\,Cot(\theta)] = 0. \tag{3.29c}$$

For a cone and plate geometry, the shear rate and therefore the shear stress does not vary in the radial direction. This is not the case for normal stress components and they vary in the radial direction. Since the purpose of this study was to model the material behavior based on the measured response (average response across the cross-section), it was assumed that the normal stresses do not vary in the radial direction. This assumption simplifies the problem and leads to the unique solution. For example, a radially varying normal stress would result in non-unique solutions while calibrating the model and obtaining model constants. Assuming no change in normal stresses in the radial *r* direction and considering the traction free rim (boundary condition) implies that the normal stress in *r* direction σ_r is equal to zero. Consequently, the state of the stress in the

specimen can be computed by solving the system of differential equations (three equations and three unknowns):

$$-\sigma_{\phi} - \sigma_{\theta} = 0, \tag{3.30a}$$

$$\frac{\partial \sigma_{\theta}}{\partial \theta} + [(\sigma_{\theta} - \sigma_{\phi}) Cot(\theta)] = 0, \tag{3.30b}$$

$$\frac{\partial \tau_{\phi\theta}}{\partial \theta} + [2\tau_{\phi\theta} Cot(\theta)] = 0. \tag{3.30c}$$

Equation 3.30*a* indicates that the two nonzero normal stresses are equal and opposite in sign. Thus, Equations 3.30*b* and 3.30*c* can be rewritten as

$$\frac{\partial \sigma_{\theta}}{\partial \theta} + 2\sigma_{\theta} Cot(\theta) = 0, \tag{3.31a}$$

$$\frac{\partial \tau_{\phi\theta}}{\partial \theta} + 2\tau_{\phi\theta} Cot(\theta) = 0. \tag{3.31b}$$

This shows that the rate of change in all of nonzero stress components is the same and follows the above differential equation. The solution for this first order differential equation is

$$\tau_{\theta\phi} = \frac{c_1}{(Sin\theta)^2}, \tag{3.32a}$$

$$\sigma_{\theta} = -\sigma_{\phi} = \frac{c_2}{(Sin\theta)^2}, \tag{3.32b}$$

where c_1 and c_2 are constant and can be found using boundary conditions. Cone angles used in rheology are generally less than 6^{o} and therefore the θ would vary between 84^{o} and 90^{o}. Table 1 shows the percentage change in the nonzero stress components (the difference between stresses on the flat plate ($\theta = 90^{o}$) and the cone plate surface), for typical cone angles.

Table 3.1: Change in Stresses within the Cone and Plate Specimen.

Cone angle θ_0	**$1/(Sin\theta)^2$**	**Percent change in stresses within the**
1	1.0003047	0.03047
2	1.0012195	0.12195
3	1.0027466	0.27466
5	1.0076543	0.76543

As can be seen, the change in stresses is less than one percent. Therefore, it can be assumed that the stresses are uniformly distributed in the bulk of specimen.

To find the constants in Equation 3.32, we need to consider the boundary conditions and equilibrium. To this end, the relation between the shear stress $\tau_{\phi\theta}$ and the applied torque M was obtained using the toque equilibrium on the flat plate ($\theta = 90^o$):

$$M = \int_0^{2\pi}\int_0^R \tau_{\phi\theta}\, r\, r\, dr\, d\phi = \\ = \int_0^{2\pi}\int_0^R c_1 r^2\, dr\, d\phi = \frac{2\pi R^3 c_1}{3}. \tag{3.33}$$

Knowing that at $\theta = 90^o$ the shear stress $\tau_{\phi\theta} = c_1$ (Equation 3.32), we can rewrite Equation 3.33 as

$$\tau_{\phi\theta} = \frac{3M}{2\pi R^3}, \tag{3.34}$$

where R is the radius of cone plate. Similarly, the normal stresses can be obtained by considering the force equilibrium on the flat plate ($\theta = 90^o$):

$$F_z = \int_0^{2\pi}\int_0^R \sigma_\theta\; r\, dr\, d\phi = \pi R^2 \sigma_\theta. \tag{3.35}$$

Therefore, σ_θ can be written based on the thrust normal force F_z:

$$\sigma_\theta = \frac{F_z}{\pi R^2}. \tag{3.36}$$

This result is in accord with the general solution for the first normal stress difference N_1:

$$N_1 = \sigma_\theta - \sigma_\phi = \frac{2F_z}{\pi R^2}, \tag{3.37}$$

for the case of $\sigma_\theta = -\sigma_\phi$. This stress analysis allows us to find the octahedral shear stress in the specimen,

$$\tau_{oct} = \frac{1}{3}\sqrt{(\sigma_\phi - \sigma_\theta)^2 + (\sigma_\theta - \sigma_r)^2 + (\sigma_r - \sigma_\phi)^2 + 6(\tau_{\phi\theta}{}^2 + \tau_{\theta r}{}^2 + \tau_{r\phi}{}^2)}\ , \tag{3.38}$$

and calibrate Schapery's model constants against the octahedral shear stress invariant.

Conducting the creep and recovery snapshots at different levels of octahedral shear stress τ_{oct} (as shown in Figures 3.4 and 3.5) allowed us to find the nonlinear model parameters as a function of τ_{oct}. To obtain the material parameters in this study, the author followed the approach was originally set forth by Schapery (*1969*). Considering Equation 3.18, it can be shown that the shear strain under step stress τ follows

$$\gamma(t) = \left[g_0 J_0 + g_1 g_2 J_1 \left(\frac{t}{a_\sigma} \right)^n \right] \tau. \tag{3.39}$$

During unloading it becomes

$$\frac{\gamma_r(t)\, g_1}{\gamma_T(t_1)} = [1 + a_\sigma \lambda]^n - (a_\sigma \lambda)^n, \tag{3.40}$$

where $\gamma(t)$is the measured strain during creep; $\gamma_T(t_1)$ is the time dependent strain at time t_1, the end of creep; $\gamma_r(t)$ is measured strain during recovery; and λ is

$$\lambda = \frac{t - t_1}{t_1}. \tag{3.41}$$

Using Equation 3.40 and recovery data from each creep and recovery snapshot, the first two parameters (g_1 and a_σ) were obtained at different levels of interaction. Then, using Equation 3.39 and creep data from each creep and recovery snapshot, two other parameters (g_0 and g_2) were obtained. Applying this approach to obtain nonlinear

parameters ensures the uniqueness of solution. Figures 3.6 through 3.9 show the nonlinear model parameters as a function of τ_{oct}, for the asphalt binder PG 76-22 at 28°C. Exponential and polynomial functional forms that best fit the data for the nonlinear parameters were chosen with the realization that these functions are effective only within the range of octahedral shear stress that were measured and must not be extrapolated.

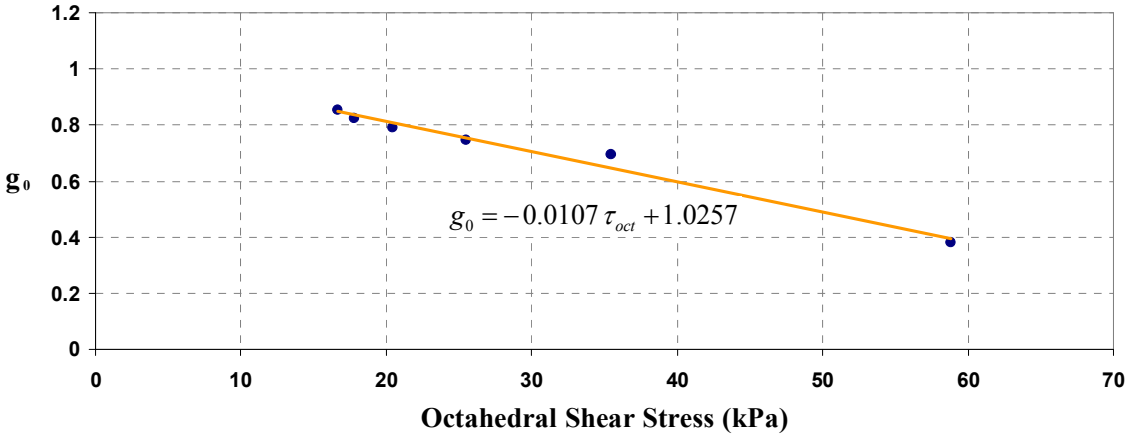

Figure 3.6: Parameter g_0 as a function of τ_{oct}, for PG 76-22 at 28 °C.

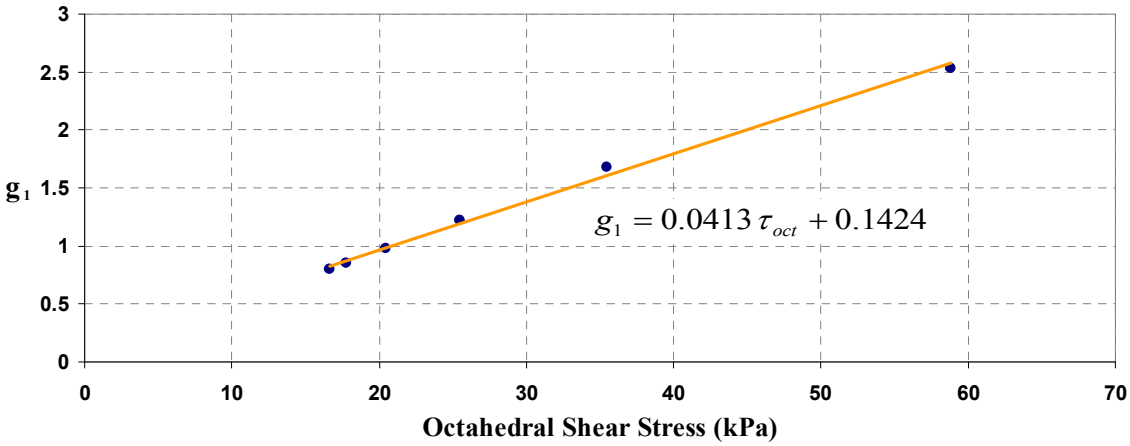

Figure 3.7: Parameter g_1 as a function of τ_{oct}, for PG 76-22 at 28°C.

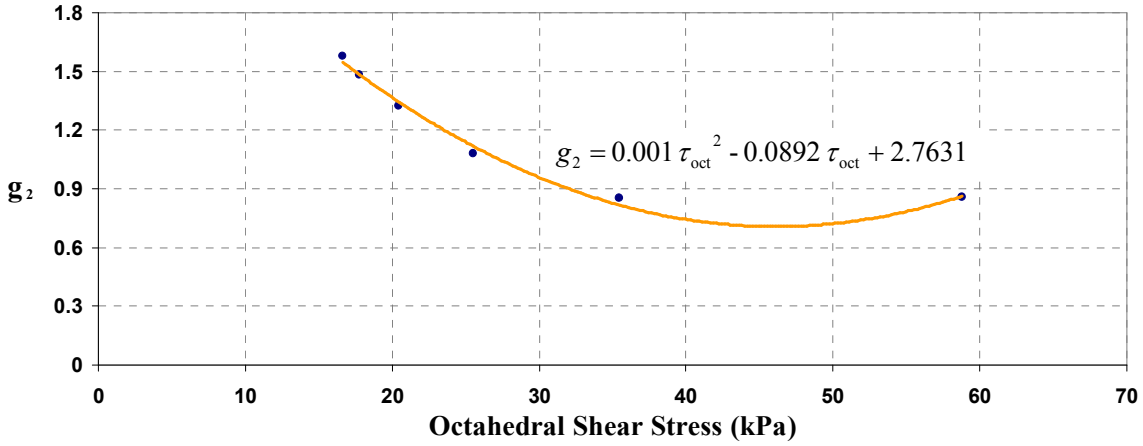

Figure 3.8: Parameter g_2 as a function of τ_{oct}, for PG 76-22 at 28 °C.

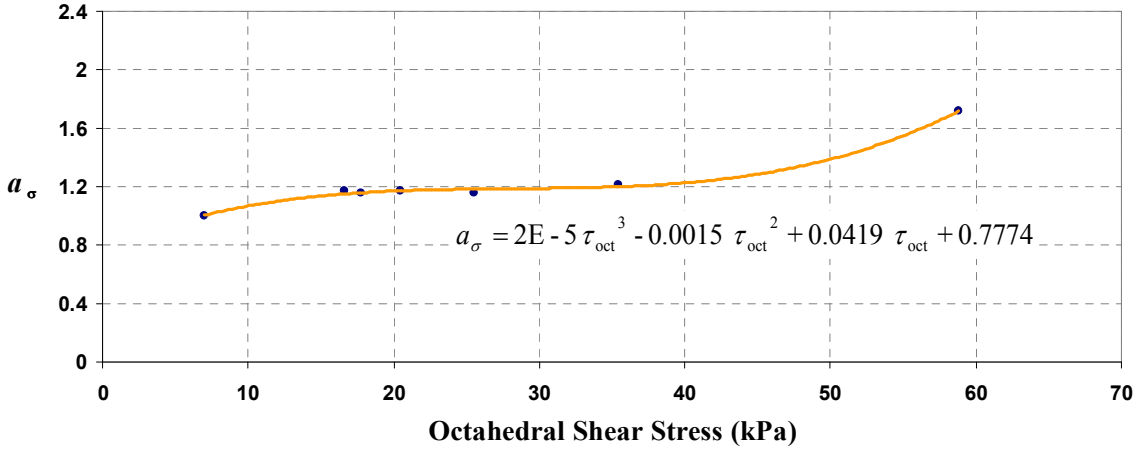

Figure 3.9: Parameter a_s as a function of τ_{oct}, for PG 76-22 at 28 °C.

3.6.3. Model Verification

After defining all the model parameters in Schapery's model (Equation 3.18), the proposed nonlinear model was evaluated under loading conditions different from those used to obtain the parameters. To perform the integration in Equation 3.18 and predict the shear strain, the author made use of trapezoidal numerical integration with small time steps. First, the model was verified for an oscillatory type of loading to evaluate whether the interaction nonlinearity can explain the observed nonlinear behavior under an amplitude sweep test (Figure 3.2). To this end, the material response under sinusoidal loading (with different amplitudes and frequencies) were predicted using the model and compared to the measured response using a DSR. Figure 3.10 compares the predictions from the nonlinear model to the laboratory measurements for asphalt binder PG 76-22, tested at the stress amplitude of 48.1 kPa and frequency of 0.1 Hz. The testing temperature was 28^{o}C at which the model parameters were calibrated. As can be seen, the predictions from nonlinear model are in good agreement with the laboratory measurements. For a better comparison, Figure 3.10 also shows the prediction for a linearly viscoelastic material, obtained using the Boltzmann superposition integral. These comparisons demonstrate that (i) there is a significant deviation from linear behavior (approximately 31%), and (ii) the observed nonlinear behavior can be modeled by accounting for the interaction nonlinearity. Similar comparisons for different frequencies and stress levels further corroborated these findings. Figure 3.11 shows similar results for a stress level of 34.4 kPa and a frequency of 1 Hz.

To further validate the model, the asphalt binder response was measured under stress controlled ramp loading. Figures 3.12 and 3.13 show the applied shear stress, measured shear strain, and the developed normal stress for two different loading rates (900 Pa/s and 450 Pa/s, respectively). The stress increased linearly from 0 to 45 kPa. The testing temperature was 28^{o}C, the same temperature at which the model parameters were calibrated.

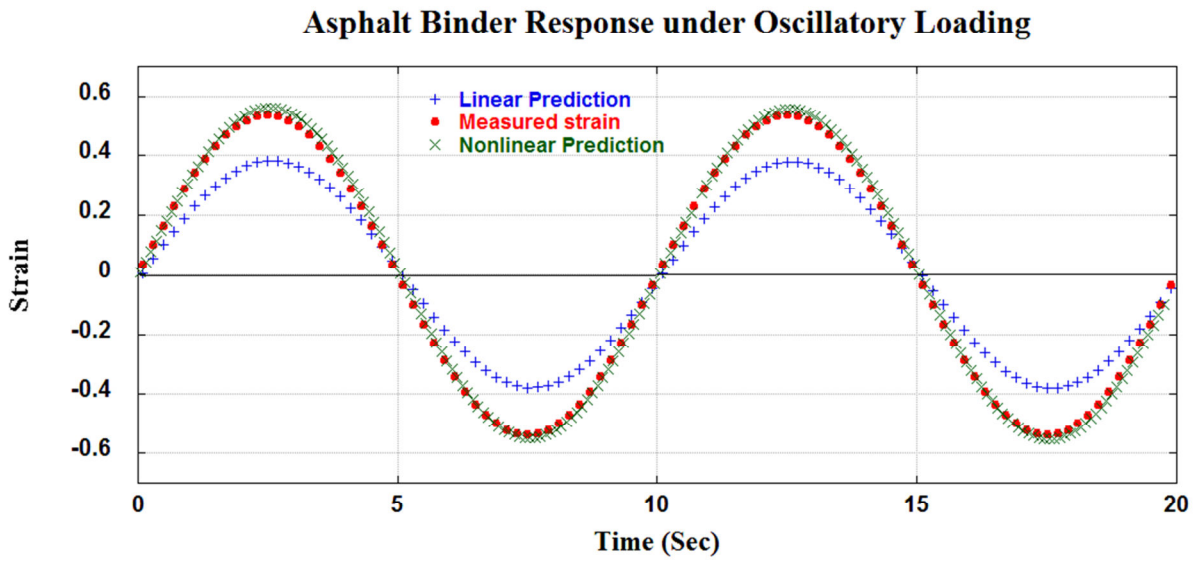

Figure 3.10: A comparison of model computations and laboratory measurements for asphalt binder PG 76-22, at a 48.1 kPa shear stress level, 0.1 Hz, and 28°C. The average measured first normal stress difference (N_1) was 151 kPa.

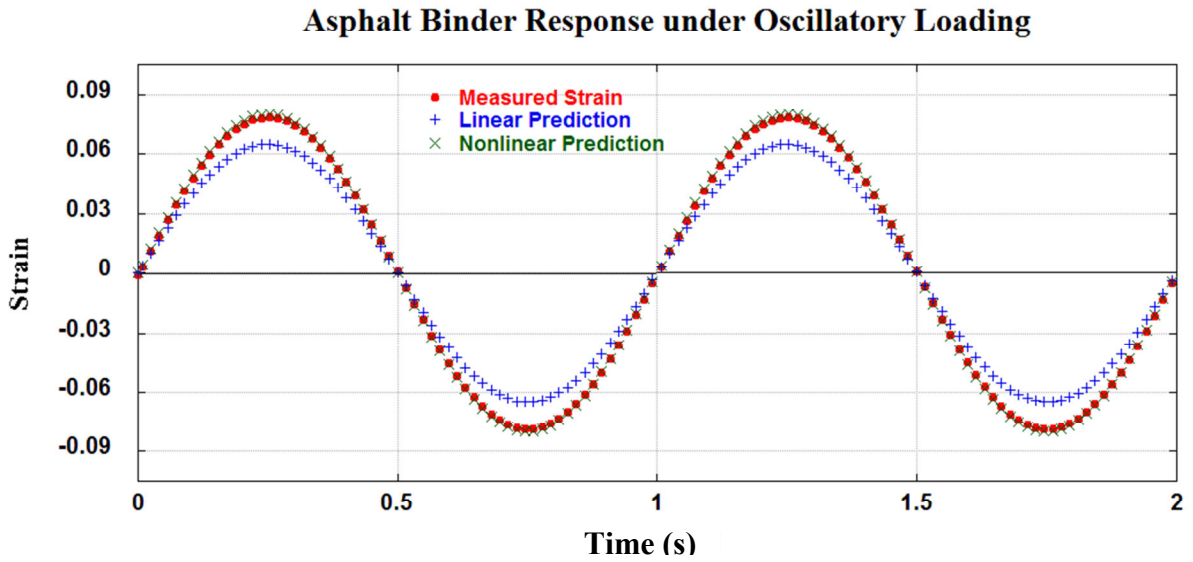

Figure 3.11: A comparison of model computations and laboratory measurements for asphalt binder PG 76-22, at a 34.4 kPa shear stress level, 1 Hz, and 28°C. The average measured first normal stress difference (N_1) was 90.6 kPa.

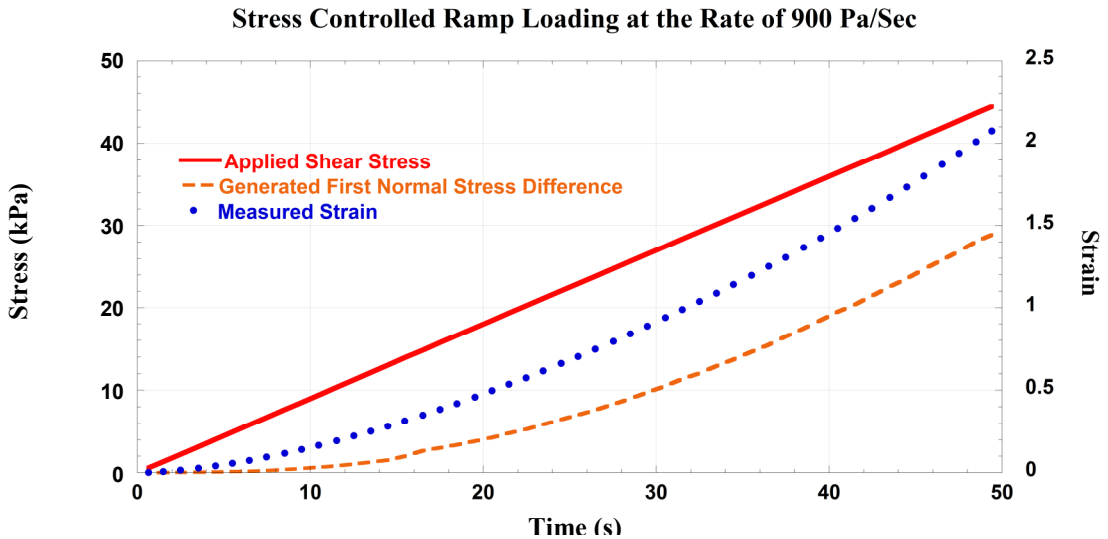

Figure 3.12: The response of asphalt binder PG 76-22 under ramp loading with the rate of 900 Pa/s at 28°C. Where N_1 is the first normal stress difference.

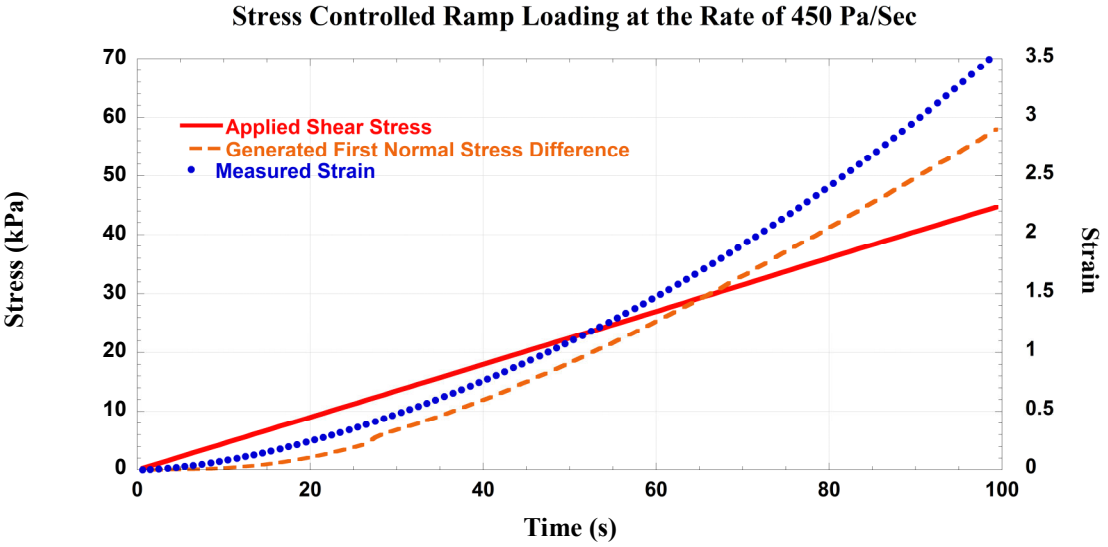

Figure 3.13: The response of asphalt binder PG 76-22 under ramp loading with the rate of 450 Pa/s at 28°C. Where N_1 is the first normal stress difference.

The test results show that the lower rate of loading led to more shear deformation and generated higher normal force levels. Similar to the case of oscillatory loading, the proposed nonlinear model was utilized to predict the asphalt binder response. The octahedral shear stress was determined using the stress history (the state of stress) illustrated in Figures 3.12 and 3.13. Schapery's model (Equation 3.18), which had been calibrated against the octahedral shear stress (using the creep and recovery snapshots), was then applied to predict the material response. Figures 3.14 and 3.15 compare the predictions from the nonlinear model with the laboratory measurements for asphalt binder PG 76-22 tested at the loading rates of 900 Pa/s and 450 Pa/s, respectively.

In addition, the linearly viscoelastic response was also obtained for comparison with the nonlinear response and data. The linear prediction matches the measured response for the first few seconds of loading. As the deformation and generated normal stress increase, the material response deviates notably from linearity. In contrast to the linear model, the predictions from nonlinear model are in good agreement with the laboratory measurements. This demonstrates that the observed nonlinear behavior in an asphalt binder can be modeled by considering the three-dimensional state of stress in the material when it is being characterized in a dynamic shear rheometer under large strains.

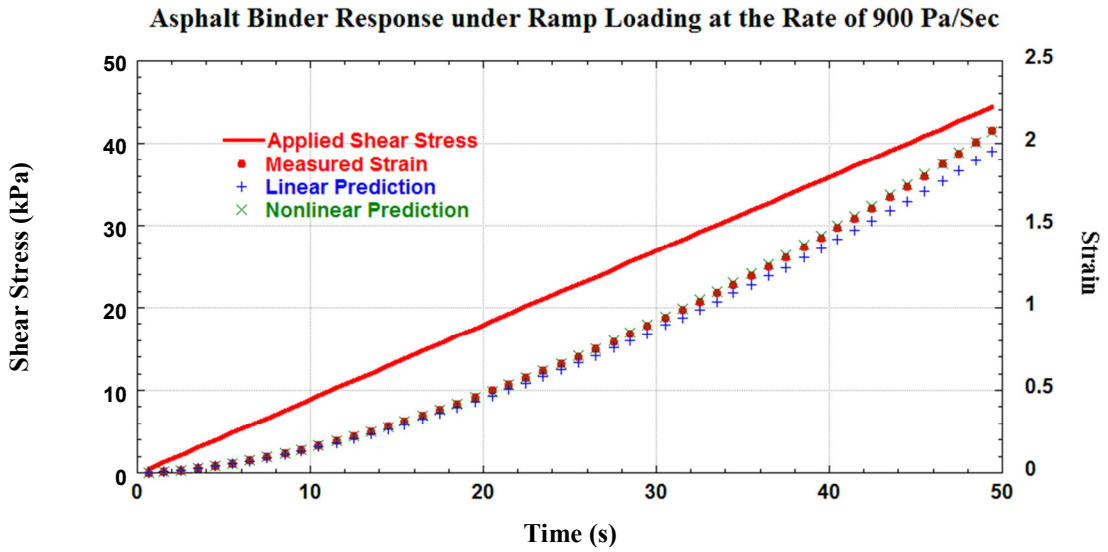

Figure 3.14: A comparison of model computations and laboratory measurements for asphalt binder PG 76-22 under ramp loading with the rate of 900 Pa/s at 28°C.

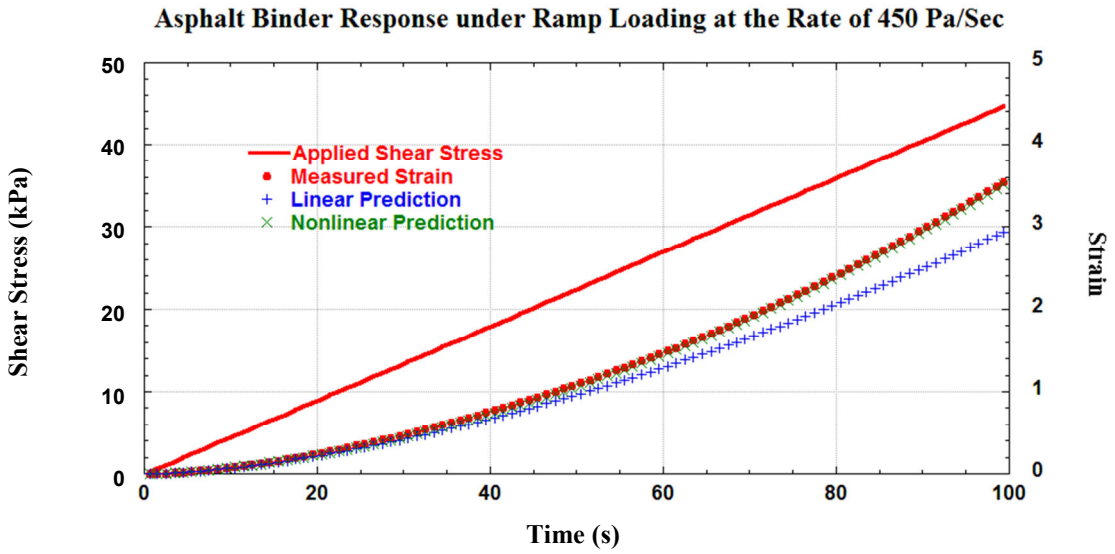

Figure 3.15: A comparison of model computations and laboratory measurements for asphalt binder PG 76-22 under ramp loading with the rate of 450 Pa/s at 28°C.

3.7. SUMMARY AND CONCLUSION

Asphalt binders experience a change in free volume or dilatation when subjected to shear stresses. The change in free volume along with the geometric nonlinearity in an axially constrained specimen subjected to torsion will result in the generation of normal stresses, which in turn leads to an interaction nonlinearity. In other words, the response of the asphalt binder to shear stresses also depends on the magnitude of normal stresses. Given the fact that asphalt binders are used as the matrix in asphalt mixture composites and experience a variety of stress states due to traffic loads, it is important to develop an appropriate constitutive model that accommodates this interaction nonlinearity.

This research extended the previous study on the source of nonlinear response in asphalt binders by modeling the interaction nonlinearity. The overall state of stress in the material was represented by the octahedral shear stress. In order to model both intrinsic and interaction nonlinearity, Schapery's nonlinear viscoelastic equation was modified and the model parameters (as a function of octahedral shear stress) were obtained by conducting creep and recovery snapshots at different levels of octahedral shear stress. The resulting model was used to predict the material response under oscillatory and ramp loadings. The results were in good agreement with DSR measurements. The model verification under different loading histories further corroborates the existence of an interaction nonlinearity. This model can be incorporated into computational methods for more realistic modeling of the micromechanics of asphalt mixtures in order to better predict pavement performance.

Chapter 4: Bulk Modulus of Asphalt Binders[1]

4.1. OVERVIEW

The properties of asphalt binders strongly influence the overall mechanical response of asphalt mixture composites. A thorough understanding of the mechanistic behavior of asphalt binders is important in order to fully and accurately characterize the behavior of the asphalt mixture. The mechanical properties of the asphalt binder, the matrix in the asphalt mixture composite, are time and temperature dependent and have a lower stiffness compared to the inclusions (aggregate particles). However, computational methods used to model the micromechanics of asphalt mixtures typically assume a constant bulk modulus or Poisson's ratio for asphalt binders. This chapter investigates the time-dependence of the bulk modulus of an asphalt binder. Several approaches for measuring the bulk modulus were explored and the poker-chip geometry was found to be the most suitable one. The boundary value problem for the poker-chip geometry was solved to determine the bulk modulus and Poisson's ratio of an asphalt binder as a function of time. The findings from this research improve the understanding of asphaltic materials behavior, and also guide important assumptions typically made during computational modeling of asphaltic materials.

1- A significant portion of this chapter has been submitted for publication to the Journal of Mechanics of Time Dependent Materials; Motamed, A., Bhasin, A., Liechti, K.M.: Using the poker chip test for determining the bulk modulus of asphalt binders. *J. Mech. Time-Depend. Mater.,* (2012)

4.2. INTRODUCTION AND MOTIVATION

Computational methods are being increasingly used to model the mechanical response of asphalt composites based on the properties of their constituent materials (mineral aggregate, asphalt binder, and air). These methods are also used in a micromechanics framework to characterize damage evolution in the composites. Therefore, computational methods not only save time and resources in evaluating the performance of different asphalt mixtures, but they also allow industry to innovate and develop newer technologies to design more efficient highway structures and materials. However, the success of computational methods is contingent upon the accuracy of the constitutive relationships that are used to describe the constituent materials behavior.

The mechanical properties of the asphalt binder or mastic, the matrix in the asphalt mixture composite, are time and temperature dependent and have a lower stiffness compared to the inclusions (aggregate particles). Several research studies demonstrated that the properties of the asphalt binder significantly influence the overall mechanical response of the asphalt mixture composite (*Di Benedetto et al., 2004; Delgadillo, 2008*). Therefore, accurate constitutive relationships for the asphalt binder are crucial to ensuring accurate predictions of the mixture behavior. However, computational methods to model the micromechanics of asphalt mixtures typically use (i) linear viscoelastic models to describe the shear properties of the asphalt binder, and (ii) a constant bulk modulus or Poisson's ratio for the asphalt binder. The previous studies by the author examined the sources of nonlinear response in asphalt binders subjected to shear (Chapter 2), and introduced a thermodynamic-based constitutive equation to model these nonlinearities (Chapter 3). This chapter further investigates the viscoelastic behavior of asphaltic materials by measuring the time-dependence of the bulk modulus of asphalt binders.

Different assumptions are typically employed regarding the time-dependent behavior of the bulk modulus of asphalt materials during computational modeling. For example, it can be assumed that the material is elastic in dilatation [e.g., in the work of You et al. (*2007*)]. This assumption implies that the Poisson's ratio changes with time

while the bulk modulus is constant. An alternative to this assumption is that the bulk modulus and shear modulus have similar time dependency [e.g., in the works of Kim and Lutif (*2008*), and Karki (*2010*)]:

$$\frac{K(t)}{G(t)} = c, \tag{4.1}$$

where $K(t)$ is the bulk modulus, $G(t)$ is the shear modulus, and c is a constant. This assumption, which is known as synchronous shear and bulk moduli, implies that the Poisson's ratio does not change with time. Finally, some studies have also assumed the asphalt binder to be incompressible (*Read and Whiteoak, 2003; Al-Khateeb et al., 2006; Delgadillo, 2008*; *Johnson, 2010; Luo and Lytton, 2011*). This implies that the bulk modulus is infinite and the Poisson ratio is 0.5. Investigating the validity of these assumptions is important to ensure the accuracy of computational models at the material and mixture length scale. Although many researchers have measured the bulk modulus of asphalt mixtures (*Lee, 1976; Stroup-Gardiner et al., 1997; Read, 2000; Long, 2001; Maher and Bennert, 2008; Kim et al., 2010*), there have only been few studies (*Kim, 2009; Di Benedetto et al., 2007*) intended to measure the bulk modulus of asphalt binders. Since these approaches, which will be discussed in the next section, were either not successful or hard to implement, this study further investigates the time-dependence of the bulk modulus of asphalt binders.

Section 4.3 presents a review of the different approaches that can be used to measure the bulk modulus. This review was conducted to identify the most appropriate method to measure the bulk modulus (and any time dependence) of asphalt binders. Section 4.4 solves the boundary value problem for the selected poker-chip geometry. This is followed by the description of the experiment (Section 4.5) and the analysis of the results (Section 4.6).

4.3. BACKGROUND

Four different approaches were considered for measuring the bulk relaxation modulus of asphalt binders:

- The use of two separate tests (uniaxial and shear)
- The use of a long cylindrical test geometry in tension or compression
- The use of the confined compression test
- The use of Poker-chip geometry in tension or compression.

Uniaxial and shear tests are often conducted separately in order to determine the bulk behavior through inter-conversion. This approach appears to be relatively simple but requires special attention due to the fact that (i) any changes in bulk modulus may occur in a shorter period of time than the viscoelastic transition in tension or shear (*Park, 2004*); and (ii) when materials are nearly incompressible (rubbery regime), small errors in the measurements of shear or tensile properties will lead to significant errors in the calculation of the bulk property. This can be seen from the interrelation

$$\widetilde{K} = \frac{\widetilde{G}\,\widetilde{E}}{3(3\widetilde{G} - \widetilde{E})}, \tag{4.2}$$

in the Carson-transformed domain. In the rubbery regime, the material becomes incompressible and therefore $\widetilde{E}$ approaches $3\widetilde{G}$. This implies that the denominator will approach to zero and consequently a small error in measuring $\widetilde{E}$ or $\widetilde{G}$ will result in significant errors in the calculation of $\widetilde{K}$. Furthermore, it is not generally feasible to fabricate a bulk test specimen of an asphalt binder at or above room temperature for uniaxial tests. Kim (*2009*) used this approach to measure the bulk modulus of asphalt binders at low temperatures (below 5°C). Kim first measured the dynamic Young's modulus E^* using Hollow Cylinder Tensile Tester (HCT). Then, he measured the dynamic shear modulus G^* using a Dynamic Mechanical Analyzer (DMA). Applying

interrelations, Kim obtained the dynamic Poisson's ratio ranging from -0.5 to 1.14. Kim (*2009*) concluded that these unrealistic values of Poisson's ratio should be due to errors in the measurement or in the test setup.

The second possible approach to measure the bulk modulus is to conduct a tension or compression test using long cylindrical test specimens and measure the axial and radial displacements (*Arzoumanidis and Liechti, 2003*). This approach directly measures the Young's modulus and Poisson's ratio of the material, while the other material constants can be obtained using the interrelations. Although this method is more robust and does not need special care regarding the measurements in the rubbery regime, it has the same limitation as the previous method, in that it is not feasible to fabricate and test a bulk test specimen of an asphalt binder at or above room temperature for uniaxial tests. The other drawback of this approach could be difficulties in test set up and specimen fabrication. Di Benedetto and coworkers (*2007*) used this approach to measure the three-dimensional linear properties of asphalt binders at low temperatures (below 0°C). They investigated the time and temperature dependence of Poisson's ratio and demonstrated that asphalt binders are not necessarily incompressible. While the findings from their research were insightful, their approach was also limited to measurements at low temperatures.

The third possible approach to measure the bulk modulus is to use the confined compression test (*Ma and Ravi-Chandar, 2000; Park et al., 2004; Qvale and Ravi-Chandar, 2004*). This approach is very efficient and can measure both bulk and shear modulus by only conducting one test. However, the confined compression test requires frictionless contact between the material and the confining cylinder. Since satisfying this condition for asphalt binders is difficult and in view of the aforementioned limitations of the other approaches, the author selected the poker-chip geometry to measure bulk modulus of the asphalt binder. The poker-chip test method, also known as the longitudinal bulk relaxation modulus test, is described in the next section.

4.4. Analytical Solution for Poker-Chip Geometry

The poker chip geometry was selected to measure the bulk relaxation modulus. To this end, we can apply a step strain load and measure the axial stress as it relaxes. For small axial deformations, the relationship between strains and displacements are linear (verified later). Furthermore, the poker chip geometry typically has a high diameter to thickness ratio, and consequently the lateral displacement in the specimen can be neglected. Under these conditions, it can be shown that the axial stress is a function of bulk and shear modulus.

The stress and strain tensors can be decomposed to the hydrostatic and deviatoric components:

$$\sigma_z = S_z + \frac{1}{3}\sigma, \tag{4.3}$$

and

$$\varepsilon_z = e_z + \frac{1}{3}\varepsilon, \tag{4.4}$$

where σ_z is the normal stress in the *z*-direction (the direction of axial loading), S_z is the deviatoric stress in the *z*-direction, σ is the sum of the normal stresses, ε_z is the normal strain in the *z*-direction, e_z the deviatoric strain in the *z*-direction, and ε in the sum of normal strains. Under a small step axial displacement, the lateral displacements and strains will be negligible:

$$\varepsilon = \varepsilon_r + \varepsilon_\theta + \varepsilon_z = \varepsilon_z . \tag{4.5}$$

Thus, the deviatoric strain in the *z*-direction is

$$e_z = \frac{2}{3}\varepsilon_z . \tag{4.6}$$

Using the linearly elastic, isotropic constitutive relationships

$$S_z = 2G e_z \tag{4.7}$$

and

$$\sigma = 3K\,\varepsilon\,, \tag{4.8}$$

Equation 4.3 can be rewritten as

$$\sigma_z = 2G e_z + K\,\varepsilon = \frac{4}{3} G\,\varepsilon_z + K\,\varepsilon_z = \left[\frac{4}{3}G + K\right]\varepsilon_z\,. \tag{4.9}$$

Using the correspondence principle, material response can be obtained in the Laplace domain:

$$\overline{\sigma}_z(s) = s\left[\frac{4}{3}\overline{G}(s) + \overline{K}(s)\right]\overline{\varepsilon}_z(s). \tag{4.10}$$

Finally, by applying the inverse Laplace transform, the material response (the axial stress as a function of time) can be obtained in the time domain:

$$\sigma_z(t) = \int_0^t \left[\frac{4}{3}G(t-\xi) + K(t-\xi)\right]\frac{\partial \varepsilon_z(\xi)}{\partial \xi}\,d\xi. \tag{4.11}$$

For a step strain loading

$$\varepsilon_z(t) = \varepsilon_0\,H(t), \tag{4.12}$$

the axial stress would be

$$\sigma_z(t) = \left[\frac{4}{3}G(t) + K(t)\right]\varepsilon_0\,, \tag{4.13}$$

where $K(t)$ is the bulk modulus, $G(t)$ is the shear relaxation modulus, $H(t)$ is the step function, and ε_0 is the magnitude of the step strain. Therefore, to find the bulk modulus $K(t)$ from the poker-chip test, one first needs to find the shear relaxation modulus $G(t)$ by conducting a creep or relaxation test in shear.

It should be noted that this formulation is valid for small axial deformations and away from the edges. At the edges, the stress and strain field are complicated and do not follow the abovementioned assumptions. Masuoka and Nakao (*1978*) investigated the displacement field at the edge of square test geometry in tension and demonstrated that there is a lateral displacement close to the edges. Therefore, this formulation can only be used for high aspect ratios (diameter/thickness), for which the edge effect is minimal. Section 4.5.2.3 discusses the effect of aspect ratio on the apparent elastic modulus of thin films. The next section presents the laboratory test procedures used in this study.

4.5. LABORATORY TESTING

4.5.1. Materials and Test Method

Two different asphalt binders were selected with similar performance grades following the Superpave specification: PG 64-16 (*Binder 1*) and PG 67-22 (*Binder 2*). A Dynamic Shear Rheometer DSR (Model TA AR2000Ex) was used to measure the mechanical response of the asphalt binders when subjected to different shear stress levels. The poker-chip test in compression was conducted to measure the bulk modulus of the asphalt binders. In order to conduct the poker-chip test, a tension-compression dynamic mechanical analyzer (DMA- Model Instron ElectroPuls E1000) was used. The tests were conducted at 20ºC. To ensure the same testing temperature inside these two testing devices, dummy specimens with a thermocouple in the middle were used for calibration of the temperature controller. The asphalt binders were RTFO-aged to simulate the short-term aging during production and placement. The test temperature was well above the glass transition temperature (T_g) of asphalt binders; which is typically in the range of *-30* $^{\circ}C$ to *-5* $^{\circ}C$. The next two subsections present the test geometry and procedure used in this study.

4.5.2. Test Geometry

4.5.2.1. Shear Test

The selection of appropriate test geometry for use with the DSR is important to accurately characterize the shear properties of the asphalt binders. There are two different geometric configurations that are typically used to test asphalt binders with a DSR at intermediate to high temperatures. The first and the most common is the cylindrical specimen between two parallel plates with the top plate being subjected to torsion and the bottom plate being fixed. The use of parallel plate has some disadvantages such as non-uniform stress and strain distribution across the cross section of specimens, and instability flow at intermediate to high temperatures (*Motamed and Bahia, 2011*). Therefore, it is not recommended to use the parallel plate geometry to determine the true material properties (*Motamed and Bahia, 2011; Carreau et al., 1997*).

The second configuration, although not as commonly used for asphalt binders, is the cone and plate geometry. The difference between the cone and plate geometry and the parallel plate geometry is that the former has a conical shaped top plate. This geometry ensures that the shear strain rate is approximately uniform throughout the specimen. Therefore, this geometry is more suitable for accurate measurement of material properties and was selected in this study to characterize the shear behavior of the asphalt binders. The diameter of the cone and plate was 25 mm. The cone had an angle of 2° (2:17':42") and a truncation gap of 56 μm. Additional details comparing these two geometries can be found in the text book by Macosko (*1995*).

4.5.2.2. Poker Chip Test

To conduct tests using the poker-chip geometry, disc-shaped specimen holders were fabricated to avoid singular corners. Metal discs were fabricated with two different diameters of 14.6 mm and 40 mm. The discs with smaller diameter were used for conducting a set of preliminary test and analysis. The larger diameter discs allowed the

fabrication of thicker test specimens without compromising the aspect ratio. Consequently, these could be used to have a better precision in the measurements of vertical displacement.

Poker-chip test specimens with different aspect ratios were fabricated using the following procedure. First the end plates were clamped to the tension-compression DMA and the device was conditioned for 3 hours at the testing temperature. After the instrument reached steady state, the zero gap was established. Then the asphalt binder was placed on the lower metal plate and the temperature was raised to 100°C. Raising the temperature to 100°C, (i) allows the asphalt binder to spread uniformly, (ii) releases any trapped air bubbles in the asphalt binder, and (iii) promotes bonding between the binder and the metal plates. The high temperature will also minimize the effect of physical hardening (*Bahia, 1991*) on the test results. After holding the temperature at 100°C for 5 minutes, the temperature was decreased to 60°C, which seems to be an appropriate temperature for squeezing the asphalt binder. Finally, thin films with different thickness were prepared by lowering the upper plate and squeezing the asphalt binder between two metal end plates. To avoid any thermal stresses in the specimen, first the upper plate were lowered to a gap larger than the target gap. Then, as the temperature was lowered to the testing temperature, the material and system were allowed to shrink by maintaining zero normal force in the specimen. It was observed by the author that almost forty minutes was required to reach the thermal and concomitant shrinkage equilibrium. Therefore, specimens were conditioned for one hour at the testing temperature before trimming the edge of the specimen. Trimming was followed by another hour of conditioning before the displacement controlled test starts. Figure 4.1 illustrates the compression test set-up for the poker-chip geometry with different aspect ratios.

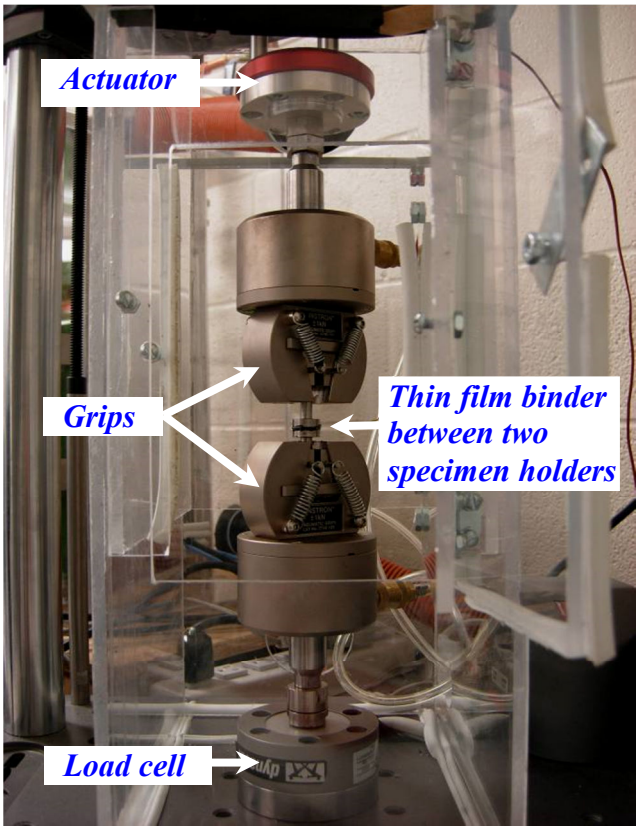

a) Load string in the tension-compression dynamic mechanical analyzer. The disc specimen has a diameter of 14.6 *mm* and a height of 300 μm.

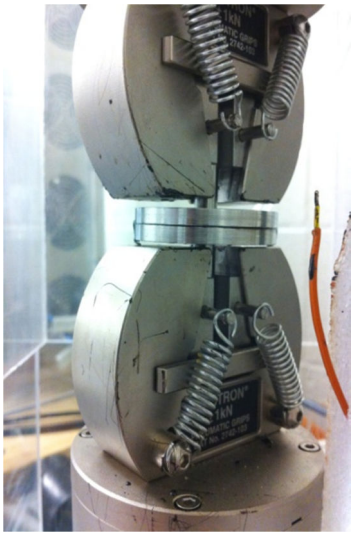

b) A close up of the poker-chip test geometry with a diameter of 40 *mm* and a height of 200 μm.

Figure 4.1: The set up for the poker-chip test geometry.

4.5.2.3. Aspect Ratio in the Poker-chip Test

Gent and Lindley (*1959*) used an analytical approach to the stress analysis of the poker chip specimen and developed a load-displacement relationship for incompressible materials. They showed that for a cylindrical disc with a radius *a* and height *h*

$$E_c = E(1+2S^2), \tag{4.14}$$

where E_c is the apparent modulus of the poker-chip specimen (defined as the ratio of the nominal vertical stress to the nominal vertical strain), E is the elastic modulus of the material, and *S* is the shape factor. The shape factor *S* for a circular disc of the radius *a* and layer thickness *h is*

$$S = \frac{a}{2h}. \tag{4.15}$$

Lindley (*1979*) extended this work by developing the load-displacement relationship for compressible materials. Lindley assumed parabolic displacement profiles through the thickness of the specimen and by using energy considerations and classical elasticity theory showed that

$$E_c = \lambda + 2\mu - \frac{\lambda^2}{15(\lambda+\mu)}\frac{w_2}{w}(8-\frac{w_2}{w}), \qquad (w > w_2) \tag{4.16}$$

where the λ and μ are Lame's constants, *w* is the diameter of the specimen, and w_2 is the diameter at which bulk strain just equals the applied compressive strain (*e*) at *x=0*:

$$w_2^2 = \frac{64(\mu+\lambda)}{15\mu}h^2 \tag{4.17}$$

Lindley examined the accuracy of his model by comparing the model predictions and finite element (FE) simulations, Figure 4.2. As can be seen, at high shape factors (or aspect ratios) the amount of error is less than two percent and for lower values of Poisson's ratio approaches to zero.

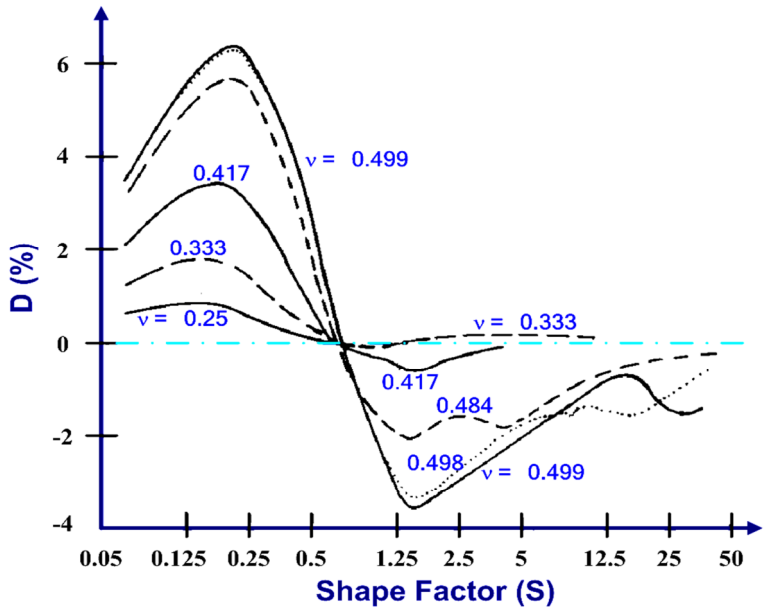

Figure 4.2: The amount of error in the prediction of the apparent elastic modulus of the cylindrical disc specimen (Equation 4.16), compared to FE simulation results, adopted form Lindley (*1979*).

Shariff (*1988*), by making more realistic assumptions, was able to obtain a simpler and more accurate solution:

$$E_c = G\left\{2(1+\nu)+\frac{0.75\,\nu\,k^2}{1+\frac{1-2\nu}{2\nu}+\frac{3(1-2\nu)\,k^2}{16\,\nu}}\right\}, \qquad (4.18)$$

where E_c is the apparent elastic modulus, G is the shear modulus, and ν is the Poisson's ratio, and k is the aspect ratio (diameter/height). Shariff validated his solution by comparing the model predictions with published (experimental and theoretical) data. He showed that his formulation is not only simpler but is also more accurate. Shariff (*1988*) using the Equation 4.18 clearly demonstrated that the apparent elastic modulus is a function of material properties (shear modulus and Poisson's ratio) and the test geometry

(aspect ratio). These analyses also concluded that in two cases the apparent modulus is independent of the test geometry (Figure 4.3). The first case is when the specimen is a long cylinder with a shape factor less than 0.1. In other words, the length of the specimen should be at least 10 times bigger than the diameter of the specimen (recall that this analysis is for cylinders bonded to the end plates). The other case is when the test specimens are thin films with shape factors greater than 20. Fabricating long cylindrical specimens of asphalt binders even at low temperatures is not practical. Therefore, based on the results presented in Figures 4.2 and 4.3, the author decided to use thin films with a high shape factor of 40 or above to eliminate the effect of test geometry on the test results. The author verified the test geometry effect (shape factor) on the test results by conducting a series of preliminary compression tests on thin films of different thickness and 14.6 *mm* diameter. Further evaluations were also conducted using specimens with a larger diameter, 40 *mm*. After verifying the appropriate gap size, the larger diameter discs were used to have a better precision in the measurements of vertical displacement. Thus, considering the radius of the metal disc (20 *mm*) and the selected shape factor (40), the specimen height could be at most 250 μm. This configuration was considered to be optimal for following reasons. Using a higher aspect ratio entailed using a larger diameter substrate disc or smaller film thickness. A larger diameter substrate would reduce the uniformity with which specimens can be fabricated whereas a smaller film thickness would reduce the accuracy of vertical strain measurements.

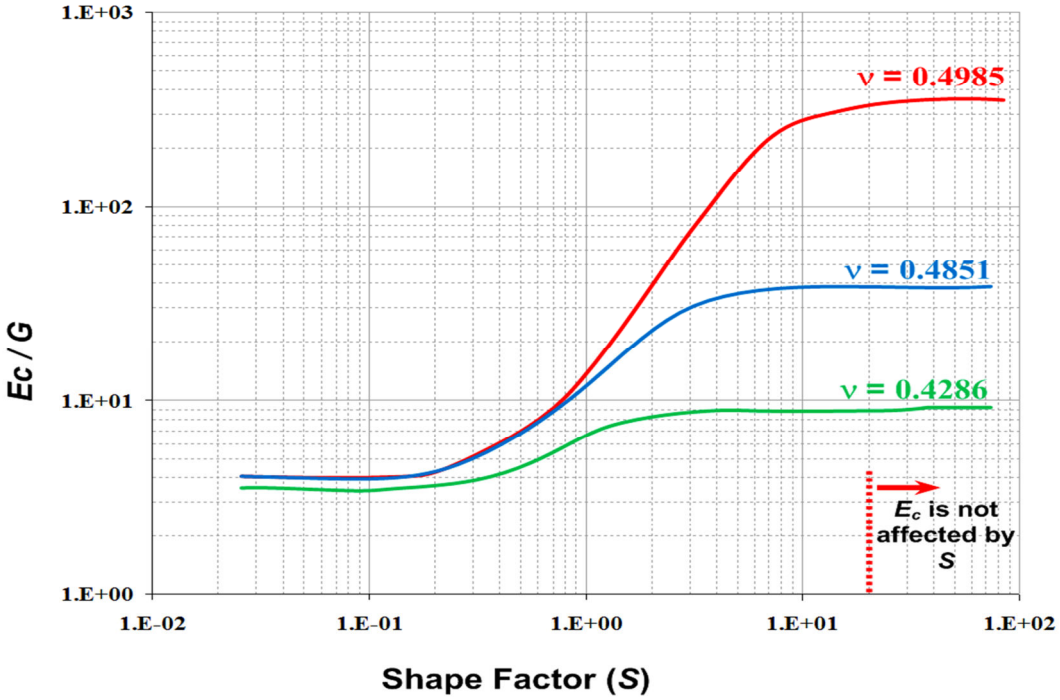

Figure 4.3: The influence of Poisson's ratio and shape factor (aspect ratio) on the apparent elastic modulus of the cylindrical disc specimen, adopted form Shariff (1988).

4.5.3. Test Procedure and Data Collection

Creep and recovery tests were conducted to determine the viscoelastic properties of asphalt binder in shear. Creep and recovery tests were conducted at different stress levels of 1 kPa, 5 kPa, and 20 kPa to examine whether the material behaves linearly in shear. The creep part of the test was twenty seconds long. This loading time was long enough to collect the time dependent response of material for the typical time spans of interest. The selected loading time was much greater than the rise time of the instrument, which is on the order of 10^{-4} second. This ensured the accuracy of the measured data. On the other hand, the loading time was not too long so as to risk damaging the material and causing tertiary flow. In this context, tertiary flow refers to the accelerated unstable creep that is preceded by steady-state creep, due to the change in material or creation of microcracks and cavities (*Lakes, 2009*). The minimum stress amplitude of 1 kPa was

selected to ensure that the lowest stress was well within the linearly viscoelastic limit of the binder (*Delgadillo, 2008; Huang, 2008*). This stress level also caused deformations that were significantly larger than the precision level of the instrument.

The recovery time of 1000 seconds was considered long enough to achieve significant recovery. The creep and recovery at each stress level were repeated twice before proceeding to the next stress level. Results from the second repeat were compared to the first repeat in order to detect whether there was any permanent change or damage to the material during the loading period. Figure 4.4 illustrates the creep and recovery test protocol used in this study.

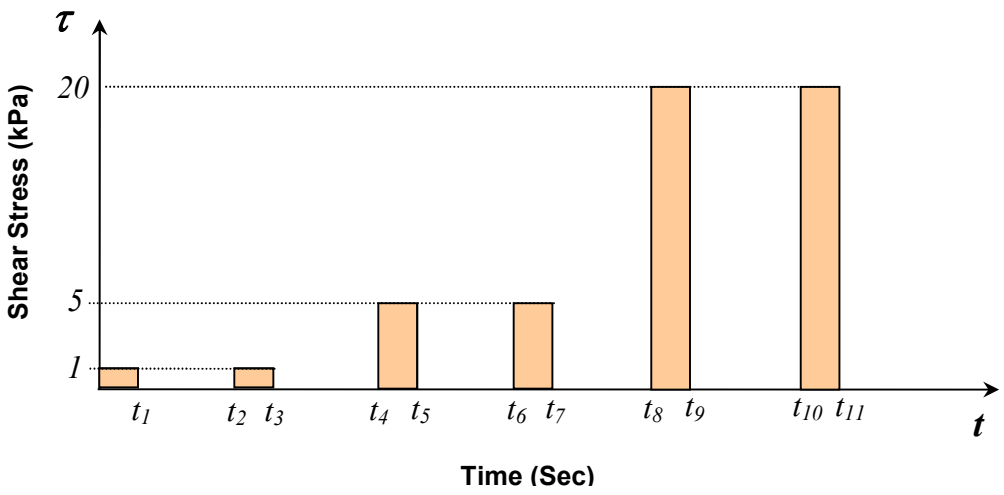

Figure 4.4: Schematic of creep and recovery test protocol in shear.

An identical response under same loading condition would be an indication that no damage or permanent change in the material has occurred. Figure 4.5 illustrates the creep and recovery test results at different stress levels. Figure 4.5*a* shows the measured shear strain under the abovementioned loading condition for *Binder 1* at 20°C. Figure 4.5*b* is the close up of the first creep and recovery test at 5 kPa. These measurements were used to obtain the shear creep compliance of the asphalt binders. Figure 4.6 compares the creep compliance of two asphalt binders at different stress levels. The

results clearly show that the creep compliance of these two asphalt binders does not change at different stress levels. This implies that (i) these two asphalt binders behave linearly at the stress levels below 20 kPa, and (ii) there is no damage or change in materials at these stress levels. It should be also noted that while these two binders behave similarly at very short period of time, their strain response could deviate significantly at a longer periods of time. Each test was replicated three times with consistent results.

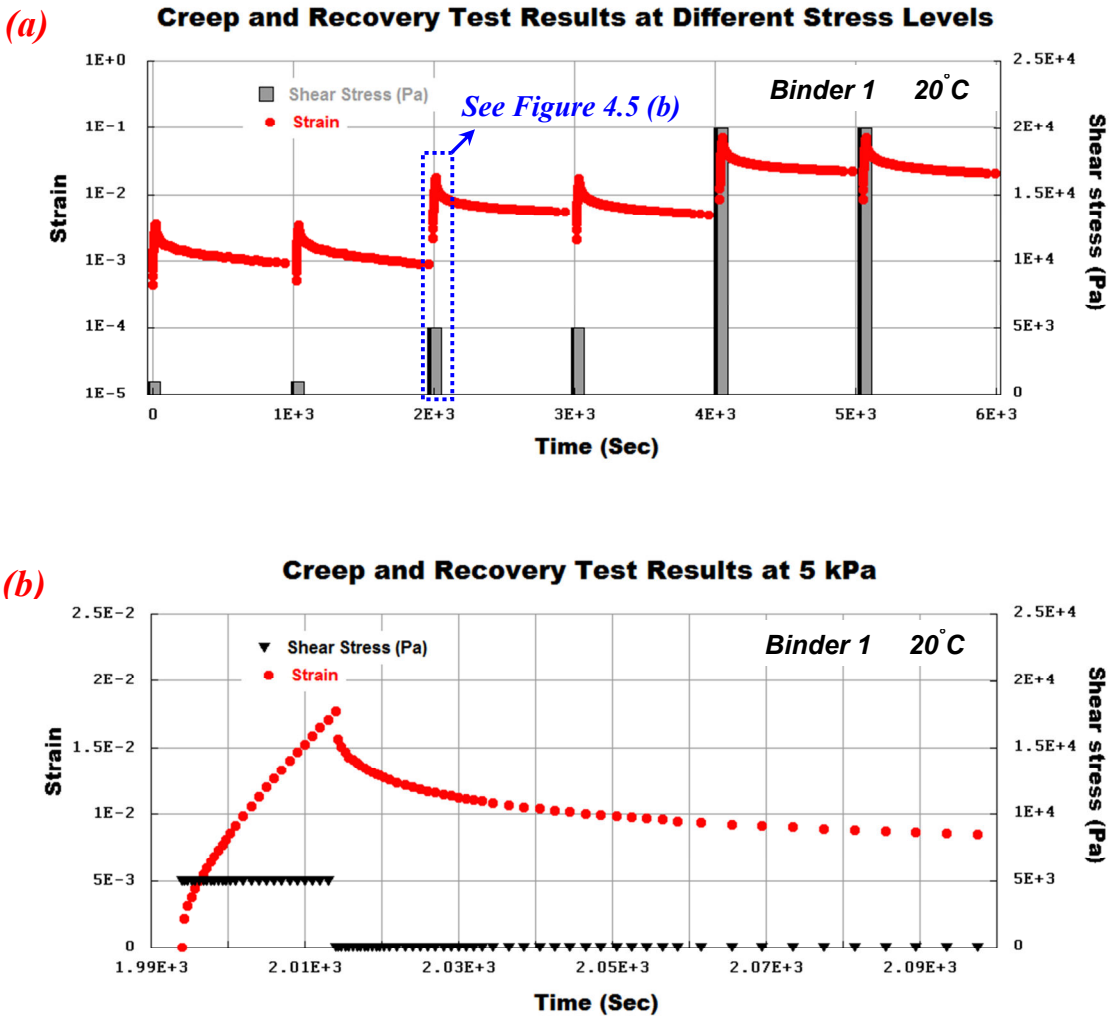

Figure 4.5: Creep and recovery test results at 20°C and different stress levels of 1 kPa, 5 kPa, and 20 kPa.

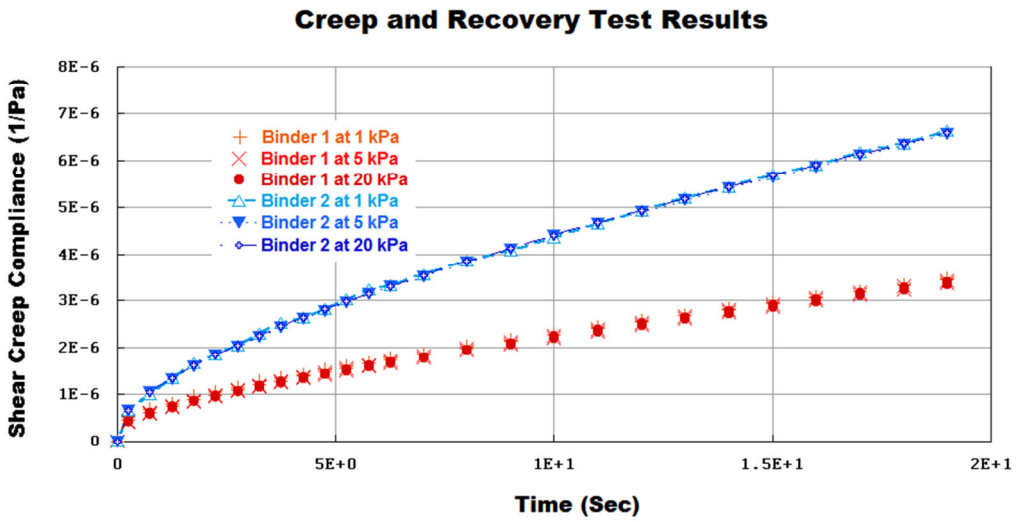

Figure 4.6: Measured shear creep compliance at 20°C and different stress levels.

To measure the bulk properties of asphalt binders, compression tests with poker-chip test geometries were conducted under step displacement. The shape factors for the cylindrical disc specimens were above 40. To examine whether asphalt binders behave linearly in compression, the tests were conducted at two different strain levels (about 3% and 4%) on the same specimen. These strain levels were well above the lowest axial displacement that could be precisely applied by the instrument, but not excessively high to violate the assumption of small deformations. The apparent relaxation modulus of the test specimens was measured for 1000 seconds at each strain level.

The relaxation tests at each strain level were repeated twice before proceeding to the next strain level. Similar to the creep and recovery tests in shear, results from the second repeat were compared to the first repeat in order to detect any permanent change or damage to the material during the loading period. To minimize the effect of loading history, materials rested (zero axial force) for one hour after each relaxation test. Figure 4.7 illustrates the test protocol used for compression relaxation test. Figure 4.8 demonstrates the results from compression relaxation test at 20°C and two different strain

levels. Figure 4.8*b* is the close up of the first 5 seconds of the test at 3 percent strain. As can be seen in Figure 4.8*b*, the rise time of the compression test is almost 0.4 second. To eliminate the effect of rise time on the measured response, the first 2 seconds (five times the rise time) of the collected data should be discarded. It should be noted that the displacement fluctuates within one micron. This is the resolution of the digital encoder for measuring axial displacement. Each test was replicated three times with consistent results. The effect of test geometry on measured apparent modulus was also examined by testing asphalt binder specimens with shape factors ranging from 40 to 60. The test results verified that the apparent Young's modulus is independent of test geometry for this range of shape factors. The next section presents the analysis of the shear and compression test results in order to obtain the bulk properties of asphalt binders.

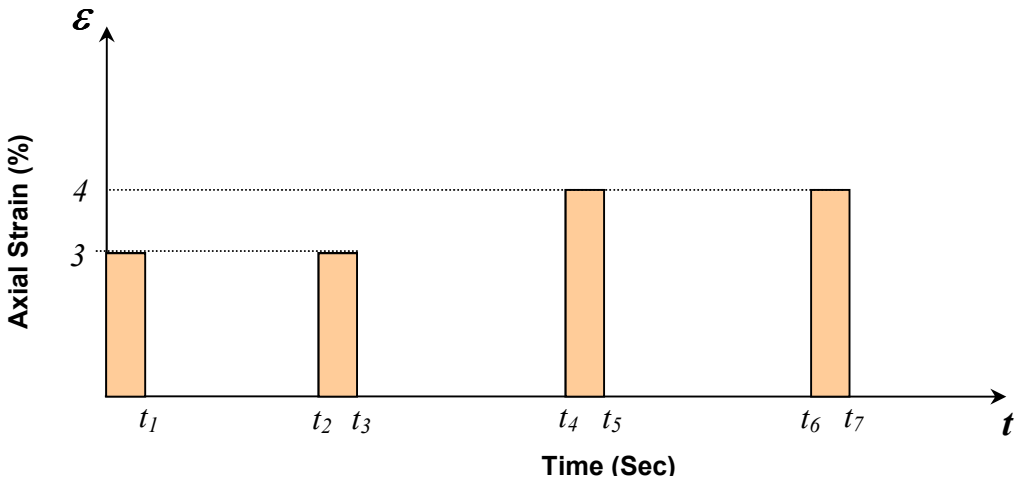

Figure 4.7: Schematic of the test protocol for compression relaxation test.

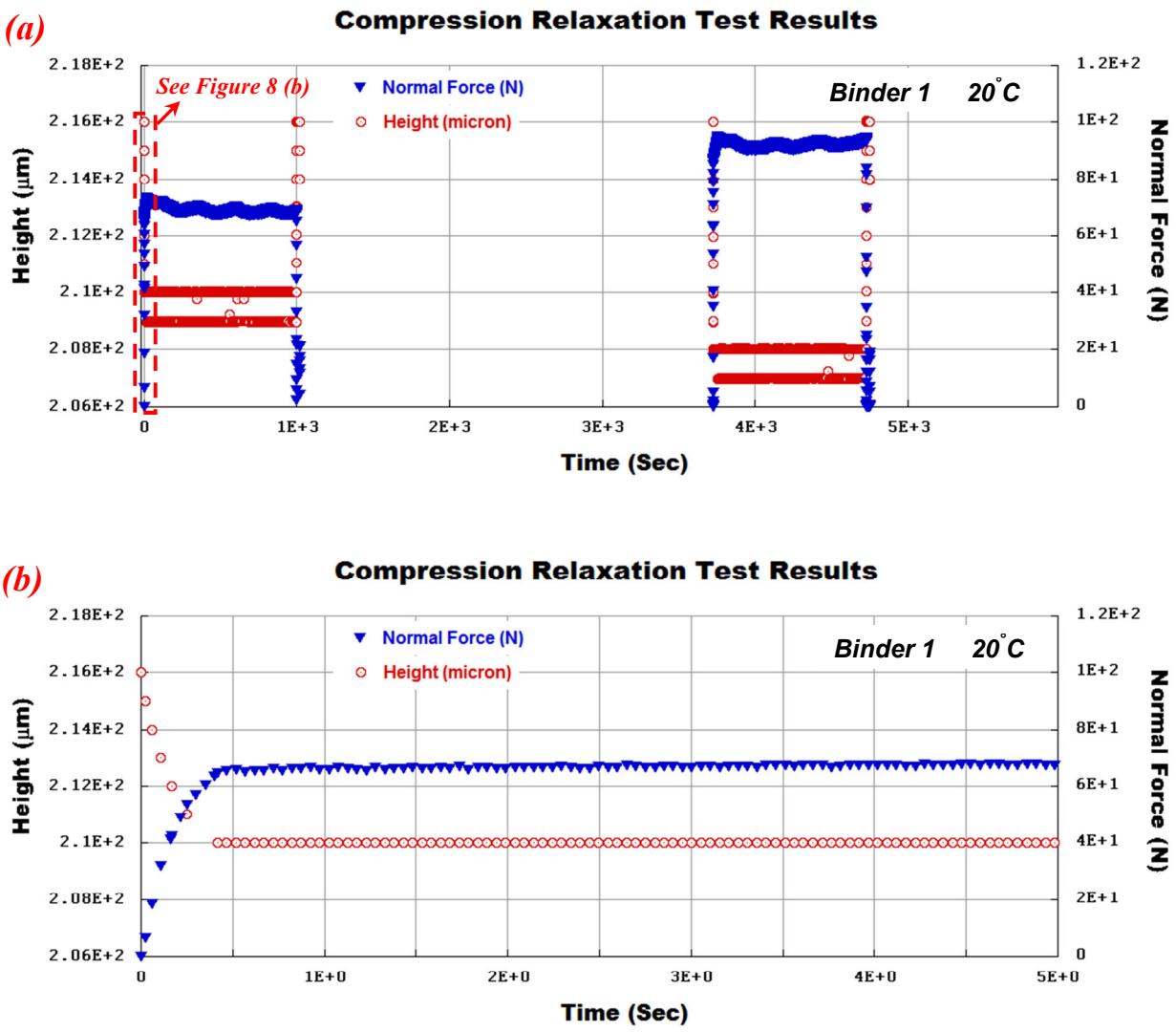

Figure 4.8: Compression relaxation test results at 20°C and different strain levels.

4.6. RESULTS AND ANALYSIS

Using Dynamic Shear Rheometer DSR, material response under creep and recovery shear loading were measured. It was observed by the author that a power-law equation fits well to the measured creep and recovery data:

$$J(t) = J_0 + J\,t^n, \tag{4.19}$$

where J_0, J , and n are material constants. Due to higher sensitivity of these constants to the test duration in creep, these material constants were obtained using only the recovery test data (*Hiel et al., 1984*). Table 4.1 summaries the shear properties of two asphalt binders. Figure 4.9 shows the measured creep and recovery test results (at 1 kPa) and the fitted power-law curves. The material response was estimated using Boltzmann integral and the creep compliance obtained from the recovery at 1 kPa.

Table 4.1: Shear Properties of Asphalt Binders at 20°C.

Asphalt Binder	Creep Compliance (1/Pa)
Binder 1	$J(t)_{Binder\ 1} = (3.32E-7) + (3.16E-7)t^{0.767}$
Binder 2	$J(t)_{Binder\ 2} = (5.73E-7) + (7.43E-7)t^{0.708}$

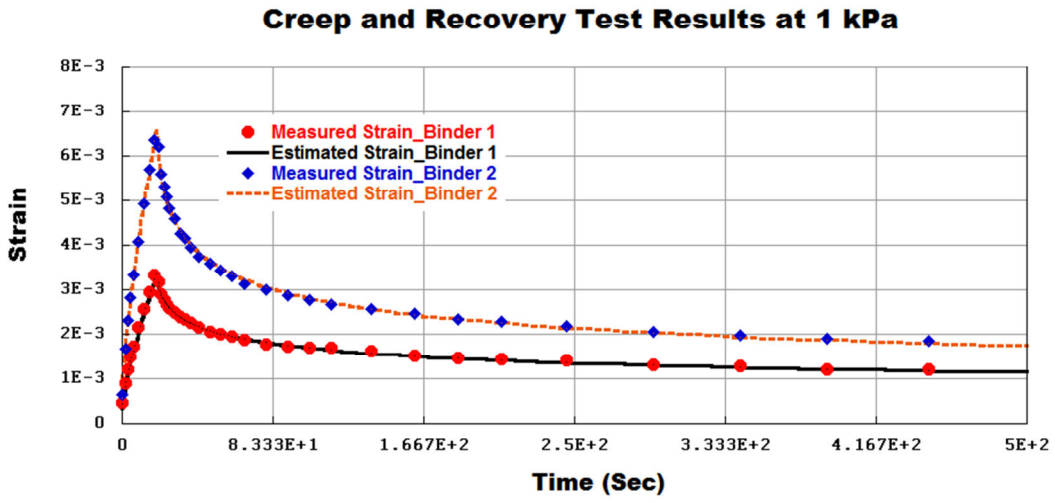

Figure 4.9: Creep and recovery test results at 20°C and 1 kPa, under torsion. Response follows the power-law.

In the next step, using the power-law-based interrelationship, the shear relaxation modulus was obtained from the measured creep compliance (*Leaderman, 1958*) through

$$G(t)\ J(t) = \frac{\sin(n\pi)}{n\pi}, \tag{4.20}$$

where *J(t)* is the shear creep compliance, *G(t)* is the shear relaxation modulus, and *n* is the exponent in the power law equation.

In order to obtain the time-dependent bulk modulus of asphalt binders, a compression relaxation test was conducted to measure the apparent elastic modulus $E_c(t)$ of the poker-chip test geometry:

$$E_c(t) = \frac{\sigma_z(t)}{\varepsilon_0}, \tag{4.21}$$

where $\sigma_z(t)$ in the normal stress in the direction of loading, and ε_0 is the strain level in the axial direction. Figure 4.10 illustrates the measured apparent modulus at 20°C. The results demonstrate that the apparent elastic modulus of the asphalt binders, used in this study, follows the power law. Similar to the case of creep and recovery in shear, the modulus (apparent elastic modulus) of *Binder 2* is more time-dependent and it changes with a higher rate comparing to *Binder 1*. This can be easily seen by comparing the results on a log-log scale plot. In a log-log plot, these two graphs will be represented by straight lines with slopes that are equal to the exponent in the power-law equation. It should be noted that the rate of change in apparent elastic modulus is significantly slower than the rate of change in shear modulus (comparing the exponent of power-law equation for the apparent elastic modulus and shear modulus).

Therefore, the apparent elastic modulus can be considered as a constant for a short period of time.

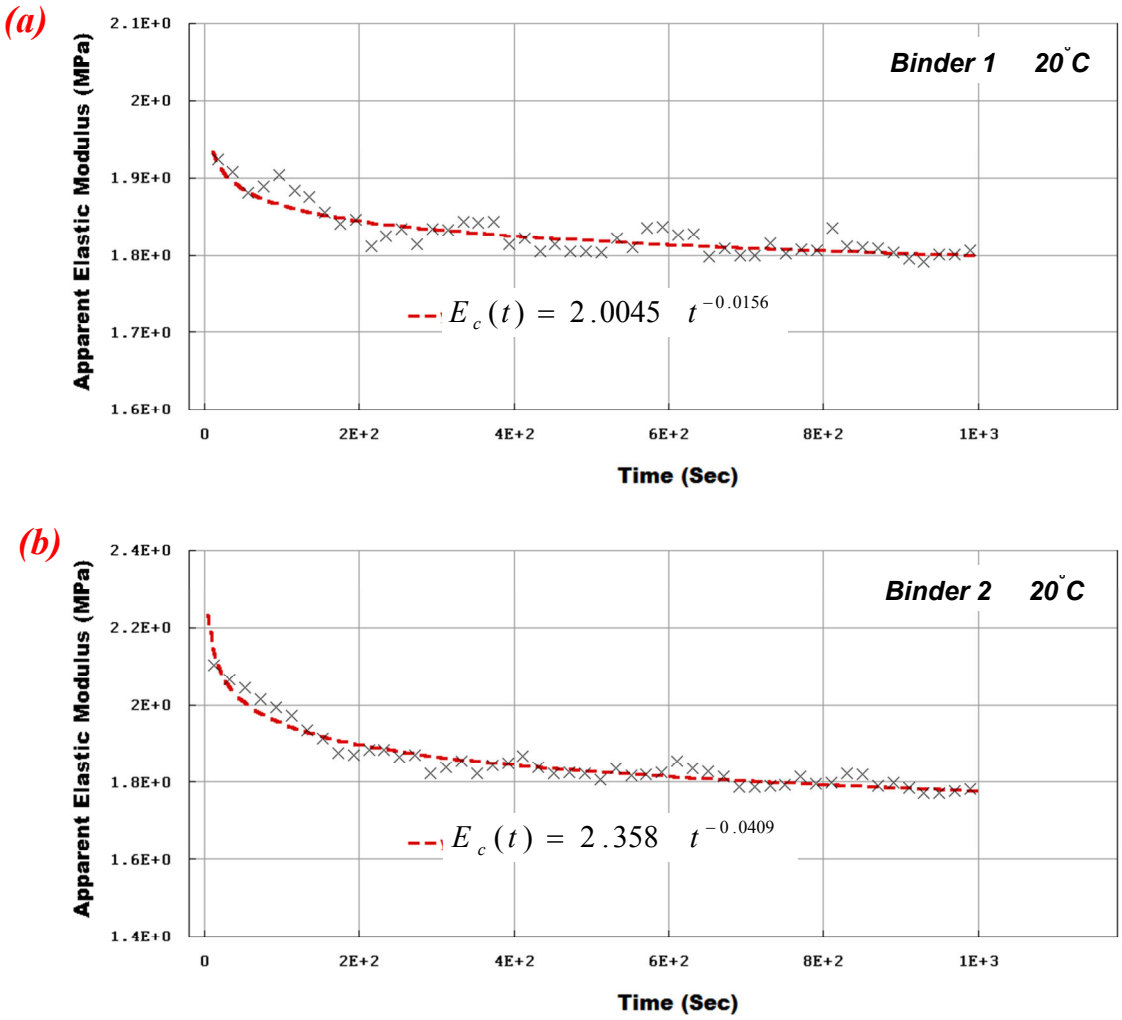

Figure 4.10: Measured apparent elastic modulus of asphalt binders at 20°C.

After obtaining the shear and the apparent elastic modulus, the bulk modulus was calculated as

$$K(t) = E_c(t) - \frac{4}{3}G(t). \tag{4.22}$$

Figure 4.11 illustrates the measured shear and bulk modulus as a function of time at 20°C. The analyses quantify the time dependence of the bulk modulus of asphalt binders. It should be noted that these results do not include the glassy behavior of asphalt binders.

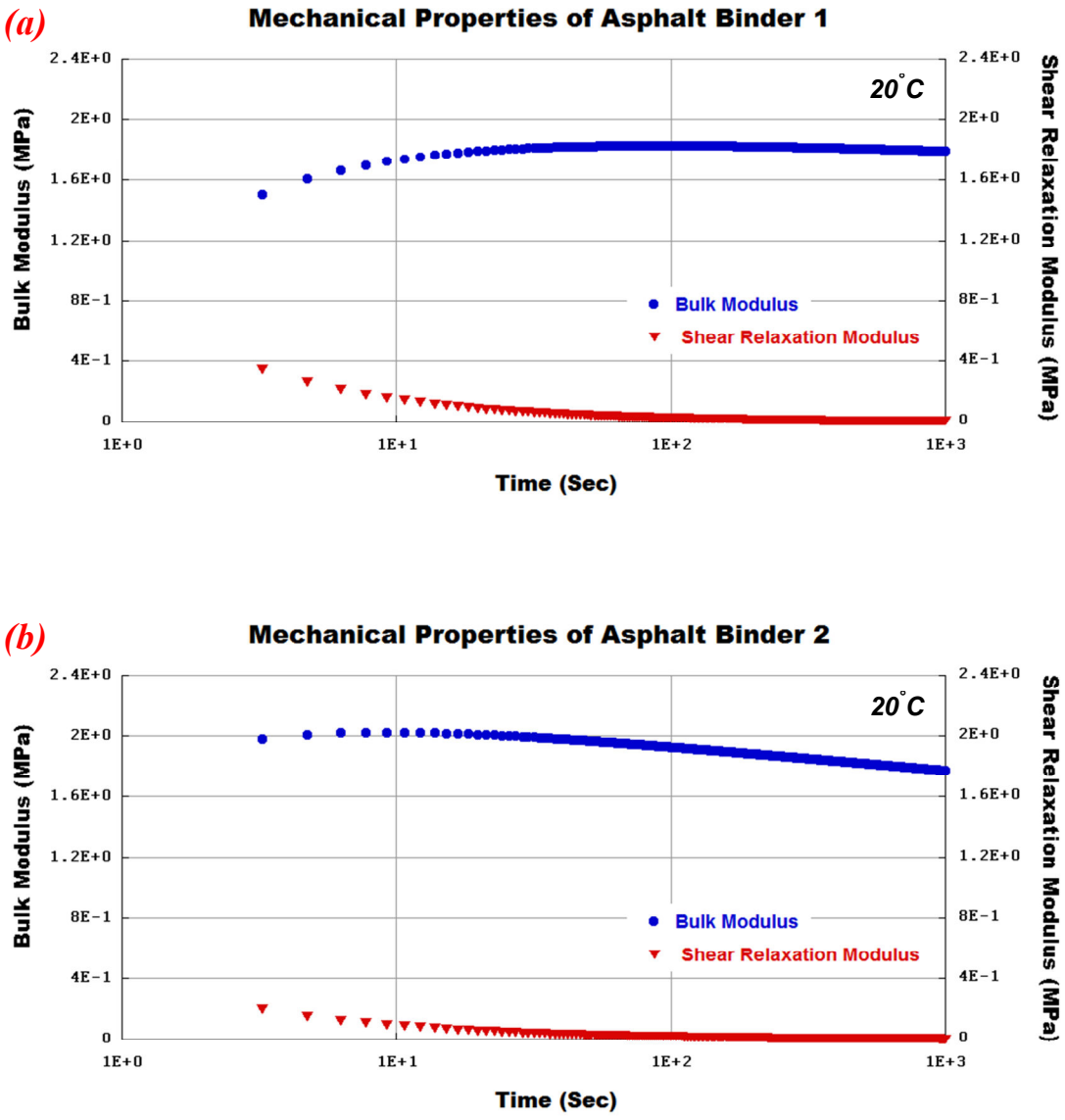

Figure 4.11: Measured mechanical properties of the asphalt binders at 20°C.

This is because of the experimental limitations that precluded the test data immediately after loading (the first two seconds) due to the effect of rise time. This can be mitigated by testing at lower temperatures and using the time-temperature superposition. It should

be also noted that the bulk modulus is computed using the measured shear and apparent elastic modulus as a function of time. Therefore, the slight increase in the bulk relaxation modulus (occurs in the first 10 seconds) could be due to the errors in estimation of the apparent relaxation modulus during the first few seconds of loading due to the effect of the rise time, molecular rearrangements within the asphalt binder, or a combination of these two. The author will further investigate this variation in his future work.

Finally, the measured shear and bulk moduli of the asphalt binders were used to examine the time-dependence of Poisson's ratio. Poisson's ratio as a function of time $\nu(t)$ was calculated using Equation 4.23, and plotted in Figure 4.12. The results also show that Poisson's ratio was indeed a function of time, and it increases with time.

$$\nu(t) = \frac{3K(t) - 2\mu(t)}{6K(t) + 2\mu(t)}. \tag{4.23}$$

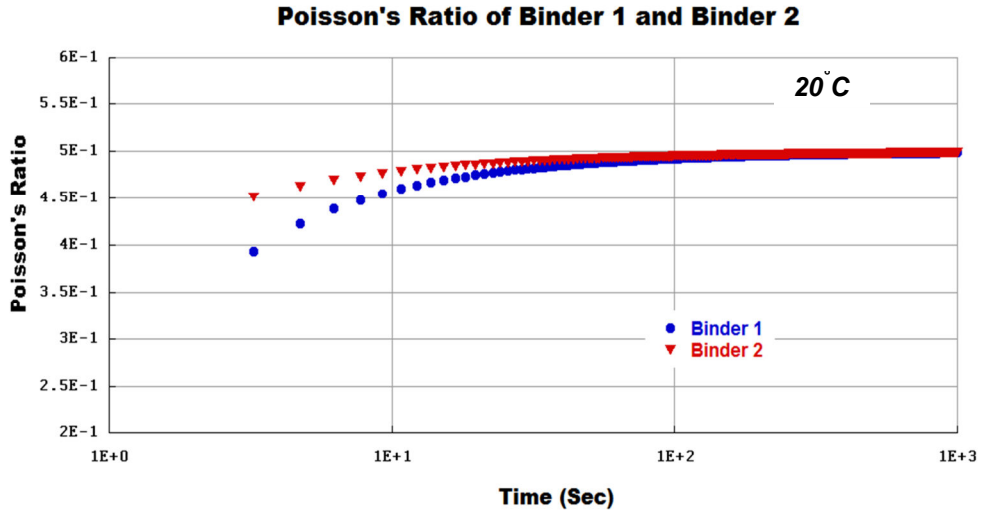

Figure 4.12: Measured Poisson's ratio of the asphalt binders at 20°C.

Figure 4.12 illustrates that although the initial value and time-dependence of Poisson's ratio varied from a binder to another, the Poisson's ratio for both binders reaches an asymptotic value of 0.5. These results indicate that asphalt binders are not initially incompressible, and they become nearly incompressible under long term loadings.

The author verified the linearity of the bulk response by conducting the compression relaxation test at different strain levels. The effect of test geometry on compression test measurements was also examined by conducting tests with different aspect ratios. The author demonstrated that there is no geometry effect when geometries with shape factor greater than 40 are being used. The shape factor of the test geometry used in these tests was 50 to minimize the edge effects, and the applied strain was three percent.

This research study developed a methodology to measure the bulk properties of asphalt binders. The test results demonstrated that both the bulk modulus and Poisson's ratio of asphalt binders change with time (albeit one can be regarded as more time sensitive than the other), and can be measured using a poker-chip geometry with a high aspect ratio. In the future, this work can be extended to measure the bulk properties of mastic and fine aggregate mixtures (FAM). Testing FAM or mastic has the advantage of including the interaction between asphalt binder and fine aggregates. This provides the required information for modeling the behavior of hot mix asphalt composite (coarse aggregate - mortar - air composite) in a computational framework. As a result, the developed model can be easily implemented in computational methods to improve the field performance predictions for asphalt pavements.

4.7. SUMMARY AND CONCLUSIONS

The objectives of this research were (i) to investigate the bulk behavior of asphalt binders, and (ii) to propose an approach to measure the bulk modulus of asphalt binders. The author used the poker-chip geometry with a high aspect ratio to measure the bulk modulus of asphalt binders. The proposed test procedure was able to measure the

mechanical properties of asphalt binders required for three-dimensional analyses. The time dependent bulk modulus and Poisson's ratio for two different binders were measured and reported at 20°C. The initial value and time-dependence of Poisson's ratio can be different from a binder to another one. However, the limited test data illustrated that the Poisson's ratio reaches an asymptotic value of 0.5, under long period of loading. This indicates that asphalt binders are not incompressible in short time scales of loading, and they become nearly incompressible under long loading duration. The analyses also demonstrated that the rate of change in apparent elastic modulus is significantly slower than the rate of change in shear modulus.

The methods and results from this research can be used to improve the understanding of the asphaltic materials behavior and can also help significantly improve the accuracy of computational analysis of asphaltic materials. In the future, this work will be extended to measure the bulk modulus of the fine aggregate mixtures and mastics. This will provide the information required in computational methods, and improves the performance predictions in simulations.

Chapter 5: Summary of Findings

The literature shows that localized stress concentrations in an asphalt mixture can result in very high and complex stress/strain states in asphalt binder. Therefore it is important to develop a comprehensive constitutive model for asphalt binder that is capable of reflecting the true response of the material under these stress states.

To investigate the shear behavior of asphaltic materials, this study evaluated the response of asphalt binders subjected to a range of cyclic stress levels using a Dynamic Shear Rheometer (DSR). The results demonstrate that asphalt binder specimens subjected to cyclic shear loads with stress amplitudes of 5 kPa and above, while axially constrained, experience the generation of a compressive axial force that changes the state of stress within specimen. The contribution of excessive geometric distortion to the generation of normal force was examined using finite element (FE) simulation. FE simulation revealed that the normal force generated under pure torsion can only be partially attributed to geometric distortion or the Poynting effect. The change in free volume and tendency of the specimen to axially dilate must be considered to fully explain the normal force that were observed in the laboratory tests.

It was also observed that asphalt binder subjected to cyclic loads over a range of stress amplitudes exhibits nonlinear behavior even at stress amplitudes as low as 5 kPa. This observation was consistent with the findings from other research studies. However, the decrease in dynamic modulus observed during a stress sweep test is commonly attributed to intrinsic nonlinearity of the material or damage. A systematic study was conducted to investigate the nature of nonlinear response in asphalt binders. The results from this study demonstrate that the nonlinear response of asphalt binders observed using measurements with the DSR can be explained by considering the interaction between normal stresses and applied shear stresses, referred to here as an interaction nonlinearity or three dimensional effects. Furthermore, the analysis indicated that the other sources of

nonlinear response such as damage, hysteretic heating, or stress history dependence did not contribute significantly to the observed nonlinear response. It should be noted that under a loading condition different from what is used in this research (such as higher stress levels), asphalt binder might experience damage. Although modeling of damage evolution in asphaltic materials was beyond the scope of this research, accounting for interaction nonlinearity is the cornerstone in developing the failure criteria for asphaltic materials.

In summary, asphalt binders experience a change in free volume or dilatation when subjected to shear stresses, which in turn leads to an interaction nonlinearity. In other words, the response of the asphalt binder to shear stresses also depends on the magnitude of axial stress. Given the fact that asphalt binders are used as the matrix in asphalt mixture composites and experience a variety of stress states due to traffic loads, it is important to develop an appropriate constitutive model that accommodates this interaction nonlinearity.

This research introduced an approach to model the interaction nonlinearity by modifying Schapery's nonlinearly viscoelastic equation. The overall state of stress in the material was represented by the octahedral shear stress. In order to model both intrinsic and interaction nonlinearity, Schapery's nonlinear viscoelastic equation was modified and the model parameters were obtained as a function of octahedral shear stress. The model parameters were obtained by developing a novel test method that captures the shear behavior of asphalt binders under different levels of normal force and associated octahedral shear stress. The resulting model was used to predict the material response under oscillatory and ramp loadings. The results were in good agreement with DSR measurements. The model verification under different loading histories further corroborated the existence of an interaction nonlinearity. The detailed development, calibration, and validation of this model were presented in Chapter 3 of this document.

Finally, to provide the necessary tools for three-dimensional modeling of asphaltic materials, this research investigated the bulk behavior of asphalt binders, and also proposed an approach to measure the bulk modulus of asphalt binders. A poker-chip

geometry with a high aspect ratio was used to measure the bulk modulus of asphalt binders. The proposed test procedure was able to measure the mechanical properties of asphalt binders required for three-dimensional analyses. The time dependent bulk modulus and Poisson's ratio for two different binders were measured at an intermediate temperature. The results demonstrated that the initial value and time-dependence of Poisson's ratio can be different from a binder to another one. However, the limited test data illustrated that the Poisson's ratio reaches an asymptotic value of 0.5, under long period of loading. This indicates that asphalt binders are not incompressible in short time scales of loading, and they become nearly incompressible under long loading duration.

The methods and results from this research can be used to improve the understanding of the asphaltic materials behavior, and can also help significantly improve the accuracy of computational analysis of asphaltic materials. This will improve pavement performance predictions and consequently help engineers develop more efficient pavement management policies. In the future, this work will be extended to the fine aggregate mixtures and mastics. This will include the asphalt binder and fine aggregates interactions, and therefore provides more accurate information required to improve the performance predictions in simulations.

References

Abaqus Theory Manual, Version 6.7, (2007)

Airey, G.D., Rahimzadeh, B., Collop, A.C.: Linear rheological behavior of bituminous paving materials. J. Mater. Civ. Eng. 16(3), 212–220 (2004)

Al-Khateeb, G., Shenoy, A., Gibson, N., Harman, T.: A new simplistic model for dynamic modulus predictions of asphalt paving mixtures. J. Association of Asphalt Paving Technologists 75, 1254-1293 (2006)

Anderson, D.A., Christensen, D.W., Bahia, H.U., Dongre, R., Sharma, M.G., Antle, C.E., Button, J.: Binder characterization and evaluation, Vol. 3: physical characterization. Strategic highway research program. Report shrp-a-369, National Research Council, Washington, ISBN 0-309-05767-1 (1994)

Arzoumanidis, G. A., Liechti, K. M.: Linear viscoelastic property measurement and its significance to some nonlinear viscoelasticity models. J. Mech. Time-Depend. Mater. 7, 209-250 (2003)

Bahia, H. U.: Low-temperature isothermal physical hardening of asphalt cement. Ph.D. Dissertation, The Pennsylvania State University (1991)

Bahia, H.U., Hanson, D.I., Zeng, M., Zhai, H., Khatri, M.A., Anderson, R.M.: Characterization of Modified Asphalt Binders in Superpave Mix Design. Publication NCHRP, vol. 459. National Academy Press, Washington (2001)

Bailey, R.: The utilization of creep test data in engineering design. Proc. Inst. Mech. Eng. 131, 131–349 (1935)

Bernstein, B., Kearsley, E.A., Zapas, L.J.: A study of stress relaxation with finite strain. Trans. Soc. Rheol. 7, 391–410 (1963)

Biot, M.A.: Mechanics of Incremental Deformations. John Wiley & Sons, (1965)

Brinson, H.F., Brinson, L.C.: Polymer Engineering Science and Viscoelasticity: An Introduction. Springer, Berlin (2008)

Carreau, P.J., De Kee, D.C.R., Chhabra, R.P.: Rheology of Polymeric Systems—Principles and Applications. Hanser/Gardner, Cincinnati (1997)

Cheung, C. Y., Cebon, D.: Deformation mechanisms of pure bitumen. Journal of Materials in Civil Engineering ASCE 9(3), 117-129 (1997)

Coleman, B.D., Noll, W.: Foundations of linear viscoelasticity. Rev. Mod. Phys. 3, 239–249 (1961)

Darvish, K.K., Crandall, J.R.: Nonlinear viscoelastic effect in oscillatory shear deformation of brain tissue. Med. Eng. Phys. 23, 633–645 (2001)

Delgadillo, R.: Nonlinearity of asphalt binder and the relationship with asphalt mixture permanent deformation. Ph.D. thesis, University of Wisconsin at Madison (2008)

Delgadillo, R., Bahia, H.U.: The relationship between nonlinearity of asphalt binders and asphalt mixture permanent deformation. Road Mater. Pavement Des. 11(3), 653–680 (2010)

Di Benedetto, H., Olard, F., Sauzeat, C., Delaporte, B.: Linearly viscoelastic behavior of bituminous materials: from binders to mixes. Road Mater. Pavement Des. 5, 163–202 (2004)

Di Benedetto, H., Delaporte, B., Sauzéat C.: Three-dimensional linear behavior of bituminous materials: experiments and modeling. Int. J. Geomechanics (ASCE) 7(2), 149-157 (2007)

Dinzart, F., Molinari, A., Herbach, R.: Thermomechanical response of a viscoelastic beam under cyclic bending; self-heating and thermal failure. Sixty Years of the Archives of Mechanics, Warszawa, 59-85 (2008)

Drakos, C., Roque, R., Birgisson, B.: Effect of measured tire contact stresses on near-surface rutting. Transp. Research Record 1764, National Research Council, Washington, D.C., 59-69 (2001)

Ferry, J.D.: Viscoelastic Properties of Polymers. Wiley, New York (1980)

Findley, W.N., Lai, J.S., Onaran, K.: Creep and Relaxation of Nonlinearly Viscoelastic Materials with Introduction to Linearly Viscoelasticity. North-Holland Series in Applied Mathematics and Mechanics. North-Holland, Amsterdam (1976)

Freudenthal, A.M., Ronay, M.: Second order effects in dissipative media. Proc. R. Soc. Lond. A 292, 14–50 (1966)

Fung, Y.C.: Foundations of Solid Mechanics. Prentice-Hall Inc, (1965)

Fung, Y.C.: Stress-strain-history relations of soft tissues in simple elongation. Biomechanics, Its Foundations and Objectives. Prentice Hall, New York (1972)

Gent, A. N., Lindley, P. B.: The compression of bonded rubber blocks. Proc. Inst. Mech. Eng. 173(1), 111-122 (1959)

Gould, P.L.: Introduction to Linear Elasticity, 1st edition, Springer, (1983)

Green, A.E., Rivlin, R.S.: The mechanics of nonlinear materials with memory. Part I. Arch. Ration. Mech. Anal. 1, 1–21 (1957)

Green, A.E., Rivlin, R.S.: The mechanics of nonlinear materials with memory. Part III. Arch. Ration. Mech. Anal. 4, 387–404 (1960)

Haward R.N.: Heating effects in the deformation of thermoplastics. Thermochim Acta 247, 87–109 (1994)

Hiel, C.C., Cardon, A.H., Brinson, H.F.: Viscoelastic modeling of epoxy-resins for adhesive and composite applications. In: Proc. of the 5th International Conference on Experimental Mechanics, Montreal, pp. 263–267 (1984)

Huang, Y.H.: Pavement Analysis and Design, 2nd edn. Pearson/Prentice-Hall, New York (2004)

Huang, C.: Development and numerical implementation of nonlinear viscoelasic–viscoplastic model for asphalt materials. Ph.D. thesis, Texas A&M University (2008)

Johnson, C. M.: Estimating asphalt binder fatigue resistance using an accelerated test method, PhD thesis, University of Wisconsin at Madison (2010)

Karki, P.: Computational and experimental characterization of bituminous composites based on experimentally determined properties of constituents, PhD thesis, Univ. of Nebraska at Lincoln, (2010)

Kim, H.J., Swan, C.C., Lakes, R.S.: Computational studies on high stiffness, high damping SiC-InSn particulate reinforced composites. Int. J. Solids and Structures 39, 5799-5812 (2002)

Kim, Y.R., Little, D.N.: Linearly viscoelastic analysis of asphalt mastic. J. Mater. Civ. Eng. 16(2), 122–132 (2004)

Kim, Y., Lutif, J.S.: Computational micromechanics modeling for damage-induced behavior of asphalt mixtures considering viscoelasticity and cohesive zone fracture. Special Publication of ASCE Geo-Institute, Minneapolis, Minnesota, May 18-21, 17-25 (2008)

Kim, M.: Development of differential scheme micromechanics modeling framework for predictions of Hot-Mix Asphalt (HMA) complex modulus and experimental validations. PhD thesis, University of Illinois at Urbana-Champaign (2009)

Kim, J., Lee, H., Kim, N.: Determination of shear and bulk moduli of viscoelastic solids from the indirect tension creep test. J. Eng. Mech., 136(9), 1067–1075 (2010)

Knauss,W.G., Emri, I.J.: Nonlinearly viscoelasticity based on free volume consideration. Comput. Struct. 13, 123–128 (1981)

Kose, S.: Development of a virtual test procedure for asphalt concrete. Ph.D. thesis, University of Wisconsin at Madison (2001)

Lai, J.S., Anderson, D.: Irrecoverable and recoverable nonlinearly viscoelastic properties of asphalt concrete. Highw. Res. Rec. 468, 73–88 (1973)

Lakes, R.S., Kose, S., Bahia, H.U.: Analysis of high volume fraction irregular particles damping composites. J. Eng. Mater. Technol. 124, 174–178 (2002)

Lakes, R.S.: Viscoelastic Materials. Cambridge University Press, Cambridge (2009)

Leaderman, H.: Viscoelasticity phenomena in amorphous high polymeric systems. J. Rheology 2, New York, 1-61 (1958)

Lee, M. A.: Resilient modulus and dynamic Poisson's ratio of asphaltic concrete mixes. Master Degree thesis, McMaster University, (1976)

Lianis, G.: Constitutive equations of viscoelastic solids under finite deformation. Purdue university report a & ES 63-11 (1963)

Lindley, P. B.: Compression moduli for blocks of soft elastic material bonded to rigid end plates. J. Strain Analysis for Eng. Design 14(1), 11-16 (1979)

Long, F. M.: Permanent deformation of asphalt concrete pavements: a nonlinear viscoelastic approach to mix analyses and design, PhD thesis, University of California at Berkeley, (2001)

Lu, H., Knauss, W.G.: The role of dilatation in the nonlinearly viscoelastic behavior of PMMA under multiaxial stress states. Mech. Time-Depend. Mater. 2(4), 307–334 (1999)

Luo, R., Lytton, R. L.: Self-consistent micromechanics models of an asphalt mixture. J. Mater. Civ. Eng. (ASCE) 23(1), 49-55 (2011)

Ma, Z., Ravi-Chandar, K.: Confined compression: a stable homogeneous deformation for constitutive characterization. Experimental Mechanics 40, 38-45 (2000)

Macosko, C.W.: Rheology Principle, Measurements, and Applications. John Wiley & Sons Inc., New York, (1995)

Maher, A., Bennert, T.: Evaluation of Poisson's ratio for use in the mechanistic empirical pavement design guide (MEPDG). Reported to FHWA, Report No.: FHWA-NJ-2008-004, (2008)

Marasteanu, O., Anderson, D.A.: Improved model for bitumen rheological characterization. Eurobitume Workshop on Performance Related Properties for Bituminous Binder, Luxembourg, Paper No. 133, (1999)

Masad, E., Somevadan, N., Bahia, H.U., Kose, S.: Modeling and experimental measurements of strain distribution in asphalt mixes. J. Transp. Eng. 127(6), 477–485 (2001)

Masad, E., Huang, C., Airey, G., Muliana, A.: Nonlinearly viscoelastic analysis of unaged and aged asphalt binders. Constr. Build. Mater. 22(11), 2170–2179 (2008)

Masuoka, M., Nakao, K.: Effect of aspect ratio on tensile bond strength for butt joint of internal fracture: theoretical and experimental analysis. Adhesion Measurement of Thin Films, Thick Films and Bulk Coatings, ASTM, 342-359 (1978)

McGuirt, C.W., Lianis, G.: Experimental investigation of non-linear, non-isothermal viscoelasticity. Int. J. Eng. Sci. 7, 579–599 (1969)

Molinari, A., Germain,Y.: Self-heating and thermal failure of polymers sustaining a compressive cyclic loading. Int. J. Solids Structure 33, 3439-3462 (1996)

Motamed, A., Bahia, H.U.: Influence of test geometry, temperature, stress level, and loading duration on binder properties measured using dynamic shear rheometer. J. Mater. Civ. Eng. 23(10), 1422-1432 (2011)

Motamed, A., Bhasin, A., Liechti, K.M.: Interaction nonlinearity in asphalt binders. J. Mech. Time-Depend. Mater. 16(2), 145-167 (2012*a*)

Motamed, A., Bhasin, A., Liechti, K.M.: Constitutive modeling of the nonlinear viscoelastic response in asphalt binders; incorporating three-dimensional effects. J. Mech. Time-Depend. Mater., DOI: 10.1007/s11043-012-9178-9, (2012*b*)

Norton, F.: Creep of High Temperatures. McGraw Hill, New York (1929)

Park, S.J., Liechti, K.M.: Rate-dependent large strain behavior of a structural adhesive. J. Mech. Time-Depend. Mater. 7, 143–164 (2003)

Park, S.: Durability of adhesive joints between concrete and FRP reinforcement in aggressive environments. PhD thesis, The University of Texas at Austin (2004)

Park, S.J., Liechti, K.M., Roy, S.: Simplified bulk experiments and hygrothermal nonlinearly viscoelasticity. J. Mech. Time-Depend. Mater. 8, 303–344 (2004)

Park, S., Liechti, K.M., Roy, S.: A nonlinearly viscoelastic fracture analysis of concrete/frp delamination in aggressive environments. Int. J. Fract. Mech. 142(1), 9–27 (2006)

Popelar, C.F., Liechti, K.M.: Multiaxial nonlinearly viscoelastic characterization and modeling of a structural adhesive. J. Eng. Mater. Technol. 119, 205–210 (1997)

Popelar, C.F., Liechti, K.M.: A distortion-modified free volume theory for nonlinearly viscoelastic behavior. J. Mech.Time-Depend. Mater. 7, 89–141 (2003)

Poynting, J.I.-I.: On pressure perpendicular to the shear-planes in finite pure shears, and on the lengthening of loaded wires when twisted. Proc. R. Soc. Lond. 82, 546–559 (1909)

Qvale, D., Ravi-Chandar, K.: Viscoelastic characterization of polymers under multiaxial compression. J. Mech. Time-Depend. Mater. 8, 193-214 (2004)

Read, J.M.: An assessment of Poisson's ratio for bituminous materials. Institute of Asphalt Technology Yearbook, 37-41 (2000)

Read, J., Whiteoak, D.: The Shell Bitumen Handbook. Shell UK Oil Products Limited, (2003)

Reinke, G., Glidden, S., Engber, S., Herlitzka, D.: Rheological properties of polymer modified binders and mixtures related to mixture resistance to permanent deformation. In: Proceedings of the Fifty-First Annual Conference of the Technical Asphalt Association, Prince Edward Island, pp. 57–85 (2006)

Riddell, M.N., Koo, G.P., O'Toole, J.L.: Fatigue mechanisms of thermoplastics. Polymer Engineering & Science, October, 363-368 (1966)

Rittel, D.: An investigation of the heat generated during cyclic loading of two glassy polymers; Part I: Experimental. Mechanics of Materials 32, 131-147 (2000)

Schapery, R.A.: Approximate methods of transform inversion for viscoelastic stress analysis. In: Proceedings of 4th US National Congress of Applied Mechanics (ASME 2), New York, pp. 1075–1085 (1962)

Schapery, R.A.: Thermomechanical behavior of viscoelastic media with variable properties subjected to cyclic loading. J. Applied Mechanics 32, 611- 619 (1965)

Schapery, R.A.: Further development of a thermodynamic constitutive theory: stress formulation. Purdue university report AA&ES 69-2 (1969)

Schapery, R.A.: On the characterization of nonlinear viscoelastic materials. Polym. Eng. Sci. 9(4), 295–310 (1969)

Shames, I.H.: Mechanics of Fluids. McGraw-Hill Professional, (2002)

Shariff, M.H.B.M.: An approximate analysis of infinitesimal deformations of bonded elastic mounts. J. Strain Analysis for Eng. Design 23(3), 115-120 (1988)

Shuku, T.: Effect of geometric non-linearity on the deformation behavior of linear elastic ground. Proceedings of the Nineteenth International Offshore and Polar Engineering Conference, (2009)

Stroup-Gardiner, M., Newcomb, D.E., Drescher, A., Zhang, W.: Influence of test method variables on Mn/Road hot mix asphalt mixture test results. Reported to U.S. Army Corps of Engineer, Report No.: MN/RC - P2000-03, (1997)

Taylor, G.I., Quinney, H.: The latent energy remaining in a metal after cold working. Proceeding of Royal Society of London, A143, 307-326 (1934)

Tormey, J.F., Britton, S.C.: Effect of cyclic loading on solid propellant grain structure. AIAA Journal 1, 1763-1770 (1963)

Turner, S.: The strain response of plastics to complex stress histories. Polym. Eng. Sci. 6, 306–316 (1966)

You, Z., Adhikari, S., Dai, Q.: Two dimensional and three dimensional discrete element models for HMA. The Special Publication of ASCE Geo-Institute. Blacksburg, Virginia, June 3-6, 117-126 (2007)

You, Z., Dai, Q.: A review of advances in micromechanical modeling of aggregate–aggregate interaction in asphalt mixture. Can. J. Civ. Eng. 34(2), 1519–1528 (2007)

Vita

Mr. Arash Motamed has earned a Bachelor's degree in Civil Engineering as well as two Masters of Science in the field of Pavement and Materials with first class honors. Arash joined the PhD program at The University of Texas at Austin in 2008, and he has been involved in constitutive modeling of asphaltic materials. His PhD research, sponsored by the *Federal Highway Administration* (*FHWA*), identifies the reasons why current practice to evaluate pavement materials does not accurately represent the observed field performance and provides a resolution to this shortcoming in the form of new experimental test methods and mechanistic analysis of test results.

In addition to his research on pavement materials at UT Austin, he continued his collaboration with his second MS supervisor at the University of Wisconsin at Madison (Professor Bahia) on modeling the permanent deformation in asphaltic materials. As a result, he extended the constitutive equation for permanent deformation in asphalt binders, and also examined the influence of test geometry on the measured properties of asphalt binders. Besides conducting fundamental research on material characterization, Arash was actively involved in applied research (funded by *Texas Department of Transportation*) that addresses the immediate needs of industry. For instance, he investigated the performance of asphalt mixtures produced by using different environmental-friendly techniques. Furthermore, his research experience and knowledge includes pavement management and analysis which was the focus of his first MS degree. As a part of his research on the topic of "*Back-Calculation of Pavement Layers Moduli Using Genetic Algorithm,*" he developed a unique way of using a genetic algorithm to reduce the time required for back-calculation.

During the last few years, Mr. Arash Motamed has made significant contributions to the fields of pavement and transportation infrastructure. These contributions, along with his academic performance, made him eligible to receive several prestigious awards such as ***IRF*** Fellowship (awarded by the International Road Federation), the ***AAPT***

Scholarship (awarded by the Association of Asphalt Paving Technologists), and the ***NAPA*** Professor Training Fellowship (awarded by the National Asphalt Pavement Association).

Permanent address (or email): motamed@utexas.edu

This dissertation was typed by Arash Motamed.